2024

# Contributions of the dentate gyrus to episodic and spatial memory

BOSTON UNIVERSITY

ARAM V. CHOBANIAN & EDWARD AVEDISIAN SCHOOL OF MEDICINE

Dissertation

# CONTRIBUTIONS OF THE DENTATE GYRUS TO EPISODIC AND SPATIAL MEMORY

by

**LUCIUS KELTON WILMERDING**

B.A., Macalester College, 2017

Submitted in partial fulfillment of the

requirements for the degree of

Doctor of Philosophy

2024

Approved by

First Reader

Michael E. Hasselmo, D.Phil.
William Fairfield Warren Distinguished Professor
Professor of Psychological and Brain Sciences
Professor of Biomedical Engineering

Second Reader

Steve Ramirez, Ph.D.
Assistant Professor of Psychological and Brain Sciences

## DEDICATION

I would like to dedicate this dissertation to my family: Orion, Liz, Austin, Mary and Olivia whose wisdom, feedback, support, and humor made the long journey brighter and worth traveling.

To Mom: The original Dr. Wilmerding, your power of intellect is matched only by your love and kindness. Thank you for showing me the way.

To Dad: You once told me to learn from my mistakes. There is no better place, nor no more complete way, to digest that lesson than in a PhD program. Failure is a tool for growth, not a commentary on our worth as human beings.

To Orion: You are my twin and my foundation. Words are too paltry a currency to express everything. They shall not try. Thank you.

To Olivia: You have taught me to be a better communicator and to believe in myself. A little, anyway. I could not have made it this far without your feedback, kindness, and wit.

To Achilles, Clio and Pepper: The second law of thermodynamics can be interpreted as 'entropy always increases'. I salute all three of you for your adorable contributions to this process.

## ACKNOWLEDGMENTS

It goes without saying that the following work would not have been possible in the absence of my small team in the Hasselmo lab, Ivan Kondratyev and Wen Bing Shi. But the two of you contributed far more than the hours of your time. You pushed me to be a better teacher, a better mentor, and a halfway competent project manager. In theory it works, it's just broken. Thank you both.

Secondly, I must acknowledge the sacrifice made by each and every animal used in the course of my research in the Hasselmo lab to develop my own selfish understanding of the brain. I also thank those animals from my previous research experience, in particular, subjects B, S, T, U, K and N from Matt Johnson's Neuromodulation Research and Technology Lab. Even subject A who bit the hell out of me. I also thank the generous funding sources from the NIH and ONR that made my time at BU possible.

Many thanks to the Hasselmo and Ramirez labs who have been my home and community in the lab these last years. In particular, thanks to Andy, Bill, Lucas, Kaitlyn and Amy who donated their valuable time to helping me learn. Thanks to our lab manager, Jun Shen as well. Going forward I hope to emulate some of Mike Hasselmo's incisive intellect, encyclopedic knowledge of the field, and infinite patience for good science to take the time it needs. Thank you for indulging my peculiarities, in particular one final surprise at the defense. So too do I hope that I have inherited some of Steve Ramirez's willingness to entertain a good hypothesis, his boundless enthusiasm for all things science, and his wisdom in knowing when to celebrate success and failure. I am

pleased to acknowledge all of the feedback, ideas and technical support of my advisory committee, Dr. Ben Scott, Dr. Emily Stephen, and Dr. Shantanu Jadhav.

A career in science does not begin on your first day in graduate school, nor even your first year of undergrad. I will be forever grateful to the teachers who indelibly changed the way I look at the world – Fred Shaw, Mr. Keogh, Ms. Estep, and Jonathan Heiles. A special thanks tinged with admiration to Eric Wiertelak and Julia Manor at Macalester. How did you do it?

To the Graduate Program in Neuroscience community: Thank you. It has been my pleasure and privilege to learn and grow with you. In particular, grateful thanks must be made to Shelley Russek and Sandi Grasso who have been the patient, nurturing gardeners of the GPN biome, helping each of us find optimal conditions. Mine was alongside my excellent cohort – Beverly, Kylie, Spencer, Rifqi, Amy, Ashley, and Dr. Allison Tipton. Nor could I forget my friends/mentors Dr. Lucas Carstensen and Dr. Kaitlyn Dorst and those excellent companions in the cohorts behind me, including Naomi, Sam M, and Quan. I will miss you all deeply, but only until the next time we reconnect as colleagues and friends.

**CONTRIBUTIONS OF THE DENTATE GYRUS**

**TO EPISODIC AND SPATIAL MEMORY**

**LUCIUS KELTON WILMERDING**

Boston University Aram V. Chobanian & Edward Avedisian School of Medicine, 2024

Major Professor: Michael E. Hasselmo, D.Phil., Professor of Psychological and Brain Sciences

ABSTRACT

Animals learn from past experience to guide future behavior and improve survival. This ability relies in part on specific episodic memories of past events encoded by neuronal activity and stored by updated connectivity between neurons. The unique architecture and activity of the hippocampus and related cortical regions are crucial for supporting these episodic memories. Hippocampal models propose the need for a pattern separation function to disambiguate similar memories and a pattern completion function to recall the full breadth of an experience from a partial cue. Past work suggests that neuronal activity in the dentate gyrus (DG) of hippocampus contributes to memory-guided navigation and plays a role in pattern separation. We tested the role of specific DG neuronal ensembles (i.e. engrams) in supporting the pattern separation function and altering downstream neural activity and, ultimately, behavior. To that end, we used an activity-dependent labeling paradigm to identify and manipulate engram ensembles during navigational and contextual fear conditioning (CFC) tasks. The results of our first experiment revealed that the DG partially disambiguates specific maze trajectories while still exhibiting greater overlap than chance levels. These findings suggest that the DG contributes to memory-guided navigation by both pattern separation and completion. Our

second experiment manipulated nonspecific memory-related DG populations to assess the functional role of these cells in task generalization across contexts and ongoing spatial working memory. Optogenetic activation of these ensembles disrupted performance accuracy and exhibited a time-dependent impairment effect suggesting a role of the DG in task generalization between contexts. The final experiments investigated the physiological ramifications of artificial memory ensemble reactivation during ongoing navigation behavior. We recorded local field potential (LFP) and single unit responses in mouse DG and CA1 during artificial reactivation of a DG-mediated CFC memory engram. Stimulation of the DG entrained LFP and individual cell spiking in a subpopulation of CA1 pyramidal cells. Their spatial information was disrupted by stimulation despite stable navigational representation before and after the manipulation. Further, the presence of stimulation could be reliably decoded by the firing rate of the network, suggesting that engram reactivation forced the CA1 to adopt a repeatable state, perhaps to support behavioral expression of memories. In summary, my dissertation work presents empirical and theoretical evidence for the role of the dentate gyrus as a single node of an extended separation/completion circuit distributed anatomically and temporally as a neural mechanism supporting episodic memory.

## TABLE OF CONTENTS

## LIST OF FIGURES

## LIST OF ABBREVIATIONS

5-HT ..... Serotonin

AD ..... Alzhiemer's Disease

Ach ..... Acetylcholine

BDNF ..... Brain Derived Neurotrophic Factor

BU ..... Boston University

CA1 ..... Cornu Ammonis 1

CA2 ..... Cornu Ammonis 2

CA3 ..... Cornu Ammonis 3

cm ..... centimeter

DA ..... Dopamine

D/V ..... Dorsal / Ventral

DG ..... Dentate Gyrus

EC ..... Entorhinal Cortex

GC ..... Granule Cell

HD ..... Head Direction

HPC ..... Hippocmapus

IACUC ..... Institutional Care and Use Committee

IN ..... Interneuron

KO ..... Knockout

LFP ..... Local Field Potential

LTP ..... Long Term Potentiation

m ..... meter

M/L ..... Medial / Lateral

MC ..... Mossy Cell

ms ..... millisecond

NMDA ..... N-methyl D-aspartate

PVB ..... Parvalbumin

PVC ..... Population Vector Correlation

sec ..... second

Sub ..... Subiculum

SI ..... Spatial Information

SWM ..... Spatial Working Memory

# CHAPTER ONE: INTRODUCTION

## Organization of Dissertation

This dissertation is organized as follows: Chapter One introduces the reader to episodic memory, neuroanatomy, hippocampal physiology, and engrams; Chapter Two presents data supporting the hypothesis that ensembles of the dentate gyrus (DG) partially separate different spatial trajectories made within an overall environmental context; Chapter Three discusses the results of a study employing optogenetics to manipulate learning-associated cellular ensembles in DG to disrupt ongoing navigational memory in novel environments; Chapter Four summarizes the findings of a pilot experiment manipulating DG fear memory ensembles during freely moving behavior and the associated changes in hippocampal network activity recorded using extracellular electrophysiology; and lastly Chapter Five summarizes the key findings of each study and discusses reasonable interpretations of the data, the nature of pattern separation and completion, limitations of the experiments, and future directions of the field.

Chapter Two tested the degree of overlap in DG granule cell populations associated with spatial memory in which I designed the experiment, performed data collection, analyzed data and wrote the published manuscript. Prior studies have implicated ensembles of DG cells in both contextual fear memories (Liu et al., 2012; Ramirez et al., 2013; Denny et al., 2014; Kitamura et al., 2017) and specific spatial representations (GoodSmith et al., 2017, 2019; Hainmueller & Bartos, 2018; Cholvin et al., 2021). We tested the degree of cellular ensemble overlap recruited by partially non-overlapping spatial trajectories within a memory-guided T-maze task. Using endogenous

c-Fos driven cell ‘tagging’ with fluorescent labels, we visualized DG ensembles associated with exposure to a full T-maze, partial T-maze, or novel open field and compared them to ensembles recruited by full T-maze experience. Our results suggest the DG partially disambiguates specific maze trajectories while still exhibiting greater overlap than chance levels. Our results support a hypothesis that the DG contributes to memory-guided navigation by a simultaneous pattern separation and completion process.

Chapter Three sought to examine the functional role of learning-related DG ensembles in task generalization across contexts and ongoing spatial working memory in which I did experimental design, carried out procedures and data analyses, and wrote the manuscript. The DG is involved in successful performance of spatial working memory tasks (Xavier et al., 1999; Costa et al., 2005; Sasaki et al., 2018) and is upstream to regions such as CA1 that mediate successful task generalization for flexible decision making (Wang & Cai, 2006; Hyman et al., 2010; Spellman et al., 2015). This raises the question of how the ensembles of DG cells participate in these cognitive functions. We expressed the light-activated excitatory ion channel, ChannelRhodopsin2, in memory-associated DG cell ensembles during learning of a spatial working memory T-maze task. Optogenetic activation of these ensembles disrupted memory accuracy and exhibited a time-dependent impairment effect suggesting a role of the DG assemblies in task generalization between contexts.

Chapter Four aimed to investigate the physiological ramifications of artificial memory ensemble reactivation during ongoing behavior for which I designed the experiments, conducted recordings, analyzed data, and organized the preliminary findings

for the present dissertation. Artificial reactivation of DG engram ensembles leads to behavioral fear expression (Liu et al., 2012; Ramirez et al., 2013; Redondo et al., 2014; Ryan et al., 2015), but only one study has attempted to examine the HPC circuit response to artificial memory perturbation during freely-moving behavior (Jou et al., 2023). Understanding the circuit-level consequences of engram reactivation is an important step for potential therapeutic benefit of memory stimulation. We recorded local field potential (LFP) and single unit responses in mouse DG and CA1 during artificial reactivation of a DG-mediated CFC memory engram. Optogenetic stimulation of the DG entrained LFP and individual cell spiking in a subpopulation of CA1 pyramidal cells. Their spatial information was disrupted by stimulation despite stable navigational representation before and after the manipulation. Further, the presence of stimulation could be reliably decoded by the firing rate of the network, suggesting that engram reactivation forced the CA1 to adopt a repeatable state, perhaps to support behavioral expression of memories.

Chapter Five includes a summary of the central findings of each previous chapter, a holistic discussion and interpretation of the experimental outcomes with specific reference to the nature of memory pattern separation and completion as well as limitations of the present work and future directions for the field.

## Overview of Neuroanatomy

Forecasting future states allows biological agents to reach goals or avoid injuries by modifying their actions appropriately. The nervous system makes extensive use of prior experience, memory, to improve the survival of the organism and the evolutionary

fitness of its genes. Even the neurons of ‘simple’ organisms such as the sea slug *Aplysia*, whose mollusk ancestors first appeared in the Cambrian period, exhibit mnemonic (memory) behavior such as habituation, sensitization, and even classical and operant conditioning (Kandel & Tauc, 1964; Kupfermann & Kandel, 1969; Kandel et al., 2014). Comparative anatomical and transcriptomic studies in amniote species (birds, reptiles and mammals) suggest a high degree of conservation of the memory-associated hippocampal region, even to the level of transcription factors for neurons in specific subfields of hippocampus (Tosches et al., 2018). Clearly, the ability to record fragments of previous states through memory processes offered our ancestors an immense survival advantage. By happy circumstance, this adaptation allows us to remember the rich detail and charming peculiarities of our lives.

Much work has been devoted to reaching a satisfying mechanistic interpretation of memory processes in the brain. Episodic memories, specific recollections in time and space, have been extensively tied to the function of regions in the temporal and parietal lobes including the hippocampus (HPC), subiculum (Sub), and entorhinal cortex (EC). Computational researchers established a standard model for HPC function in episodic memory which has been extensively adopted (Marr, 1971; McNaughton & Morris, 1987; O’Reilly & McClelland, 1994; Treves & Rolls, 1994; Hasselmo et al., 1995). Based largely on architectural evidence and computational theory at the time, the model proposes the role of the HPC and other cortical regions in memory formation and storage.

In summary, functions are assigned as follows: the EC serves as gateway into and out of the HPC for new information and cues the recall of specific memories; the dentate

gyrus (DG) acts to separate similar input patterns from EC; the CA3 acts to complete partial inputs into whole memory outputs via auto-association; and the CA1 integrates and compares CA3 outputs to the invoked memory cued by EC (McNaughton & Morris, 1987; Treves & Rolls, 1994; Hasselmo et al., 1995). In particular, the roles of pattern separation and completion are often contrasted with one another as serial stages within an overall learning and retrieval process. An illustrative example of this view would be the rich recall of a memory about a red-clad Viking winning a mock tournament as separate from the memory of a female knight jousting on a field, despite both memories occurring at Renaissance fairs alongside similar cues such as minstrels and mead. How then is this computational theory realized at the level of HPC circuitry? Further, how well do these theories capture the mnemonic phenomenon to yield potential clinical benefit and satisfactorily explain our most cherished experiences?

### *Hippocampal anatomy and organization*

Extensive work has documented the cell types and connectivity within HPC and associated cortices. A comparatively brief overview will be made. First, the EC receives highly processed multimodal and unimodal sensory and non-sensory information from the rest of neocortex including visual, auditory, and olfactory information (Suzuki & Amaral, 1994; Kerr et al., 2007). The EC itself is divided between a lateral and medial portion, with the LEC implicated in carrying information related to nonspatial features in the environment, while the MEC is implicated in the coding of spatial position of those features (Mumby & Pinel, 1994; Hargreaves et al., 2005; Eichenbaum et al., 2012). In addition to extensive projection to the neocortex (Insausti et al., 1997), layer 2 outputs of

EC synapse onto the dendrites of granule cells (GCs) in the DG and pyramidal cells in CA3, while layer 3 outputs synapse onto pyramidal cell dendrites in CA1 (Squire et al., 1989). Notably, LEC inputs and MEC inputs contact with the outer and middle strata of GC dendrites (Amaral & Witter, 1989), suggesting that GCs play some role in integrating the identity and position of the elements encoded in episodic memory (Eichenbaum et al., 2012; Fernández-Ruiz et al., 2021).

The amygdala also represents an important extrinsic connection to HPC. The basolateral and to a lesser extent basomedial subnuclei of the amygdala project to the CA3 and CA1 stratum radiatum and oriens layers (Pikkarainen et al., 1999; Yang et al., 2016; Yang & Wang, 2017). This connection is particularly strong in the rodent ventral HPC, suggesting a functional specialization in emotionally salient memories (Felix-Ortiz et al., 2013; Yang et al., 2016). The HPC reciprocally connects to amygdala via the CA1 (Van Groen & Wyss, 1990).

Within the HPC proper, DG granule cells send their axonal projections, the mossy fibers, to the CA3 pyramidal cells, as well as to the mossy cells (MCs) and interneurons of the DG hilus (Ribak et al., 1985; Amaral et al., 2007; Scharfman, 2016). These mossy fibers form multiple boutons *en passant* with many CA3 cells along the curve of the pyramidal layer (Amaral et al., 2007). These CA3 pyramidals display a remarkable feature – their recurrent fibers synapse onto other CA3 pyramidal cells both ipsilateral and contralateral with about 2-4% probability (Amaral & Witter, 1989; Ishizuka et al., 1990; Treves & Rolls, 1994), yielding a sparse auto-associative network (Marr, 1971; McNaughton & Morris, 1987). The CA3 also projects fibers (Schaffer collaterals) to the

CA1. In addition to CA3 inputs, CA1 receives inputs from layer 3 of EC (Amaral et al., 1990) and indirectly from the medial prefrontal cortex (mPFC) via the nucleus reuniens of the thalamus (Vertes et al., 2007; Griffin, 2015). Lastly, the CA1 pyramidal cells mediate the direct output connections of HPC to the Sub and layer 5 of EC, as well as a small connection to mPFC (Tamamaki et al., 1987; Van Groen & Wyss, 1990; Naber et al., 2001). Recently, superficial layer CA1 pyramidals were shown to have anatomical and functional preference for mPFC in contrast to deep layer pyramidals which preferred connection to MEC (Harvey et al., 2023). To commit a vast oversimplification, the EC projects to DG, the DG onto CA3, and the CA3 finally to CA1 forming the classic 'tri-synaptic circuit' of memory.

Lastly, the multifarious interneuron (IN) subtypes of HPC will be discussed. INs show remarkable diversity in their gene expression patterns, axonic arborization, and response to circuit dynamics relative to the few HPC excitatory cell types (Freund & Buzsáki, 1996; Klausberger & Somogyi, 2008). Several common cell types are identified by gene expression profiles in combination with their projection specificity onto pyramidal cell compartments. For example, the axons of the parvalbumin (PVB) expressing basket cells extensively enmesh the soma and proximal dendrites of principal cells while PVB axo-axonic cells target the initial axon segment (Freund & Buzsáki, 1996; Klausberger & Somogyi, 2008). Bistratified cells in CA1 target the pyramidal dendrites in stratum radiatum and oriens, matching the excitatory inputs of CA3 pyramidal cells while oriens-lacunosum moleculare INs inhibit the dendritic layer associated with EC input (Freund & Buzsáki, 1996; Klausberger & Somogyi, 2008). The

presence of INs that target other INs leading to disinhibition implies a highly flexible circuit with nonlinear dynamics. While an exhaustive description is beyond the scope of the present work, suffice to say that INs are crucial to the function of HPC in health and disease states.

*The hilus – anatomy and interconnectivity with DG*

The DG is peculiar among the HPC subfields for its multiple types of excitatory cells – the granule cells (GCs) of the dentate granular zone and the mossy cells (MCs) of the dentate hilus (polymorphic layer; sometimes "CA4"). In brief, the GCs send their mossy fiber axons (not to be confused with MC axons) to synapse on CA3 pyramidals and hilar MCs via giant boutons, and onto interneurons of both CA3 and the hilus via smaller boutons (Amaral et al., 2007; Scharfman, 2016). These MCs, partly characterized by large somas with thorny excrescences, send glutamatergic efferents to a diverse range of cells, including interneurons, other MCs both locally and distantly, and to ipsilateral and contralateral HPC (Ribak et al., 1985; Soriano & Frotscher, 1994; Scharfman, 1995). MCs return excitation to GCs by synapsing in the inner molecular layer (Ribak et al., 1985; Frotscher et al., 1991) and may represent a strong influence on GC activation. MCs also provide lateral inhibition to GCs by exciting interneurons such as the basket cells (Scharfman, 1995; Larimer & Strowbridge, 2008) leading to wide-ranging network effects. Complicating matters further, CA3 sends back-projections to contact hilar MCs, hilar INs, and the inner molecular layer of DG (X.-G. Li et al., 1994; Scharfman, 2007). The back-projection is particularly common from the cells nearest the hilus (proximal, CA3c). This extensive recurrency suggests that the DG, CA3, and hilus forms an

extended network. While much work to elucidate the interplay between GCs and MCs during memory formation and retrieval is still required, the extended DG circuitry satisfies the conditions of a hetero-associative network as previously proposed (Marr, 1971; McNaughton & Morris, 1987; Lisman, 1999).

### *Modulatory influence of the hippocampus*

To add further nuance, the contribution of neuromodulatory systems must be touched upon. Learning and memory require updating of the synaptic connections between neurons, long term potentiation (LTP) and depression (LTD), but which connections should be strengthened, weakened, or maintained? In HPC, modulation of synaptic plasticity occurs in response to acetylcholine (Ach), serotonin (5-HT), norepinephrine (noradrenaline, NE), and dopamine (DA) which act in complex but complimentary fashion to filter which experiences become lastingly stored, perhaps in response to prediction errors (Hasselmo & Schnell, 1994; Hasselmo et al., 1995; Hasselmo & Wyble, 1997; Yu & Dayan, 2005; Palacios-Filardo & Mellor, 2019). Experiences that violate expectations are salient learning opportunities for the long term benefit of the organism. The locus coeruleus in the brainstem projects both DA and NE strongly throughout HPC, activates in response to unexpected novelty, and can stabilize LTP in a retrospective fashion allowing longer term memory storage (Sara, 2009; O'Dell et al., 2015; Takeuchi et al., 2016; Edelmann & Lessmann, 2018). The median raphe nucleus provides 5-HT which prevents depotentiation of LTP and minimizes LTD in most excitatory HPC synapse types, except the CA3 recurrent synapse (Hagena & Manahan-Vaughan, 2017). Lastly, much work has demonstrated the role of Ach in gating

the flow of information into and out of HPC (Hasselmo, 2006; Hasselmo et al., 1995). The medial septum delivers cholinergic (and GABAergic and glutamatergic) afferents to the HPC (Frotscher & Léránth, 1985) These afferents suppress local connectivity and promote incoming information from EC during high cholinergic tone, and vice versa when Ach is low (Hasselmo, 1993; Hasselmo & Schnell, 1994; Hasselmo et al., 1995; Dannenberg et al., 2017). These dynamics could allow for separation of memory encoding and retrieval to orthogonalize HPC patterns of different memories (Hasselmo, 2006). Neuromodulation of INs leads to ever more complex regulation of synaptic plasticity depending on the specific receptor subtypes and the affected cellular compartments and is touched on in the many reviews cited here and above (Parra et al., 1998; Patil & Hasselmo, 1999; Palacios-Filardo & Mellor, 2019).

### *Dorsal versus ventral hippocampus and DG*

Functional specificity of the HPC is heterogeneous both across subfields but also along the longitudinal (dorsal-ventral; septo-temporal) axis. Early observations of differential impacts of HPC lesions led to assignment of spatial and contextual processing in dorsal HPC (posterior in humans) and anxiety, fear and emotional processing to ventral HPC (anterior in humans; Moser & Moser, 1998; Fanselow & Dong, 2010). Gene expression patterns offer sharp boundaries of cell types along the longitudinal axis in CA1, CA3, and DG that broadly support proposed dorsal, intermediate and ventral functional segregations (Thompson et al., 2008; Dong et al., 2009; Fanselow & Dong, 2010). Extrinsic connectivity also differs, with dHPC projecting mono- or multi-synaptically to navigational and exploration structures including EC, Sub, Retrosplenial

Cortex, Nucleus Accumbens, and the Mammillary Bodies, while vHPC favors connections to the amygdala, mPFC and hypothalamus (Fanselow & Dong, 2010). However, an updated view suggests more of a gradient in connectivity with some exceptional connections to the amygdala favored by vHPC (Strange et al., 2014). Physiological evidence also supports smoother gradients from fine- to coarse-grained representations of space in both place cells (M. Jung et al., 1994; Kjelstrup et al., 2008) and grid cells (Fyhn et al., 2004; Hafting et al., 2005) along the dorsoventral axis. Interestingly, the gradient in ratio of DG to CA1 subfield size along this axis has been used as a theoretical argument for pattern separation in dHPC (high DG/CA1) and completion in vHPC (low DG/CA1) in humans (Poppenk et al., 2013). Together, these gradients and delineations hint how the HPC can subserve both accurate navigation but also the broader emotional and motivational context of episodic memories.

Within the DG specifically, the dorsal and ventral portions appear to serve complementary functions. A study by Kheirbek et al. used transgenic mice expressing inhibitory or excitatory opsins in DG GCs for optical control over the dDG or vDG (Kheirbek et al., 2013). dDG inhibition impaired both CFC and place avoidance learning, while vDG inhibition did not. dDG excitation also drove increase exploratory behaviors while vDG excitation reduced anxiety in open field and elevated plus maze assays. Another study by Chen et al. examined the relative contributions of dDG and vDG GCs involved in fearful memories (see the section An Introduction to Engrams) using an optogenetic tagging strategy (Chen et al., 2019). Surprisingly, acute activation of either dorsal or ventral DG memory-related cells drove freezing, place avoidance or place

preference, perhaps through a memory-indexing effect. Interestingly, both dDG and vDG cells recruited by negative memories promoted anxiety-like behaviors. Therefore, while macro-scale excitation or inhibition may drive general behavioral trends, microcircuit connectivity of specific cellular ensembles may be more important for flexibility of the DG memory circuit.

## A primer on pattern separation and completion

### *Pattern separation in DG and pattern completion in CA3*

Based on the anatomical organization of the HPC outlined above, functional roles were proposed for the DG and CA3 in pattern separation and completion respectively (McNaughton & Morris, 1987; Treves & Rolls, 1994). Computational pattern separation has been defined as the relative orthogonalization of two patterns when compared across brain regions (Santoro, 2013). A relatively small number of neurons composes EC layer 2 (Squire et al., 1989; Merrill et al., 2001; Rapp et al., 2002), whereas the granule cell layer of DG has approximately 4 times as many cells (Amaral et al., 1990, p. 199; West & Gundersen, 1990) suggesting that expansion coding from a small to a large region could disambiguate an overlapping pattern in EC when projected onto DG. The output of DG is then mapped back onto relatively fewer pyramidal neurons in CA3 (Boss et al., 1987; Seress, 1988; Amaral et al., 1990; Hasselmo et al., 1995; Hasselmo & Wyble, 1997; Jinno & Kosaka, 2010), necessitating a convergence of inputs alongside those of EC. The recurrent collateral fibers of CA3 sparsely projecting to other CA3 neurons could form an auto-associative network that allows completion of a full pattern by activating a small

subset of CA3 cells via a cue from EC (Marr, 1971; McNaughton & Morris, 1987; O'Reilly & McClelland, 1994; Treves & Rolls, 1994).

Physiological studies have tested the proposed functions of each region. An early study compared the spatial tuning of individual cells within DG and CA3 as rats navigated an arena whose walls morphed between circular and square across multiple sessions (J. K. Leutgeb et al., 2007). Both CA3 and DG cells were found to separate patterns albeit at different rates, with DG cells decorrelating their activity significantly after the first arena morph while CA3 cells exhibited this decorrelation only on the third or fourth transformation. Because it is likely that the recorded DG cells in this study were mossy cells, not DG GCs (Neunuebel & Knierim, 2012; GoodSmith et al., 2017), the study can be recontextualized as evidence of different functions of the hilus and CA3. More recently, the correlation of firing rate in active populations in DG and CA3 were compared during matching or conflicting distal and local cues in a familiar arena (Neunuebel & Knierim, 2014). Once again, DG populations decorrelated activity from baseline after a mere 45 degree mismatch of cues while CA3 maintained consistent ensemble correlations during any mismatch degree. Subsequent studies have confirmed the rapid decorrelation effect in specific populations of GCs, MCs, and proximal CA3 pyramidal neurons nestled within the hilus (GoodSmith et al., 2019). Neurogenesis in DG (newborn GCs in adult animals) may also contribute to pattern separation in this region (Nakashiba et al., 2012).

Additional support for the regional specialization of pattern separation and completion comes from lesion and gene knockout strategies examining behavioral

discrimination. Behavioral discrimination is a proxy of the pattern separation/completion process observable at the level of memory-guided responses in animal models (Santoro, 2013). A Cre/loxP genetic knockout (KO) of the N-methyl D-aspartate (NMDA) receptor in CA3 recurrent collaterals left mossy fiber inputs and Schaffer Collateral outputs of CA3 intact (Nakazawa et al., 2002). With this specific deletion of CA3 autorecurrency, NMDA receptor KO mice were able to perform a spatial navigation memory task (the Morris water maze) in the presence of the full training cues but spent less time in the learned quadrant during probe trials with only partial cues. This result strongly favors the idea of NMDA receptor dependent plasticity in CA3 pattern completion. Lesions of CA3 produce linear increases in error rate as a function of cue removal in a spatial match to sample task (Gold & Kesner, 2005). NMDA receptor KO in the DG on the other hand produces deficits in behavioral discrimination of CFC environments (McHugh et al., 2007) while lesions of DG impair spatial discrimination (Gilbert et al., 2001), suggesting errors in successful pattern separation.

## The role of the dorsal DG in spatial navigation

Early behavioral experiments demonstrating latent learning of maze environments in rats led to the so-called “cognitive map” of memory (Tolman, 1948). This general theory has been largely borne out by neurophysiological evidence of map-like cells in the MTL that exhibit tuning of their firing rate to spatial aspects of the environment such as place cells (O’Keefe & Dostrovsky, 1971), head direction cells (Taube et al., 1990), grid cells (Hafting et al., 2005), and border cells (Solstad et al., 2008). HPC lesions (Scoville

& Milner, 1957; O'Keefe & Nadel, 1978; Morris et al., 1982), disruptions (Girardeau et al., 2009; Ego-Stengel & Wilson, 2010; Roux et al., 2017), and even direct stimulation of place cells (Robinson et al., 2020) can impair or alter memory-guided behavior. How these spatially tuned cells are recruited and modified by individual episodic events remains an active area of research. Further, their relationship to non-spatial aspects of episodic memory such as emotional valence, non-visuospatial sensations (olfaction, gustation, etc.), and the ever-illusive memory 'context', remains ill-defined.

### *Spatial Tuning in DG*

Historically, place cells have been recorded in CA1 and CA3 (O'Keefe & Dostrovsky, 1971; Olton et al., 1978; Muller et al., 1987) due to easy accessibility in the rodent and comparatively sparser firing probability in DG. Typical recording paradigms involve exploration of a large open field arena with the animal making multiple passes over every part of the arena while overhead video tracking marks the spatial location at which individual neurons fire action potentials. Early recordings of sparse DG cells indicated spatial tuning and place fields similar to those of the CA region, albeit with higher multi-field probability (M. W. Jung & McNaughton, 1993; J. K. Leutgeb et al., 2007). However, electrode position alone is insufficient to classify single units as GCs or MCs and updated recording and source identification suggest GCs to have single fields while MCs are more likely to have multiple fields (Neunuebel & Knierim, 2012, 2014; GoodSmith et al., 2017; Senzai & Buzsáki, 2017). Single photon calcium imaging has confirmed not only the spatial specificity of DG GCs but also their stability across multiple recording days in linear track tasks (Hainmueller & Bartos, 2018; Cholvin et al.,

2021). The DG therefore contributes to the cognitive map not only through its role in pattern separation distinguishing contexts but also by providing stable spatial input to the CA3 network and the MCs of the hilus.

### *Hippocampal indexing theory*

The cognitive map theory and spatially tuned cells across HPC predict that new memories are organized and anchored within HPC by invariant relationships between events and objects. Another theory proposes the role of HPC as an index that links disparate brain regions and cell ensembles involved in the rich computation of experiences (Teyler & DiScenna, 1986; Teyler & Rudy, 2007). Ongoing episodic experience is broadly encoded by many circuits across the brain which ultimately send efferents to the EC and HPC as described in the anatomy section. The HPC returns these connections via the EC, thus linking diverse neocortical and subcortical processing modules. The particular role of the HPC lies in its relative flexibility and rapid plasticity as compared to neocortex, allowing reversible strengthening of connections between modules via a single hub region (Teyler & DiScenna, 1986; Teyler & Rudy, 2007). Long term potentiation (LTP), or synaptic strengthening, may be mediated by many factors including NMDA-Rs, protein synthesis, and gene activation which lead to increasing levels of modification persistence (Frey et al., 1988; Malenka & Bear, 2004; Moosmang et al., 2005; Raymond, 2007). NMDA receptors on DG GCs activated by modest cortical input can induce LTP via Calcium-dependent signaling cascades (Bliss & Lømo, 1973). Neocortex may require more significant neuronal depolarization to induce more enduring LTP, with the benefit of supporting more stable cellular assemblies (Bear & Kirkwood,

1993; Werk & Chapman, 2003). In this view, memories are not so much data files stored in the hard drive of the HPC but are instead executables coordinated by HPC and played out across many modules. Hippocampal indexing theory remains agnostic to the intrinsic processes of HPC and is not mutually exclusive to the cognitive map hypothesis.

### *Sharp wave ripples and memory replay*

How then does episodic memory information functionally exit the HPC to rekindle the embers of neocortical representation? One signal, the sharp-wave ripple (SPW-R), is a strong candidate for relating HPC memory ensembles to the neocortex. SPW-Rs are HPC-originating irregular events in the local field potential (LFP) characterized by large amplitude deflections with coupled fast oscillatory activity (Buzsáki et al., 1983; Buzsáki, 2015). These events largely occur during quiet, consummatory behavior such as feeding and during slow-wave-sleep (SWS) and have been repeatedly implicated in memory consolidation. Ensembles of serially active place cells during experience reactivate in similar order during SPW-Rs of sleeping (M. Wilson & McNaughton, 1994; Skaggs & McNaughton, 1996; Louie & Wilson, 2001; A. K. Lee & Wilson, 2002) and awake animals (Foster & Wilson, 2006; Diba & Buzsáki, 2007; Karlsson & Frank, 2009; Jadhav et al., 2012; Pfeiffer & Foster, 2013; Gillespie et al., 2021) although the functional role of SPW-Rs may be different depending on brain state (Buzsáki, 2015). These reactivations, often termed replays, occur at a compressed temporal scale relative to actual experience and appear to act as a teaching signal that consolidates memory from HPC to cortex. Disruption of SPW-Rs during post-task sleep disrupts learning rate, especially for novel tasks (Girardeau et al., 2009; Ego-Stengel &

Wilson, 2010; van de Ven et al., 2016). During online memory-guided task performance, SPW-R disruption impairs spatial memory (Roux et al., 2017) while SPW-R enhancement improves it (Fernández-Ruiz et al., 2019). Computational models suggest that gently ramping stimulation of the CA3 and CA1 may optimally prolong ripples to enhance memory (Wilmerding et al., 2022). Although SPW-Rs appear to be generated in distal CA3/CA2 (Buzsáki et al., 1983; Buzsáki, 2015; Oliva et al., 2016), their power and frequency may be modulated by inputs from DG and the rest of cortex (Sullivan et al., 2011; Sasaki et al., 2018). SPW-Rs and ordered sequences of cellular activity are also found in humans (Bragin et al., 1999; Quyen et al., 2010; Vaz et al., 2020, 2023). These factors strongly suggest that the SPW-R acts as a biomarker for episodic memory consolidation from HPC to other regions.

## An Introduction to Engrams

The assemblies of neurons in models of cognitive maps and episodic memory are often vaguely defined. Here, an operational definition of those memory-related cellular ensembles will be codified and related to the central questions of how the DG participates in memory storage and recall. Zoologist Richard Semon coined the term “engram” in 1904 referring to the enduring physical changes of the brain associated with memory experience (Semon, 1921). Donald Hebb’s theory of strengthening connection between co-active cells (“neurons that fire together wire together”) lent further theoretical and eventually experimental credence to the formation of engram assemblies (Hebb, 1949; Bliss & Lømo, 1973). However, early cortical lesion studies of the rat brain during task

learning exhibited only correlation between lesion scale and error rate with no obvious localization of the engram (Lashley, 1931). Fortunately, the advance of techniques including fluorescent labeling (Shimomura, 1979; Chalfie et al., 1994) and the identification of immediate-early-genes (IEGs) regulated by neuronal activity (Sagar et al., 1988; Labiner et al., 1993; Radulovic et al., 1998; Guzowski et al., 1999) opened the door for more nuanced characterization of memory-related cellular ensembles. Transgenic and viral construct paradigms for temporally regulating IEG-driven gene expression to particular windows at last allowed for the visualization of neuronal assemblies active during specific memory experiences, suggesting sparse ensembles function as components of the engram (Reijmers et al., 2007; Liu et al., 2012). Therefore, throughout this manuscript, the term engram will refer to the relatively enduring physical and chemical changes in and around brain cells associated with the storage of memory information (Tonegawa et al., 2015; Josselyn & Tonegawa, 2020). It is also worth mentioning the term ‘ecphory’ defined by Richard Semon roughly as the reinstatement of memory activity as a result of reactivation of the engram cells. An obvious connection can be made between the process of engram formation followed by ecphory and the cognitive map hypothesis combined with hippocampal indexing of diverse cortical modules discussed above.

In some lenses, the observation of neural activity during memory recall and memory-guided decision making is a problem of reverse inference. As we have seen, assemblies of co-active cells recapitulate their past behavior during replays (M. Wilson & McNaughton, 1994; Foster & Wilson, 2006; Diba & Buzsáki, 2007) or during “theta-

sweeps" in online navigation (Johnson & Redish, 2007). This repeatable co-activity represents an ecphory which reveals the underlying enduring physical changes in the irritable substrate proposed by Semon (Semon, 1921). Indeed, rhythmic signatures such as SPW-Rs broadcast from hippocampus to the rest of the cortex (Peyrache et al., 2009; Jadhav et al., 2016; Alexander et al., 2018) and subcortically (Lansink et al., 2009; Gomperts et al., 2015) and could orchestrate more holistic recall of engram ensembles stored in disparate regions (Vetere et al., 2017; Roy et al., 2022). Of course, memory is a constructive process open to updating from new experiences which creates an ever-shifting set of goalposts. A deeper understanding of the relationship between cellular activity, IEG-expression, and engram assembly formation (Sun et al., 2020; Yap et al., 2021; Anisimova et al., 2023) in combination with functional imaging of cellular activity in engram populations *in vivo* (Pettit et al., 2022) will be a step toward untangling the self-updating nature of the engram-ecphory loop.

### *Manipulation of memory ensembles in DG and beyond*

Numerous experiments have examined the formation and activation of DG-mediated engram ensembles in particular, perhaps because of its seat at the head of the tri-synaptic loop and its putative role in pattern separation. Studies involving gain or loss of memory function have been critical in assessing the role of engram ensembles in behavior. Such studies employ IEG-mediated expression of light sensitive optogenetic (Boyden et al., 2005; Fenno et al., 2011) or drug sensitive chemogenetic (Armbruster et al., 2007; Conklin et al., 2008) proteins to alter cellular activity *in vivo* and assess behavioral outcomes. Inhibition of sparse DG (Denny et al., 2014) or CA1 (Tanaka et al.,

2014) engram ensembles during fear learning or recall reduces the behavioral expression of the learned fear response. Moreover, inhibition of protein synthesis in DG with anisomycin blocks NDMA/AMPA mediated LTP, strongly suggesting a Hebbian learning framework of forming engram cell assemblies (Ryan et al., 2015). Complimenting these findings, artificial reactivation of DG ensembles recruited by IEG c-Fos leads to conditioned fear memory expression such as freezing and place avoidance (Ramirez et al., 2013; Redondo et al., 2014; Ryan et al., 2015; Chen et al., 2019). Reactivation of DG engram ensembles can rescue memory recall in models of early stage Alzheimer's Disease in mice (Roy et al., 2016). Curiously, engram ensembles in DG and elsewhere may be heterogeneous depending on their patterns of IEG expression (Heroux et al., 2018; Jaeger et al., 2018; Jiang & VanDongen, 2021). Sun et al. reported distinct DG engram ensembles of GCs defined by IEG Fos (enhanced excitatory input) or by IEG Npas4 (enhanced inhibitory input) which mediated aspects of CFC memory generalization or discrimination respectively across similar contexts (Sun et al., 2020). Taken together, DG-mediated engram ensembles clearly have a strong impact on memory-guided behavior, likely by influencing downstream circuits within and beyond HPC.

Zooming out beyond the DG, engram networks have been examined and manipulated across the brain. A transgenic mouse line expressing GFP in c-Fos expressing neurons across the brain found distributed engram ensembles in HPC, amygdala, cortical regions including EC, RSC, and parietal cortex (Tayler et al., 2013). In an elegant series of experiments, Kitamura et al. demonstrated that cortical regions

such as PFC form engram ensembles during initial CFC learning but require contributions of HPC and amygdala engram ensembles to mature and form functional circuits for stable memory recall long after the initial experience (Kitamura et al., 2017). Chemogenetic inhibition of CFC memory hub regions identified using graph theory (albeit not in an IEG-defined engram tagging manner) found that CA1, nucleus reuniens and lateral dorsal nucleus of thalamus, and the lateral septum were integral to fear memory expression (Vetere et al., 2017). Chemogenetic activation of putative 'high engram index' regions including HPC, nucleus reuniens of thalamus, and amygdala drove freezing while co-activation of multiple such regions produced additively stronger memory recall (Roy et al., 2022). In sum, the activation of distributed engram circuits favors stronger memory recall and supports the HPC indexing theory of memory.

### *Gaps in the engram literature*

One caveat to interpretation of engram studies is their extensive reliance on aversive conditioning and behavioral expression of fear (Liu et al., 2012; Denny et al., 2014; Roy et al., 2016; Kitamura et al., 2017; Sun et al., 2020). While some papers have examined appetitive memories such as female exposure for male mice (Redondo et al., 2014; Ramirez et al., 2015; Chen et al., 2019; Shpokayte et al., 2022), behavioral readout generally defaults to freezing, place preference or avoidance and fails to capture other cardinal features of HPC function such as spatial memory. One could hardly expect to develop a full account of memory function in humans by selectively studying memories of traumatic accidents and romantic dinners. A recent study employed optogenetic silencing of DG engrams tagged during spatial navigation in a water maze and found a

modest disruption of memory in extensively trained mice (Lamothe-Molina et al., 2022). Holographic stimulation of CA1 place cell ensembles coding for specific maze positions drove mice to change their navigation patterns by over- or undershooting goal locations (Robinson et al., 2020). This study is remarkable for demonstrating a causal role of CA1 place fields in navigation as well as a stimulation-dependent remapping of spatial coding by the CA1 network including un-stimulated cells. Still, the paucity of experiments investigating low- or non-valenced memory behavior supported by specific co-active ensembles leaves many open questions about the relationship between engrams and everyday episodic memories.

Few studies have attempted to link the activity of IEG-expressing engram ensembles to circuit physiology *in vivo*. Tanaka et al. used optogenetic identification of engram cells recorded with electrophysiology in CA1 by delivering brief pulses of stimulation and sorting single unit responses based on peri-stimulus spiking (Tanaka et al., 2018). Both engram tagged and non-tagged cells had place fields, but the engram positive cells generally had poorer spatial information, larger field size, and less spatial stability of fields within the same context. However, these engram cells were able to distinguish between different contexts more readily than standard place cells. Another study found conflicting results, albeit in a different behavioral paradigm, such that high Fos neurons in CA1 (the most engram-like cells) exhibited more stable and spatially informative place cells than low Fos neurons (Pettit et al., 2022). High Fos neurons formed functional assemblies whose place fields spanned the linear track on which the mice were running, harkening to the literature surrounding SPW-R and replay in spatial

navigation. These contradictory findings may be partly reconciled by the level of experience of the animals in novel versus familiar locations. How engram cells contribute to spatial representations and how stable these representations remain during memory updating are highly topical questions for the field.

## Function of the DG in health and disease

### *Alzheimer's Disease and dementias*

Alzheimer's Disease (AD) is a progressive neurodegenerative disease that affects cognitive function, particularly memory, in over 6 million Americans (alz.org; Alzheimer, 1911). Formations of two aberrant proteins, hyperphosphorylated tau in axons and dendrites, and extracellular amyloid beta plaques are hallmarks of the disease (Fuller, 1907, 1911). Progression of cognitive impairment is strongly associated with the accumulation of neurofibrillary tangles first in EC and subsequently HPC and neocortex, casting doubt on the classic amyloid cascade hypothesis (Braak & Braak, 1991; Schönheit et al., 2004; Korczyn, 2008). Formation of layer 2 EC tangles, but not presence of amyloid plaques, is associated with extensive loss of synapses in neocortex and HPC, especially in the molecular zone of DG (Davies et al., 1987; Einstein et al., 1994; Bertoni-Freddari et al., 1996; Ohm, 2007). As perforant path EC inputs to DG degenerate, GC and PVB interneuron populations themselves remain largely spared until the most severe stages of the disease (Braak & Braak, 1991; Bobinski et al., 1997; Ohm, 2007). Neurogenesis of new granule cells appears to transiently increase, although these newborn cells may not mature properly in AD (B. Li et al., 2008). It is likely that

dendritic changes occur in GCs as a result of de-afferentation and isolation from the EC, leading to failure of memory retrieval (Ohm, 2007). Despite over a century of clinical and benchtop research, the FDA has only approved one drug which modestly reduces amyloid beta plaque levels and slows cognitive decline (Park, 2023; van Dyck et al., 2023). Another model focuses on impairment of Ach function in AD patients (Bartus et al., 1982) which led to the development of acetylcholinesterase-inhibitor drugs (Lane et al., 2005) although these show only mild slowing of symptom onset (Marucci et al., 2021).

Given the lack of panacea, other disease models and treatment options are worth exploring. Mouse models expressing mutant variations of the amyloid precursor protein (APP) and presiniln1 genes have been developed to mimic the amyloid plaques of AD pathology (Jankowsky et al., 2004; Jacobsen et al., 2006). In addition to plaque formation in EC and DG, these mice exhibit diminished LTP and spine density in DG as well as cognitive impairment in memory tasks such as CFC (Jacobsen et al., 2006; Roy et al., 2016). Optogenetic stimulation of DG-mediated engram ensembles rescues memory behavior in AD mice, suggesting that early stage memory impairment is a failure of retrieval, rather than encoding (Roy et al., 2016; Perusini et al., 2017). Despite doubt in the validity of the amyloid cascade hypothesis, these findings broadly corroborate the evidence in humans that DG GCs become synaptically disconnected from EC to leave this memory-bearing population unreachable yet spared until terminal stages of AD. While artificial stimulation of DG engram populations represents one means of recalling latent memories in AD patients, other avenues are needed to arrest or even reverse the

effects of aging. Injection of factors in the blood and blood plasma of young mice into aged, wildtype mice recovered CFC and spatial memories while increasing spine density and synaptic plasticity (Villeda et al., 2014). Other interventions, such as diet and exercise, that increase adult neurogenesis and brain-derived neurotrophic factor (BDNF) for synaptic plasticity (Choi et al., 2018) are likely the most accessible and effective means of curbing dementia especially when practiced earlier in life.

### *Epilepsy*

The hippocampus has long been associated with temporal lobe epilepsy (TLE) as a common seizure focus (Margerison & Corsellis, 1966; Lowenstein et al., 1992; Sloviter, 1994) and the role of the DG has been recently reviewed (Scharfman, 2019). While granule cells and PVB interneurons may remain largely spared, the hilar mossy cells and somatostatin interneurons appear particularly vulnerable to traumatic injury, excitotoxicity, and apoptosis leading to disruption of excitatory:inhibitory balance (Ribak et al., 1979; Sloviter, 1987). Following injury and loss of MC inputs, DG granule cells undergo numerous changes altering their excitability (Lowenstein et al., 1992; Sloviter, 1994; Santhakumar et al., 2000; Ratzliff et al., 2002). Together, these impairments as well as neuroinflammation and alterations in glial functioning have a combined effect in creating a locus for seizure in many patients (Scharfman, 2019). While an extensive discussion of epilepsy is beyond the scope of the present work which focuses largely on the mnemonic functions of the DG, this brief overview is useful to bear in mind when considering the outcomes of the tagging and reactivation experiments in Chapter 3.

# CHAPTER TWO: ROUTE-SPECIFIC SPATIAL ENGRAM TAGGING IN MOUSE DENTATE GYRUS

Data and portions of the text in this chapter were originally published as: Wilmerding, L.K., Kondratyev, I., Ramirez, S. & Hasselmo, M.E (2023). Route-specific spatial engram tagging in mouse dentate gyrus. *Neurobiology of Learning & Memory*. *200*, 107738. https://doi.org/10.1016/j.nlm.2023.107738. I designed the experiments, performed behavioral and imaging experiments, analyzed data, and wrote the published manuscript.

## Introduction

The dentate gyrus (DG), a subregion of the hippocampal formation, is hypothesized to act as a pattern separator that distinguishes between similar input patterns during memory formation and retrieval (Marr, 1971; McNaughton & Morris, 1987; O'Reilly & McClelland, 1994; Treves & Rolls, 1994; Hasselmo & Wyble, 1997; J. K. Leutgeb et al., 2007; Neunuebel & Knierim, 2014). Sparse ensembles of DG memory-associated granule cells, or engram cells, have been optogenetically targeted to successfully influence memory-associated behavior (Liu et al., 2012; Ramirez et al., 2013; Denny et al., 2014; Redondo et al., 2014) even after consolidation (Kitamura et al., 2017) and pathogenic aging leading to natural recall failure (Roy et al., 2016). These findings support the hypothesis that the DG encodes the contextual dimension of memories. Another body of literature emphasizes the spatial representations of DG granule cells, which exhibit place fields similar to those in CA1 (O'Keefe & Dostrovsky,

1971; Neunuebel & Knierim, 2012, 2014; GoodSmith et al., 2017; Hainmueller & Bartos, 2018; Cholvin et al., 2021). Lesions of the DG granule cell population impair spatial memory (McLamb et al., 1988; McNaughton et al., 1989; Nanry et al., 1989; Xavier et al., 1999; for a review, see Xavier & Costa, 2009) and reduce both spatial specificity of CA3 place cells and reward-associated sharp-wave-ripple rate (Sasaki et al., 2018). Reconciling how the DG contributes to both novel contextual learning and spatial representations would offer important insight into the contribution of this region for learning and memory.

To that end, our study investigated the role of the DG in distinguishing between multiple routes within a single T-maze context during a spatial navigation task. Male and female mice were trained on a delayed-non-match-to-position (DNMP) task with two routes. A population of active DG granule cells was visualized using an immediate-early-gene strategy of labeling cFos positive cells active during exposure on Day 1 to a novel 2-route T-maze (Guzowski et al., 1999; Reijmers et al., 2007; Liu et al., 2012; Ramirez et al., 2013). Another population of cFos positive cells activated on Day 2 by a second behavioral context was visualized with immunohistochemical staining for comparison. We hypothesized that the DG of mice exposed to a 1-route maze on Day 2 would show more overlap between the two cell populations than chance, but less overlap than mice re-exposed to the full 2-route maze from Day 1. Our findings support this hypothesis and additionally reveal the size and degree of ensemble reactivation are largely independent of behavioral performance in the arenas. Our results indicate that the DG plays a role in encoding particular sub-routes of a 2D environment during ongoing spatial navigation.

## Materials and Methods

### *Subjects*

25 wildtype (WT) C57B6J male and female mice (Jax) were segregated by sex and group-housed prior to surgery. They received food and water ad libitum and were placed on a diet containing 40 mg/kg doxycycline (dox; Bio-Serv) at least 1 week prior to surgery at the age of 17-36 weeks. Post-surgically, the mice were housed in pairs (by sex) on a reverse 12 hour light-dark cycle. Mice were split equally into groups using random assignment, counterbalancing for sex. All procedures related to mouse care and treatment were in accordance with Boston University and National Institutes of Health guidelines for the Care and Use of Laboratory animals.

### *Viral constructs and packaging*

The AAV-cFos-tTA and AAV-cFos-tTa-TRE-eYFP were constructed as described previously (Ramirez et al., 2013) and sourced from Gene Therapy Center and Vector Core at the University of Massachusetts Medical School. The viral titrations were $1.5*10^{13}$ genome copy per mL for AAV-cFos-tTA-TRE-eYFP and $1.5*10^{13}$ genome copy per mL for AAV-cFos-tTA.

### *Stereotactic injections*

All surgeries were performed under stereotactic guidance and all coordinates are reported relative to bregma. Anesthesia was induced with 5.0% isoflurane and maintained thereafter at a concentration of 1.5-2.0%. Bilateral burr holes were made at -2.2 mm (AP)

and +/-1.3 (ML) using a 0.5mm drill to allow a 10uL nanofil syringe (World Precision Instruments) to be lowered to 2.0 mm (DV). 300nL of AAV virus cocktail was injected bilaterally at a rate of 100nL/min controlled by a MicroSyringe Pump Controller (World Precision Instruments). Following injection, the needle was kept at the injection site for 5 minutes and slowly withdrawn afterwards. Bone wax was gently inserted into the burr holes to seal the skull, and two to three sterile sutures were used to close the wound. Post-operative subcutaneous injections of Buprenorphine (0.1 mg/kg) and Ketoprofen (5 mg/kg) were administered for three days following surgery and Enrofloxacin (10 mg/kg) for five days post-surgically.

*Behavioral assays and engram tagging*

All behavioral assays were performed during the light cycle of the day (7:00 - 18:00). Mice were handled 2-5 min per day for two days before behavioral training. To increase training motivation, mice were water restricted during the training period, tagging and re-exposure period to 20 minutes of ad libitum water access daily, in addition to sucrose consumed in the maze.

Behavior was run in a two-arm T-maze, as previously described (Fig. 2.1; Levy et al., 2021). The paradigm consisted of a sampling phase and a testing phase, separated by a 15-second delay period in a closed-off start box. During the sampling phase, mice were forced to run a particular arm of the maze by the application of a barrier closing off the other reward arm. In the following test phase, mice were allowed to choose either arm and reward was only delivered for choosing the opposing arm to the preceding sample phase. Each mouse received five, 15-minute sessions of pre-training on the DNMP

paradigm with gradually increasing delay in the week prior to surgery. Five additional training sessions of the same length, with full 15-second delay, were delivered after surgical recovery. All of these initial training sessions were carried out in the training maze, Context T: a grey, wooden, rectangular T-maze (66 cm long x 31 cm wide x 19 cm high), with opaque walls forming the central stem and different wall cues on each reward arm.

During the tagging window, mice were taken off dox for 48 hours and subsequently performed the DNMP paradigm in a novel T-maze, referred to as Context A: a beige, triangular, linoleum-lined T-maze (78 cm long x 78 cm wide x 18 cm high) with novel cue cards on the walls of the reward arms. The maze location, odor and floor texture were also changed relative to Context T. Context A had no walls on the stem, allowing mice to see the entire arena even when reward arm barriers were present. All mice were exposed to Context A for 20 minutes, with a minimum of ten DNMP trials performed. Food consumption was not explicitly recorded, but all animals maintained healthy body condition on both regular and dox chow. Visual observation of each subject's feces confirmed presence or absence of dox during suppression or opening of the tagging window respectively. Gene induction in hippocampus further confirmed the success of the tagging manipulation. Immediately after tagging, the mice were placed back on dox for the remainder of the study.

The following day, mice were pseudo-randomly split into three groups, counterbalancing for sex. The first group ran the full T-maze in Context A under the DNMP paradigm discussed above, for 20 minutes. The second group ran for 20 minutes

on a one-sided route inside the same physical maze and at the same room position as Context A, but with the other arm blocked by opaque barriers (Fig. 2.2C, Context B). The mice in this group were evenly split between the left and right Half-T routes via pseudorandom assignment and were counterbalanced by sex. The third group was placed in a novel arena (Context C) at the same room position as Contexts A and B and explored for 20 minutes without reward. This Open Field Context C was an empty, opaque gray box (41.5 cm long x 39.5 cm wide x 28.5 cm high) with no top.

Deeplabcut (Mathis et al., 2018) was used to extract mouse position during behavioral trials from 50fps video recorded on an overhead Mako G-131c GigE camera (Allied Vision). Video timestamps, spatially scaled position, distance, and velocity information were calculated using the CMBHome framework (https://github.com/hasselmonians/CMBHOME/wiki).

### *Immunohistochemistry*

Mice were euthanized 90 minutes after final behavior on Day 2 by administration of Euthasol (390 mg/kg) and anesthetized with Isoflurane prior to transcardial perfusion with saline and 10% formalin. Extracted brains were kept in formalin for 48 to 72 hours at 4 ℃ and transferred to 30% sucrose solution for approximately 72 hours at 4 ℃ to undergo cryoprotection. Cohorts included tissue from animals in all three groups, such that fixation and cryoprotection times were matched across groups. Brains were sliced using a cryostat into 50μm slices, and blocked for 2 hours at 4 ℃ in 1x phosphate-buffered-saline + 2% Triton (PBS-T) and 5% normal goat serum (NGS). Consistent with prior studies (Chen et al., 2019) slices were incubated for 48 hours at 4 ℃ with primary

antibodies diluted in 5% NGS in PBS-T as follows: rabbit anti-cFos (1:1000, Abcam, #190289) and chicken anti-GFP (1:1000, ThermoFisher, #A10262). Subsequently, the slices were washed three times for 10 minutes in PBS-T, followed by a 2 hour incubation in the secondary antibodies diluted in 5% NGS in PBS-T as follows: Alexa 555 goat anti-rabbit (1:200; ThermoFihser, #A21429) and Alexa 488 goat anti-chicken (1:200, ThermoFisher, #A11039). Finally, the slices were mounted on slides using VECTASHIELD® Hardset™ Antifade Mounting Medium with DAPI (Vector Labs, #H-1500) and sealed with nail polish.

*Image acquisition*

Images were acquired with an FV10i confocal laser-scanning microscope, using 60x magnification / 1.4 NA oil-immersion objective. For each image, three z-slices, separated by approximately 19.5µm, were acquired. The first z-slice was positioned at the lowest in-focus portion of the sample, the second was positioned at the center of the sample and the first was positioned at the highest in-focus portion of the imaged sample. The depth between the slices has been adjusted accordingly to ensure this composition, but was never set below 17 µm to minimize the potential of imaging the same cell in different z-planes. DAPI was acquired at 405nm with average laser power of 17.4% (SEM 1.43%), eYFP at 473nm with average laser power of 2.38% (SEM 0.17%) and cFos at 559nm with average laser power of 12.21% (SEM 0.40%). Before acquiring each image, the laser power of each channel (R, G, B) was configured to yield approximately equivalent intensity between all slices. To ensure images were collected with similar parameters across groups, we tested the laser power of each image on each channel

across groups and found no significant differences in laser power between groups (Fig. 2.1A). To rule out differences in overlap count across groups arising from the ratio of cFos and eYFP channel laser power, the ratio between the deviation of each mouse's average power away from the mean channel power was calculated as (Mouse cFos- Mean cFos Power)/(Mouse eYFP-Mean eYFP Power). No differences in R/G channel ratio was found across groups (Fig. 2.1A).

Each image was acquired as a series of 1024x1024 pixel tiles which were subsequently stitched end-to-end to produce the final image (https://imagej.net/plugins/image-stitching). Only one set of stitching parameters was used, ensuring any stitching artefacts were consistent across groups. The images used 16 bit-depth encoding and all image processing was handled in ImageJ / FIJI (https://imagej.nih.gov/ij/) with the Bioformats toolbox (https://imagej.net/formats/bio-formats).

*Cell counting*

Image acquisition was performed only on slices with successful targeting to the dorsal DG. cFos+ and eYFP+ cells in the upper and lower DG blades were counted using five 50um coronal slices of dorsal DG in each animal. Cell counts from each of the three z-planes were summed for that slice and averaged across slices for each mouse. DAPI was counted using a StarDist neural network trained and validated on a subset of the data (Fig 2.1B, Schmidt et al., 2018; Weigert et al., 2020). Segmentation metrics (precision, recall, and matching to ground truth labels) confirmed model performance over a range of label matching thresholds. An intersection-over-union threshold of 0.5% was used as a

tradeoff between match score and other metrics. The number of cFos+ and eYFP+ cells in the DG region was quantified using an automated ImageJ pipeline that carried out iterative thresholding followed by exclusion of non-circular objects (https://mcib3d.frama.io/3d-suite-imagej/plugins/Segmentation/3D-Iterative-Segmentation/). Parameters were calibrated to include cells even where stitched images showed intensity variability. In order to quantify the number of overlapping cFos+ and eYFP+ cells, an automated algorithm was used to carry out pairwise comparisons between the pixels of each eYFP and cFos cell and the results were filtered to only include overlapping cells of a comparable size (within at least 50% of each-other's size) that were mostly overlapping (85% of smaller object). The accuracy of the automatic counter was verified against a manually scored dataset created by two experimenters blind to the experimental conditions (Fig. 2.1C-E). Automated counts were used for increased reproducibility. Statistical chance for overlap was calculated as (eYFP+)/DAPI*(cFos+)/DAPI and compared against the counted overlaps normalized to the whole dentate population as (cFos+ & eYFP+)/DAPI.

*Statistical analysis*

Bar graphs are reported as means +/- SEM. One way and mixed effects ANOVA tests were used to assess group differences for both cell counts and behavior, and follow-up comparisons made where appropriate using independent T-tests (Tukey's HSD). Repeated measures comparisons including overlap against statistical chance were performed using paired t-tests while all other comparisons were made with independent t-tests. Bonferroni-Holm corrected p-values are reported where multiple t-test and

correlation tests are made. Correlations were run using Pearson's R. Percentile tests were performed against a chance distribution of P bootstrap means created by averaging n samples drawn with replacement from the statistical chance values of all mice, where n was the number of mice in the original group, and P was the number of bootstrap means. Two mice were excluded (1 Full-T, 1 Half-T) from velocity and distance comparisons (Fig. 2.4C,D) on the basis of corrupted video files but were otherwise included for all other tests. Test statistics, groups sizes, number of bootstrap samples, and p-values are reported in figure legends. All tests were performed in Matlab using publicly available functions. For all figures, * = $p < 0.05$, ** = $p < 0.01$, *** = $p < 0.001$.

### *Data availability*

All relevant data supporting the findings of this study are available from the corresponding author upon reasonable request.

## Results

### *Behavioral and viral tagging paradigm used to visualize the spatial engram*

To investigate cells in dentate gyrus (DG) associated with spatial navigation memories, we trained mice on a delayed-non-match-to-position (DNMP) task (Fig. 2.2A). A dox-inducible viral labeling strategy was used to selectively label cFos+ DG cells associated with learning (Fig. 2.2B). After pre-training and surgical recovery, dox diet was removed from the cage and mice were exposed to a novel T-maze (Context A) in which they performed the DNMP task for 20 minutes (Fig. 2.2C). The mice were

returned to dox to prevent off-target labeling and exposed on the following day to another environment in the same position with respect to room cues as Context A. The first group (Full-T) repeated the DNMP behavior in Context A as before. The second group was returned to the same physical arena as Context A, but with one arm permanently blocked (Context B). This arena was otherwise similar with respect to timing delays and sucrose rewards and allowed mice visual access to the other side of the maze. The final group was exposed to a novel open field arena without reward contingency (Context C).

### *Histological staining reveals distinct, partially overlapping spatial engram populations in DG*

We first examined the size and degree of overlap between DG cell ensembles to determine the level of representational similarity across days in each group. Immunohistochemical staining revealed two populations, the first from the Day 1 experience (eYFP) and the second from the Day 2 experience (cFos) with partial reactivation (overlap; Fig. 2.3A-F). Performance of the DNMP T-maze task on Day 1 yielded similar ensemble size across groups as expected (Fig. 2.4A). Interestingly, no difference was found in Day 2 ensemble size across groups despite the Open Field group experiencing a novel environment.

### *DG encodes different routes within a maze using partially non-overlapping populations*

Next, we normalized the number of overlapping cells to the whole dentate population and compared each group to statistical chance. This allowed testing of the primary hypothesis of the experiment as summarized in Figure 2.4B. Both the Full-T and

Half-T exposures resulted in significantly overlapping populations, while the Open Field exposure did not (Fig. 2.4B). Additionally, we found a dissociation of reactivation level across groups, with the Full-T experiencing highest overlap and Open Field experiencing the least (Fig. 2.4B). Because each group had relatively few samples, we performed an additional test of the group means and individuals against a chance distribution generated by bootstrap sampling. In agreement with the first analysis, the Full-T and Half-T group means were both above the 99th percentile of the chance distribution, while the Open Field group was not (Figure 2.4C). Taken together, these results suggest an effect of both novelty and trajectory experience on the recruitment and reactivation of the DG spatial engram ensemble.

### *DG spatial engram composition relates to experienced trajectories not distance or velocity*

To rule out the possibility of confounding effects such as task engagement, laps traversed, and behavioral activity level on engram ensemble recruitment, we analyzed behavior across groups. All groups performed the task above chance nor did we find a difference in accuracy across groups on Day 1 (Fig. 2.5A). There was no change in accuracy across days for the Full-T group. These data demonstrate that the mice grasped the task and transferred learning successfully from training Context T to the novel Context A. Next, we examined the number of laps, defined as a trajectory from the start box to the reward then back to the start box, across groups and days. The Full-T and Half-T groups performed similar numbers of laps on Day 2 despite the difference in behavioral demand between Contexts A and B, nor did either group perform differently

than its Day 1 baseline (Fig. 2.5B). For a more general comparison of behavior, we analyzed total distance traveled and average running speed in all groups across days. We found a main effect of day but no effect of group or interaction in either metric (Fig. 2.5C,D).

*Engram reactivation does not correlate to behavioral outcomes or learning across days*

To follow up this result, we tested for possible correlations between ensemble reactivation and behavior. No correlation was found between the normalized ensemble overlap and any behavioral metric (task accuracy, number of laps, distance, or average speed) on Day 2 in any group (Fig. 2.6A-D, top). Further, we correlated the overlap values against the difference in behavioral measures between Days 1 and 2 for possible effects of learning across days, but found no relationship (Fig. 2.6A-D, bottom). These analyses suggest that the degree of engram reactivation is not a result of trajectory length, self-motion cues, or differences across days, but is instead related to behavioral contingencies and experienced trajectories, as hypothesized.

*Engram composition and behavior does not appear to differ across sex or experienced trajectory in the Half-T group*

Finally, we examined our data broken down by subject sex and direction of the maze experienced in the Half-T group. While each group lacked sufficient number of subjects for rigorous comparison by sex within groups, observationally we saw little difference in average Day 1 or Day 2 ensemble size or in normalized engram reactivation (Fig. 2.7A). At the behavioral level, male and female mice exhibited little difference in

any behavioral metric on either day (Fig. 2.7B). In the Half-T group, we observed minimal difference between the Left-T and Right-T subgroups at either the ensemble level (Fig. 2.7C) or the behavioral level (Fig. 2.7D). These similarities were used as grounds to combine animals by sex and by Half-T subgroup in the previous analyses, although follow up studies with larger group sizes would be needed to confirm the lack of effect.

## Discussion

We trained mice to run a delayed-non-match-to-position (DNMP) T-maze task and used an activity-dependent viral labeling strategy to visualize cell populations from different days associated with goal-directed navigation, i.e. spatial engrams. We found that repeated experience with the same two-route spatial working memory task and physical location across days yielded the highest degree of engram similarity (Full-T; Fig. 2.4B,C). Mice performing a navigation task in the same physical arena and room position but with only one route (Half-T) showed higher reactivation of the original population than chance levels, but less than the Full-T group (Fig. 2.4B,C). The Open Field group exhibited the least overlap, no different than chance (Open Field, Fig. 2.4B,C). In addition, we observed no difference in the size of the Day 2 ensemble despite differences in memory demand and novelty based on the experienced arena (Fig. 2.4A). Together, these results are consistent with past studies implicating the DG in spatial memory processing (McNaughton et al., 1989; Emerich & Walsh, 1990; Xavier et al., 1999), including T-maze tasks with long delays (Emerich & Walsh, 1989; Costa et al.,

2005) and build on previous applications of immediate early genes (IEGs) to study the overlap of populations involved in hippocampal spatial and task-specific memories (Guzowski et al., 1999; Satvat et al., 2011).

### *Spatial vs fear engrams*

We set out to test whether methodologies typically used to label contextual memories in dorsal DG could be used to probe aspects of navigational memory for specific routes within a larger environment. Previous studies of memory ensemble, or engram, composition have largely focused on the formation and reactivation of contextual memories with strong emotional valence, in particular fear (Liu et al., 2012; Ramirez et al., 2013; Redondo et al., 2014; Chen et al., 2019; Sun et al., 2020). However, physiological recordings from DG during navigation have revealed spatial preferences of DG granule and mossy cells (M. W. Jung & McNaughton, 1993; J. K. Leutgeb et al., 2007; Neunuebel & Knierim, 2012, 2014; GoodSmith et al., 2017, 2022) which may be stable across days (Hainmueller & Bartos, 2018; Cholvin et al., 2021). While IEGs have been used to examine cell population reactivation across or within open field navigation contexts (Guzowski et al., 1999; VanElzakker et al., 2008), this approach could not distinguish an engram ensemble coding for contextual cues (e.g. odor, distal visual landmarks, etc.) from one encoding specific navigational trajectories (e.g. serially activated place fields). In our study, the Half-T group had lower ensemble reactivation than the Full-T group, but higher reactivation than the Open Field group and statistical chance (Fig. 2.4B,C). Some contribution of pattern separation as a result of differences in behavioral demand between a spatial reference memory task (Full-T) and a sensory-

guided navigation task with similar delays and rewards (Half-T) is possible (Satvat et al., 2011). However, we found largely no difference in behavior across groups (Fig. 2.5). We found largely no correlation between engram reactivation and behavioral measures or task learning across days (Fig. 2.6) in agreement with past work showing little relationship between freezing and fear engram ensemble activity (Zaki et al., 2022) or locomotion and Fos levels in hippocampus (VanElzakker et al., 2008). Based on these finding and previous evidence for spatial specificity in DG granule cells, we hypothesize that experiences of different routes are encoded by different spatial engram populations.

The relationship between Fos expression, memory encoding, and spatial correlates of cell activity is complex. One recent study linked the degree of Fos expression to the reliability and stability place fields in CA1 during familiar task performance (Pettit et al., 2022). Interestingly, clusters of co-active cells with strong Fos expression exhibited place fields across large sections of the environment, consistent with prior work in replay and theta sequences suggesting that correlated cells chunk spatial information (Foster & Wilson, 2006; Johnson & Redish, 2007; Gupta et al., 2012). Conversely, a previous engram study using electrophysiology found that cFos tagged CA1 cells displayed strong contextual firing but poorer spatial stability than non-tagged cells (Tanaka et al., 2018). One possible explanation for the disparity is the level of experience with the environment, because cFos is both driven by firing activity and helps maintain spatial coding accuracy in existing place cells (Pettit et al., 2022). In our study, mice were exposed to novel environments during tagging, likely driving formation of new engram ensembles similar to Tanaka et al. However, the animals had extensive pre-

training on the task itself and transferred learning across environments (Fig. 2.5A). It is therefore unsurprising that the Full-T group displayed reactivation above chance levels and above the Half-T group, indicating stability of the cFos tagged ensemble across days despite the novel environment, in line with the experienced animals and findings of Pettit et al. Follow up studies could compare ensembles tagged in the training context, or pre-trained versus naïve mice, to disambiguate the competing factors of pattern completion and pattern separation on spatial engram recruitment (Nakashiba et al., 2012; Santoro, 2013). Further, investigating the cellular dynamics in DG during task demand updating (as in the Half-T group on Day 2) would provide valuable insight into real-time feedback influencing memory and spatial-associated cell ensembles.

### *Size of the engram ensemble*

cFos IEG expression in granule cells arises from neural activity and plasticity-related changes within a cell (Labiner et al., 1993). Novelty is an important factor for inducing plasticity in the hippocampus, including DG (McNaughton & Morris, 1987; Kitchigina et al., 1997; Straube, Korz, & Frey, 2003; Straube, Korz, Balschun, et al., 2003; Davis et al., 2004). We observed a larger Day 1 ensemble relative to the Day 2 ensemble in all groups, consistent with a novelty effect in the Full-T and Half-T groups (Fig. 2.4A) and with prior work using similar techniques (Zaki et al., 2022). However, we made no formal comparison of this effect due to the difference in cFos detection between IHC and viral tagging methods and because animals ran less distance and at lower speed on the second day (Fig. 2.5C,D). Past work using alternate Fos detection methods similarly demonstrated increases in DG Fos expression after novel, but not familiar,

environmental exploration (VanElzakker et al., 2008). Interestingly, the Open Field group underwent a novel context exposure on each day and exhibited a similar Day 2 ensemble size to the other groups, which suggests an impact not only of novelty but also task in this study (Fig. 2.4A). Given similar ensemble detection methods to the other groups, we might have expected the Open Field group to have larger average Day 2 ensemble size, but this was not the case. The open field free-exploration task has no route constraints by design, and these mice were just as active as their Full-T and Half-T counterparts (Fig. 2.5C,D). Thus, both the navigational memory demand and reward contingencies likely play a role in DG ensemble recruitment in addition to novelty alone (Costa et al., 2005).

*Composition of sub-ensembles for pattern separation*

One question concerns whether the DG contains cells with task-modulated spatial tuning, i.e. splitter cells, like those observed in CA1 (Wood et al., 2000; Ferbinteanu & Shapiro, 2003; Griffin et al., 2007; Kinsky et al., 2020). Splitter cells can emerge early in learning and may be modulated by the turn direction, task phase, or both on the DNMP T-maze task (Levy et al., 2021). DG place fields remap based on task engagement, hinting at the flexibility of DG cells within the same physical location (Shen et al., 2021). Interestingly, CA1 splitter cells appear more stable than classic place fields across days, which might help to explain increased overlap observed in the Full-T group relative to the Half-T group which had no chance to demonstrate splitter behavior (Fig 2.4B; Kinsky et al., 2020). Splitter cells may indeed serve an additional pattern separation function in DG for this task by discriminating otherwise similar stem trajectories and improving pattern completion of orthogonal sub-ensembles coding for separate reward arm routes (O'Reilly

& McClelland, 1994; Wood et al., 2000; Ferbinteanu & Shapiro, 2003; Hasselmo & Eichenbaum, 2005; Nakashiba et al., 2012; Neunuebel & Knierim, 2012, 2014; GoodSmith et al., 2017, 2019; Senzai & Buzsáki, 2017; Hainmueller & Bartos, 2018).

### *Conclusions*

We tested whether experience with specific navigation routes could be dissected in the dentate gyrus using engram tagging and visualization strategies. We found that repeated experience of a two-route maze task across days recruited a more similar ensemble than exposure to a novel open field arena or exposure to a one-route task within the same T-maze arena. The experimental design offers a means to study aspects of spatial navigation using traditional engram tagging techniques. Additionally, our results suggest the dentate gyrus performs its role in pattern separation and spatial navigation by the activation of partially non-overlapping sub-ensembles for different routes in a larger context.

## Acknowledgments

We thank the Hasselmo and Ramirez labs for thoughtful feedback and commentary on the work.

This work was supported by the National Institutes of Health [grant numbers: R01 MH052090, MH060013, MH120073, HD101402-02; and DP5 OD023106-01], and the Office of Naval Research [grant numbers: MURI N00014-16-1-2832, N00014-19-1-2571; and DURIP N00014-17-1-2304].

## Author Contributions

Conceptualization, L.K.W., S.R., and M.E.H.; Methodology, L.K.W. and I.K.; Investigation, L.K.W. and I.K.; Writing – Original Draft, L.K.W., I.K.; Writing – Review & Editing, L.K.W., I.K., S.R., and M.E.H.; Funding Acquisition, M.E.H. and S.R.; Formal Analysis, L.K.W. and I.K.; Visualization, L.K.W.; Supervision, M.E.H. and S.R.

## Declaration of Competing Interests

The authors declare no competing interests

## Figures

**Figure 2.1**

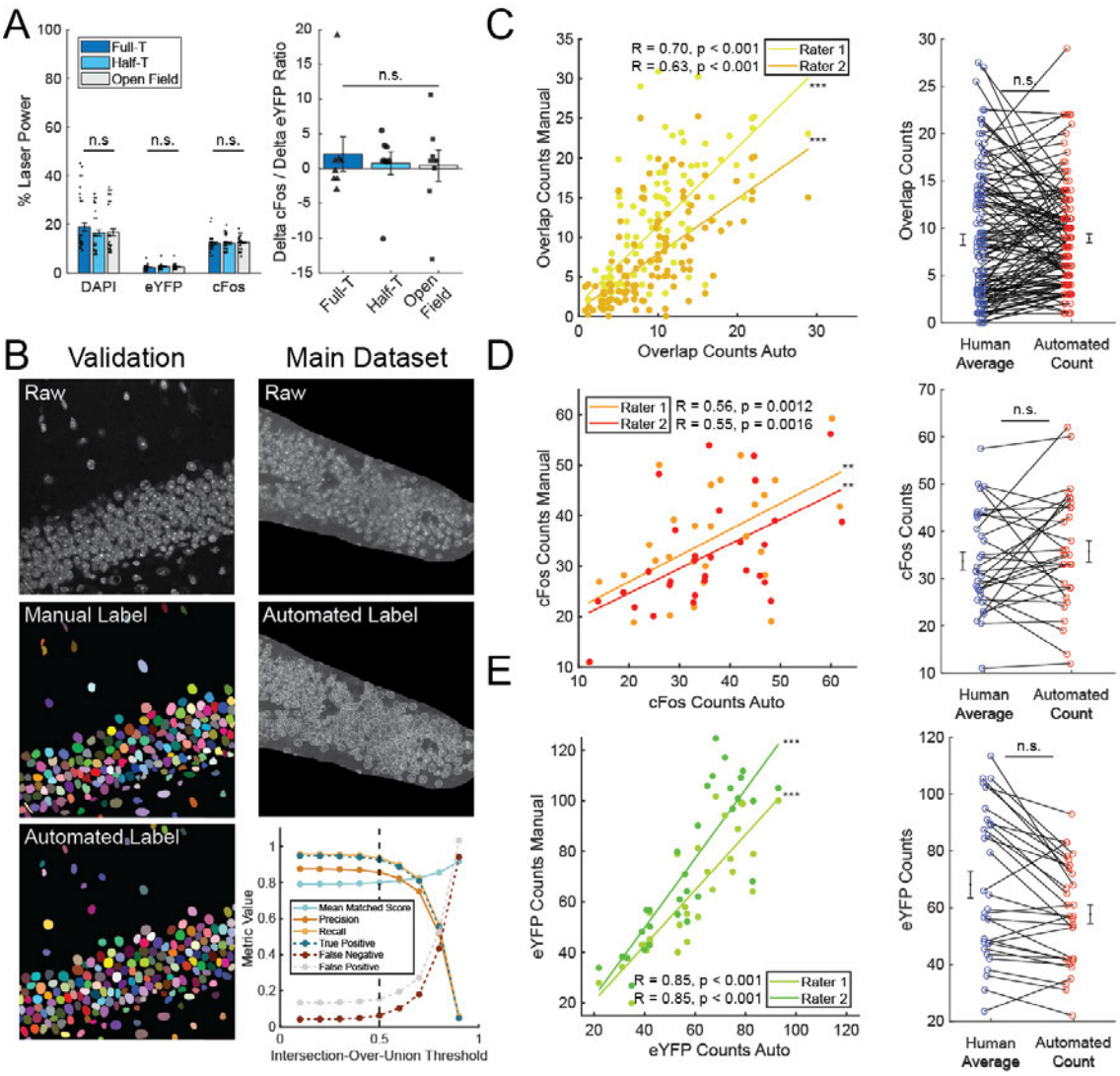


**Figure 2.1. Similarity of cell counts supports the use of automated counting methods.**

**A)** Left: Average laser power used during image acquisition across groups. No difference in power was found in the DAPI ($F_{(2,122)} = 0.83$, $p = 0.44$), eYFP ($F_{(2,122)} = 0.66$, $p = 0.52$) or cFos ($F_{(2,122)} = 0{,}21$, $p = 0.81$) channels, n = 40 images for Full-T and Half-T, 45 images for Open Field. Right: comparison of cFos to eYFP channel laser power ratio finds no difference across groups ($F_{(2,22)} = 0.17$, $p = 0.85$).

**B)** Automated DAPI cell counts. Raw, manual label and automated label example from the training validation set. Colors for visualization purpose only. Raw and automated

label example from the main data set. Bottom right: model validation metrics demonstrating high precision, accuracy, and matching to ground truth labels over a range of matching thresholds. Dashed black line indicates threshold used in dataset. True Positive, Negative, and False Negative rates shown normalized to ground truth.
**C)** Left: Automated overlap counts strongly correlate with human raters. Pearson's r and p values reported in figure. Right: no difference was found between average overlap counts of human raters and automated counting methods ($t = -0.19$, $p = 0.85$). $n = 125$ images per group.
**D)** Left: Same as C but for cFos counts. Right: No difference in human or automated counting of cFos ($t = -0.70$, $p = 0.47$). $n = 30$ images per group.
**E)** Left: Same as D but for eYFP counts. Right: No difference in human or automated counting of eYFP ($t = 1.79$, $p = 0.079$). $n = 30$ images per group.
Error bars represent +/- SEM. Scatter plots denote individual image samples jittered for clarity.

**Figure 2.2**

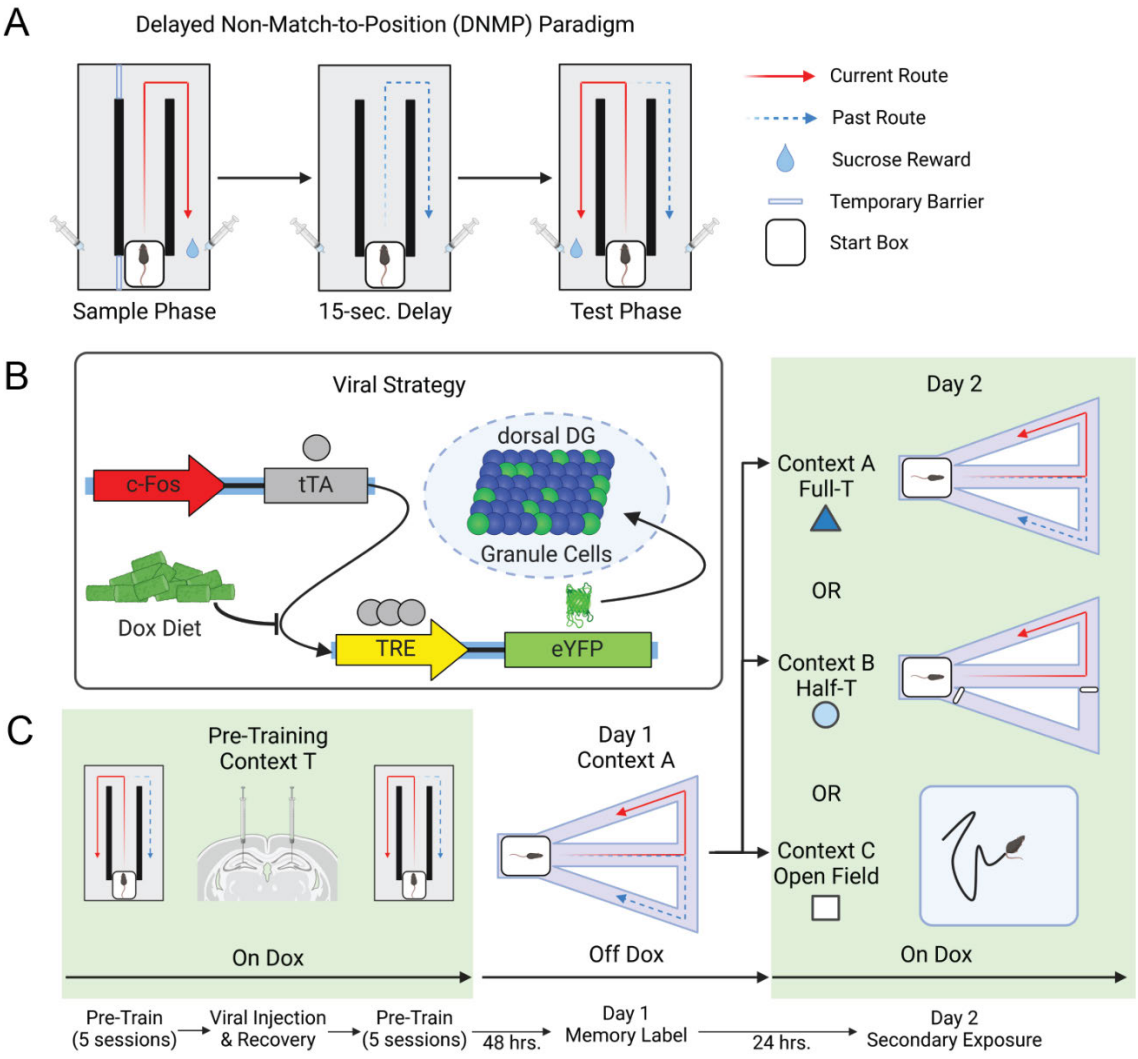


**Figure 2.2. Behavioral and viral tagging paradigm used to visualize the spatial engram.**

**A)** Schematic representation of the delayed-non-match-to-position (DNMP) T-maze task. In the sample phase, an opaque barrier is inserted to force the mouse to traverse one route and receive sucrose reward. After a 15-second start box delay, the mouse must choose to traverse the opposite route to receive a second reward in the test phase.

**B)** Viral constructs AAV9-cFos-tTA and AAV9-TRE-eYFP used in the engram labeling system. Endogenously expressed cFos in transfected Dentate Gyrus cells drives tetracycline-transactivator (tTA) which binds to the tetracycline response element (TRE) and drives expression of eYFP in the absence of doxycycline (Dox).

**C)** Behavioral timeline. Mice (n=25) were pre-trained for 10 sessions, 5 before and 5 after surgical injection of the viral constructs outlined in B. Dox diet was removed from the home cage to open a memory labeling window. Day 1 performance of the DNMP-task in a novel Context A for 20 minutes caused cFos Dentate Gyrus cells to express eYFP. On Day 2 mice were exposed for 20 minutes to the full maze task (Full-T, Context A, n=8), the same maze but with one arm blocked (Half-T, Context B, n=8), or a novel arena (Open Field, Context C, n=9). Brains were collected 90 minutes after the behavioral experience on Day 2. Created with BioRender.

**Figure 2.3**

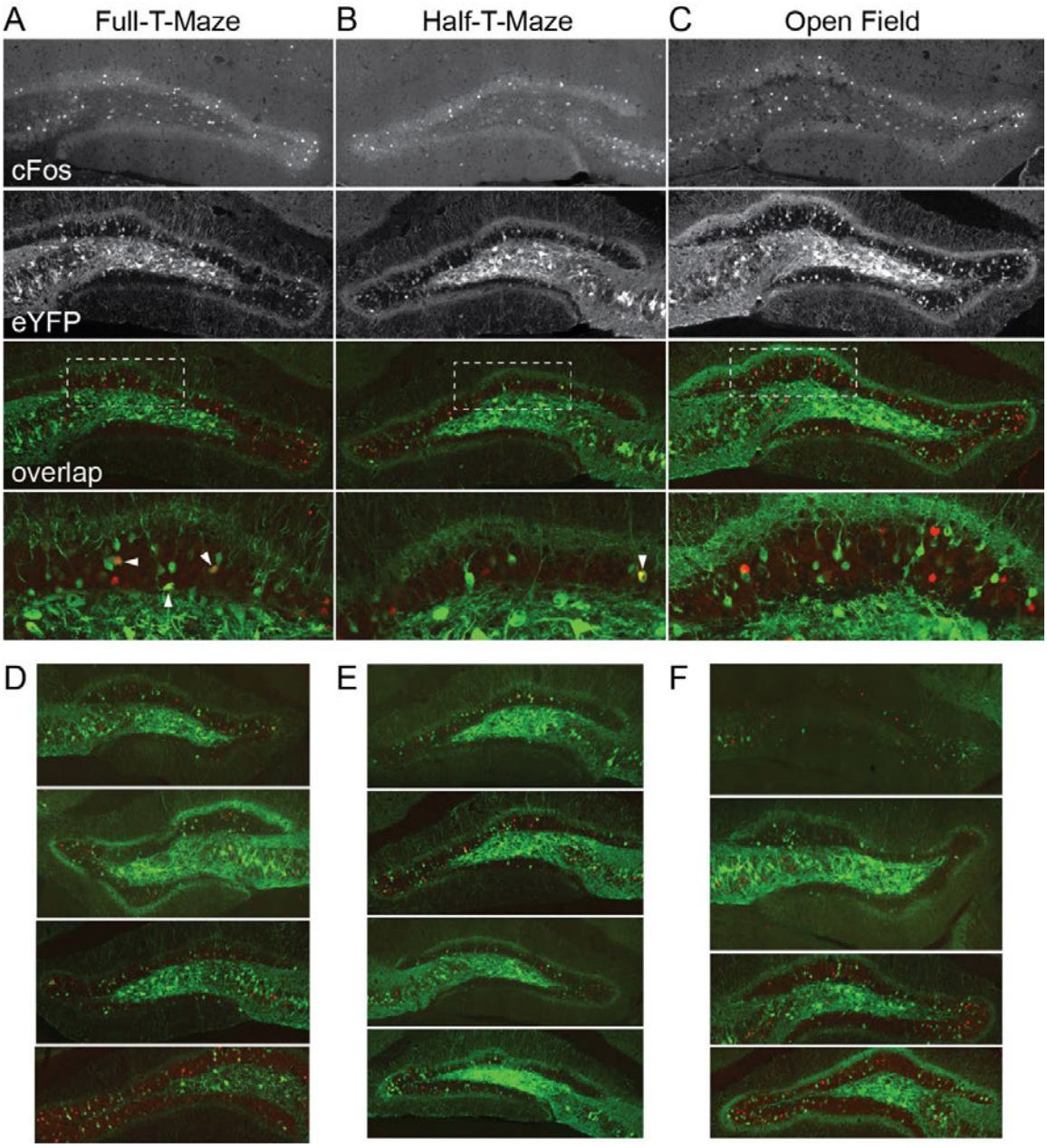


**Figure 2.3. Histological staining reveals distinct, partially overlapping spatial engram populations in DG.**

**A-C)** Representative 60x confocal images of DG from the Full-T, Half-T and Open Field groups. Top row: cFos signal. Upper middle row: eYFP signal. Lower middle row: merge of the above rows (cFos red, eYFP green). Bottom: Zoomed section from the above merge indicated by the white dashed box. White triangles indicate overlap cells active on

both days.

**D-F)** Further examples from four different animals per group outlined above in A-C.

**Figure 2.4**

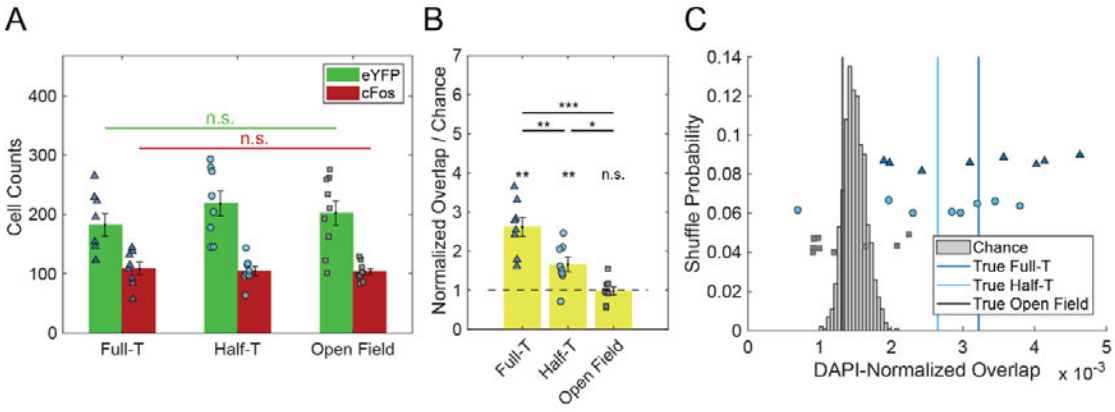


**Figure 2.4. DG encodes different routes within a maze using partially non-overlapping populations.**
**A)** There was no difference in Day 1 ensemble size (eYFP; $F_{(2,22)} = 76$, $p = 0.48$) or in Day 2 ensemble size (cFos; $F_{(2,22)} = 0.11$, $p = 0.90$) across groups.
**B)** Experience of the Day 2 environments and tasks resulted in ensemble reactivation (overlap) above statistical chance in the Full-T ($t = 6.23$, $p = 0.0012$) and Half-T ($t = 4.09$, $p = 0.0093$), but not the Open Field groups ($t = -1.04$, $p = 0.33$). Additionally, normalized reactivation in all groups differed from one another ($F_{(2,22)} = 20.44$, $p < 0.001$). Post-hoc comparisons revealed significant differences between all groups (Tukey's HSD; Full-T vs Half-T: $p = 0.0040$; Full-T vs Open Field: $p < 0.001$; Half-T vs Open Field: $p = 0.038$)
**C)** The true Full-T and Half-T DAPI-normalized ensemble overlap group means were above the 99$^{th}$ percentile of a chance distribution of shuffled overlap values (Chance; n = 1000 sample means), while the Open Field mean was not (11$^{th}$ percentile). Vertical lines indicate observed group means.
Error bars represent +/- SEM. Scatter plots denote individual subjects (triangle = Full-T, circle = Half-T, square = Open Field). N = 8 mice in Full-T and Half-T groups, 9 mice in Open Field.

**Figure 2.5**

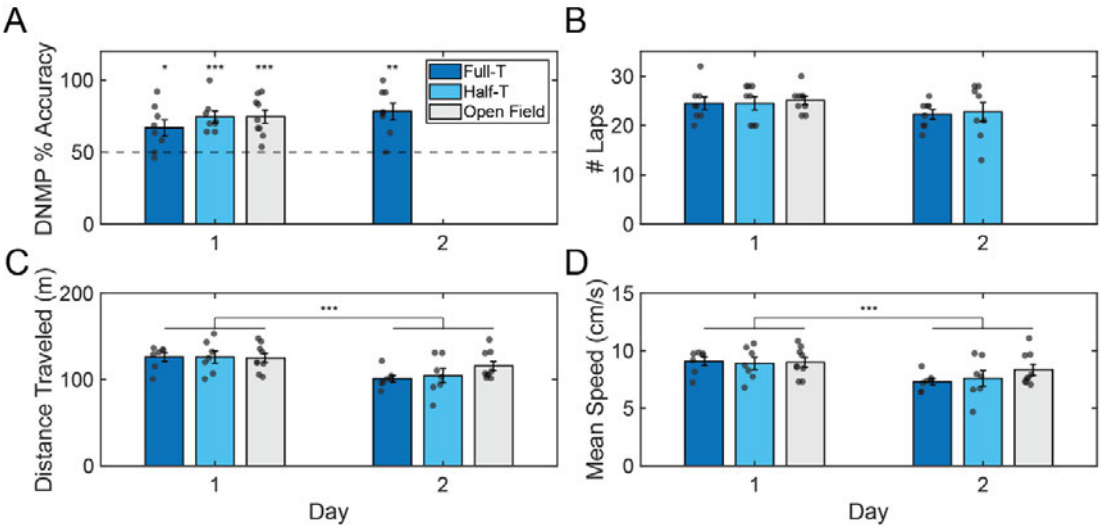


**Figure 2.5. DG spatial engram composition relates to experienced trajectories not distance or velocity.**

**A)** All groups performed above chance (One-sample t-test; Day 1: Full-T t = 3.05, p = 0.018; Half-T t = 5.99, p = 0.0022; Open Field t = 5,44, p = 0.0018; Day 2: Full-T t = 4.92, p = 0.0034). No differences in DNMP task accuracy were found across groups on Day 1 ($F_{(2,22)}$ = 0.85, p = 0.44)) nor did the Full-T group perform differently across days (t = -1.78, p = 0.12).

**B)** Groups did not run different numbers of laps on Day 1 ($F_{(2,22)}$ = 0.097, p = 0.91), nor did the Half-T group run fewer laps relative to the Full-T group on Day 2 (t = 0.217, p = 0.83). The Full-T group ran similar laps across days (t = 1.94, p = 0.28) as did the Half-T group (t = 0.90, p = 0.80).

**C)** The total distance traveled did not differ across groups ($F_{(2,20)}$ = 0.47, p = 0.63) but was lower on Day 2 ($F_{(1,20)}$ = 41.11, p < 0.001) with no interaction effect ($F_{(2,20)}$ = 2.82, p = 0.084).

**D)** The average velocity did not differ across groups on Day 1 ($F_{(2,20)}$ = 0.43, p = 0.66) but was lower on Day 2 ($F_{(1,20)}$ = 24.02, p < 0.001) with no interaction effect ($F_{(2,20)}$ = 1.77, p = 0.20).

Error bars represent +/- SEM. Scatter plots denote individual mice. N = 9 mice in the Open Field group. For accuracy and lap comparisons, N = 8 mice in Full-T and Half-T groups. N = 7 mice in Full-T and Half-T groups for velocity and distance comparisons.

**Figure 2.6**

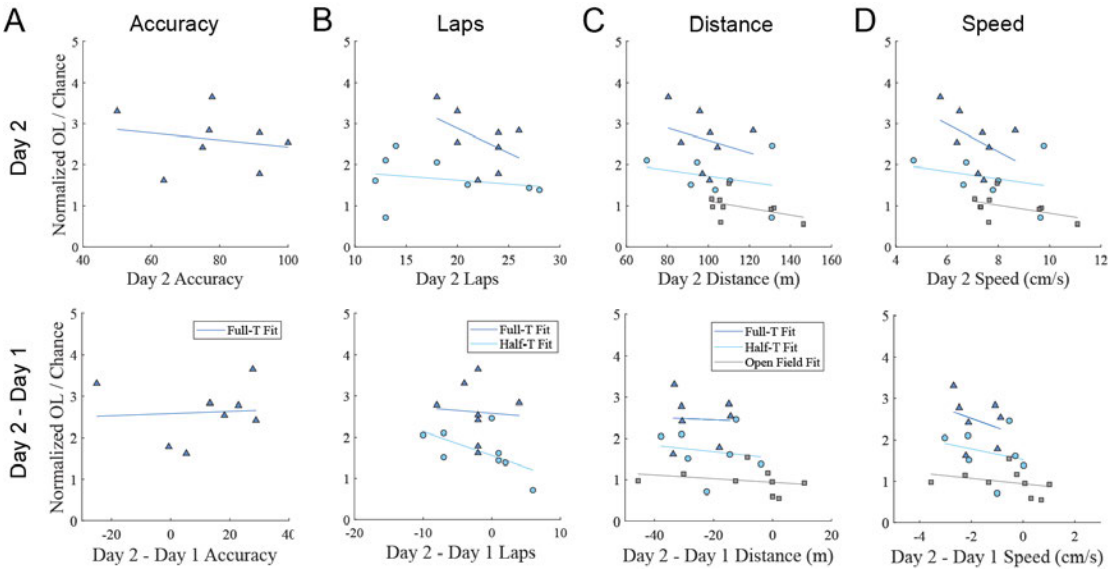


**Figure 2.6. Engram reactivation does not correlate to behavioral outcomes or learning across days.**
**A)** Top: No relationship was found between Day 2 DNMP accuracy and degree of engram reactivation in the Full-T group. (r = -0.20, p = 0.63). Bottom: Same as above but for difference in accuracy Day 1 vs Day 2 (Full-T: r = 0.07, p = 0.87).
**B)** Same as A but for number of laps on Day 2 (Full-T: r = -0.47, p = 0.47; Half-T: r = -0.23, p = 0.58) and difference in laps Day 1 vs 2 (Full-T: r = -0.07, p = 0.88; Half-T: r = -0.60, p = 0.24).
**C)** Same as B but for distance traveled on Day 2 (Full-T: r = -0.27, p = 1.00; Half-T: r = -0.28, p = 0.55; Open Field: r = -0.13, p = 0.62) and difference in distance Day 1 vs 2 (Full-T: r = -0.04, p = 0.92; Half-T: r = -0.16, p = 1.00; Open Field: r = -0.27, p = 1.00).
**D)** Same as C but for average speed on Day 2 (Full-T: r = -0.44, p = 0.55; Half-T: r = -0.28, p = 0.54; Open Field: r = -0.47, p = 0.62) and difference in average speed Day 1 vs 2 (Full-T: r = -0.30, p = 1.00; Half-T: r = -0.26, p = 0.58; Open Field: r = -0.33, p = 1.00). N = 9 mice in the Open Field group. For accuracy and lap comparisons, N = 8 mice in Full-T and Half-T groups. N = 7 mice in Full-T and Half-T groups for velocity and distance comparisons.

**Figure 2.7**

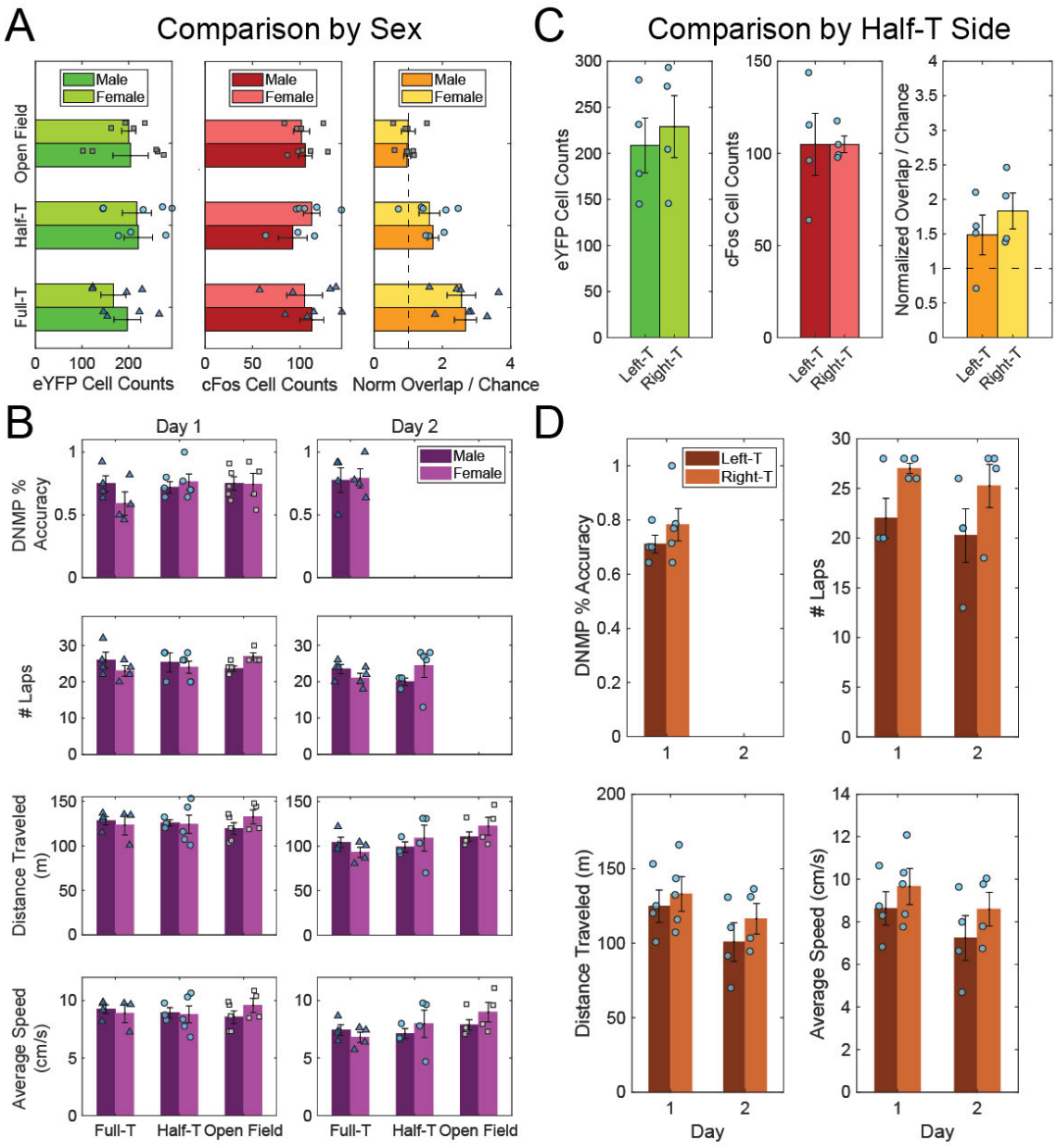


**Figure 2.7. Engram composition and behavior does not appear to differ across sex or experienced trajectory in the Half-T group.**

**A)** The size of the Day 1 and Day 2 ensembles, as well as degree of reactivation (overlap cells) appears similar between male and female mice of all groups.

**B)** Only minor sex differences were observed for any behavioral metric on either Day 1 (Left column) or Day 2 (right column) for all groups.

**C)** Same as A but comparing the Left-T and Right-T subgroups in the Half-T group,

similarly little difference observed.
**D)** Only minor subgroup differences were observed for behavioral metrics on Day 1 and Day 2.
Error bars represent +/- SEM. Scatter plots denote individual mice.

# CHAPTER THREE: NONSPECIFC ENSEMBLE REACTIVATION IN MOUSE DENTATE GYRUS DISRUPTS SPATIAL WORKING MEMORY

Data and portions of the text in this chapter were originally submitted as: Wilmerding, L.K., Kondratyev, I., Shi, W.B., Ramirez, S. & Hasselmo, M.E (2023). Ensemble reactivation in mouse dentate gyrus disrupts spatial working memory. Journal of Neuroscience. I designed the experiments, performed behavioral and imaging experiments, analyzed data, and wrote the manuscript submitted to *Journal of Neuroscience*.

## Introduction

The ability to separate recent memories of familiar locations to guide navigational decision making is an important tool for behavioral flexibility and involves structures including hippocampal region CA1 (Wang & Cai, 2006; Hyman et al., 2010; Spellman et al., 2015). Spatial working memory appears to rely on intact regions upstream of region CA1, such as the dentate gyrus (DG; Emerich & Walsh, 1989; McNaughton et al., 1989; Costa et al., 2005; Sasaki et al., 2018). The DG has been hypothesized to play a role in separating partially overlapping pattern inputs for subsequent decoding and completion by the rest of hippocampus (Marr, 1971; McNaughton & Morris, 1987; O'Reilly & McClelland, 1994; Treves & Rolls, 1994; Hasselmo & Wyble, 1997). Physiological recording studies demonstrate specific and stable spatial correlates of DG granule and mossy cells which may be used for spatial pattern separation (Neunuebel &

Knierim, 2012, 2014; GoodSmith et al., 2017; Hainmueller & Bartos, 2018; Cholvin et al., 2021). Answering how DG outputs actively shape downstream circuit computations will be important for understanding its role in spatial working memory, pattern separation and completion.

Prior work has used activity-dependent expression of immediate early genes such as c-Fos to drive the expression of fluorescent labels and optogenetic proteins to visualize and manipulate fear memory-associated cell ensembles or 'engrams' in DG (Liu et al., 2012; Ramirez et al., 2013; Redondo et al., 2014; Chen et al., 2019). One previous study used similar engram labeling to visualize populations of DG neurons associated with specific navigational trajectories in a T-maze (Wilmerding et al., 2023). In the present study, we used c-Fos driven engram tagging methods but in a non-temporally windowed fashion, allowing labeling of numerous cell ensembles in mice during multiple experiences on a spatial working memory task, the delayed-non-match-to-position T-maze. We optogenetically reactivated these 'nonspecific' ensembles during trials on a second T-maze arena to assess the contribution of DG to spatial working memory and transfer of learning between contexts. We found that nonspecific ensemble stimulation specifically disrupted spatial working memory accuracy with minimal disruption of other behavioral markers. Performance impairment was heterogeneous across days, suggesting an initial vulnerability of task representations to DG disruption as well as consistent impairment after the mice had more extensive experience of the secondary maze context. Our study suggests

a role of the DG in encoding spatial working memories as well as transferring task learning across contexts, in line with theories of its role in pattern separation and completion.

## Materials and Methods

### *Subjects*

12 wildtype (WT) C57B6J male and female mice (Jax) were segregated by sex and group-housed prior to surgery. They were housed on a reverse 12 hour light-dark cycle throughout the study. Mice received food and water ad libitum and were placed on a diet containing 40 mg/kg doxycycline (dox; Bio-Serv) at least 1 week prior to surgery at the age of 17-36 weeks. Post-surgically, the mice were returned to standard, non-dox chow and housed singly or in pairs (by sex). Mice were split equally into groups using random assignment, with 3 female and 3 male in the control group, and 5 female and 1 male in the experimental group. The bias was unintentional as several male animals whose data are not reported here were excluded from the experimental group on the basis of seizure-like activity (see Discussion section 3.3). No formal comparison of sex differences was made due to low sample size and prior work suggesting no sex difference in learning rate or spatial working memory span (number of entries prior to first error) on the radial arm maze (Bimonte & Denenberg, 2000; Harris et al., 2016). All procedures related to mouse care and treatment were in accordance with

Boston University and National Institutes of Health guidelines for the Care and Use of Laboratory Animals.

### *Viral constructs and packaging*

The pAAV9-cFos-tTA, pAAV9-TRE-ChR2-eYFP, and pAAV9-TRE-eYFP were constructed as described previously (Ramirez et al., 2013) and sourced from Gene Therapy Center and Vector Core at the University of Massachusetts Medical School. The viral titrations were $1.5*10^{13}$ genome copy per mL for the cFos-tTA and TRE-eYFP and $1.0*10^{13}$ genome copy per mL for the TRE-ChR2-eYFP virus and are consistent with prior work (Chen et al., 2019; Doucette et al., 2020).

### *Stereotactic injection and fiber placement*

All surgeries were performed under stereotactic guidance and all coordinates are reported relative to bregma. Anesthesia was induced with 5.0% isoflurane and maintained thereafter at a concentration of 1.5-2.0%. Two skull screws were inserted bilaterally above PFC without penetrating the dura. Bilateral burr holes were made at -2.2 mm (AP) and +/-1.3 (ML) using a 0.5mm drill and a pulled glass micropipette needle (Drummond Scientific, catalog no. 3-000-203 G/X) was lowered to -2.0 (DV). 300nL of AAV virus cocktail (cFos-tTA construct plus either TRE-ChR2-eYFP or TRE-eYFP) was injected bilaterally at a rate of 60nL/min controlled by a MicroSyringe Pump Controller (Drummond Scientific, Nanoject III). Following injection, the needle was kept at the injection

site for 3 minutes and slowly withdrawn afterwards. Subsequently optic fibers (200um core diameter; Doric Lenses) were lowered bilaterally at -2.2 (AP), +/-1.3 (ML) and -1.6 (DV) targeting dorsal DG. In some cases viral diffusion as well as light from the fiber may have spread to the intermediate dentate, so terminology will only refer to the dentate generally, rather than dorsal DG. Kwik-Sil (World Precision Instruments) was applied around the fiber shanks at the skull and then each fiber was fixed in place with C&B metabond (Parkell) and dental cement (Henry Schein). Post-operative subcutaneous injections of Buprenorphine (0.1 mg/kg) and Ketoprofen (5 mg/kg) were administered for three days following surgery and Enrofloxacin (10 mg/kg) for five days post-surgically. Targeting and viral expression was confirmed by histological assessment and data from off-target mice were not included in analysis.

### *Optogenetic methods*

Laser output was tested (Digital handheld optical power and energy meter console, ThorLabs) before each experiment to ensure at least 8mW power output at the end of a test fiber matching the implanted fibers. Implanted optic fibers were plugged into a branching patch-cable connected to a fiber optic rotary joint and a mono-fiber patch cable leading to a 473nm laser diode controlled by automated software (Doric Lenses). During experimental days, 20Hz square pulsatile stimulation (15ms pulse width) was delivered during the entire training phase of individual trials that were pseudo-randomly chosen. More specifically, on these trials stimulation started 5 seconds prior to trial onset, continued through

the training phase (running up the stem and into the training arm) and ended immediately upon re-entry into the start box at the start of the delay phase. Laser onset and offset was controlled manually by an experimenter in the room but did not differ between groups (Fig. S1A,B).

*Behavioral assays and ensemble tagging*

Prior to onset of behavioral training, mice were handled for 2-5 minutes per day for two days. All behavioral assays were performed during the light cycle of the day (7:00 - 18:00). To increase task acquisition speed, mice were water restricted throughout the training and experimental period to 20 minutes of ad libitum water access daily, in addition to the sucrose solution consumed in the maze. After surgery, mice were left off-dox for all subsequent days to allow activity-dependent expression of ChR2-eYFP or eYFP in the DG across behavioral training and experimental days.

The Delayed-non-match-to-position (DNMP) task was performed in a two-arm T-maze, as previously described (Fig. 1A, Levy et al., 2021; Wilmerding et al., 2023). Briefly, during the Train phase mice exited a start box and were forced to traverse one reward arm by the insertion of a temporary barrier. They received a small sucrose solution reward (30% sucrose) delivered by a blunted needle inserted through the wall. After returning to the start box for a 15-second delay phase, the Test phase began. Mice were released back to the central arm and were required to choose the previously unsampled reward arm in order to earn a second sucrose solution reward from another blunt needle at the end of that arm.

A 15-second inter-trial-interval separated each trial. Mice received ten total pre-training sessions, five prior to surgery with gradually increasing delay phase lengths, and five after surgical recovery with the full 15-second delay phase. These training sessions were carried out in one arena, Context T: a grey, wooden, rectangular T-maze (66 cm long x 31 cm wide x 19 cm high), with opaque walls forming the central stem and different wall cues on each reward arm.

Starting twenty-one days after surgery, experimental days began in a novel arena, Context A. This arena was an elevated beige, triangular, linoleum-lined T-maze (78 cm long x 78 cm wide x 18 cm high, 97.8 cm above ground) with novel cue cards, odor, floor texture, and room location. Instead of internal walls delineating the central stem, mice traversed a narrow central walkway to the choice point, allowing visual access to the reward arms. For consistency with another set of experiments (not included in this manuscript), mice experienced a 20-min exposure to a version of Context A with one reward arm blocked (counterbalanced across mice). This exposure included 15-second delays and reward delivery on the single accessible arm, but had no memory-guided component.

On the subsequent five days mice performed the full DNMP T-maze task for a minimum of twenty-five trials per day. The first five baseline trials of each day had no stimulation, while all following trials involved pseudo-randomly chosen combinations of training phase arm directions and stimulation conditions, such that on each day every mouse ran at minimum fifteen unstimulated trials,

and ten stimulated trials with counterbalanced left and right training phases. As noted above, stimulated 'light-on' trials involved 20Hz stimulation with 15msec pulse-width during the training phase of the selected trial. On the final day, mice were given a 2 hour rest after the final trial and then placed on a familiar neutral platform and given 5 minutes continuous stimulation (20Hz, 15msec pulse-width) for induction of c-Fos and later immunohistochemical visualization. Mice were sacrificed and perfused with 10% formalin 90 minutes after this stimulation.

Deeplabcut (Mathis et al., 2018) was used to extract mouse position during behavioral trials recorded on an overhead Mako G-131c GigE camera (35fps, Allied Vision). DeepLabCut outputs were further refined by interpolating across occasional tracking jumps outside the arena caused by the superposition of the optic cable over the mouse. The choice point was defined as a 10 x 10 cm box centered on the T-intersection of the maze. Video and laser pulse timestamps, spatially scaled position, distance, and velocity information were calculated and aligned using the CMBHome framework (https://github.com/hasselmonians/CMBHOME/wiki).

### *Immunohistochemistry*

Mice were euthanized 90 minutes after final neutral platform stimulation on Day 5 by administration of Euthasol (390 mg/kg) and anesthetized with Isoflurane prior to transcardial perfusion with saline and 10% formalin. Extracted brains were kept in formalin for 48 to 72 hours at 4 ℃ and transferred to 30% sucrose solution for approximately 48 to 72 hours at 4 ℃ to undergo

cryoprotection. Brains were sliced using a cryostat into 50μm slices, and blocked for 2 hours at 4 ℃ in 1x phosphate-buffered-saline + 2% Triton (PBS-T) and 5% normal goat serum (NGS). Consistent with prior studies (Chen et al., 2019; Wilmerding et al., 2023) slices were incubated for 48 hours at 4 ℃ with primary antibodies diluted in 5% NGS in PBS-T as follows: rabbit anti-c-Fos (1:1000, Abcam, #190289) and chicken anti-GFP (1:1000, ThermoFisher, #A10262). Subsequently, the slices were washed three times for 10 minutes in PBS-T, followed by a 2 hour incubation in the secondary antibodies diluted in 5% NGS in PBS-T as follows: Alexa 555 goat anti-rabbit (1:200; ThermoFihser, #A21429) and Alexa 488 goat anti-chicken (1:200, ThermoFisher, #A11039). Finally, the slices were mounted on slides using VECTASHIELD® Hardset™ Antifade Mounting Medium with DAPI (Vector Labs, #H-1500) and sealed with nail polish.

### *Cell counting*

Images of non-consecutive slices were acquired with an FV10i confocal laser-scanning microscope, using 10x magnification / 0.25 NA objective. DAPI was acquired at 405nm with laser power of 49.3%, eYFP at 473nm with laser power between 4 and 12% and c-Fos at 559nm with laser power of 19.7%.

The average DG granule cell layer c-Fos+ cell counts (indicating stimulation-induced activity) and eYFP+ cell counts (indicating total viral labeling) were obtained from three images from roughly equivalent AP positions in the dorsal DG of each animal. Each stain was counted using a StarDist neural

network trained and validated on a set of images from animals in each condition labeled by a trained, blinded rater, consistent with a prior study (Fig 1B, (Schmidt et al., 2018; Weigert et al., 2020; Wilmerding et al., 2023). Segmentation metrics (precision, recall, and matching to ground truth labels) confirmed model performance over a range of label matching thresholds. An intersection-over-union threshold of 0.5% was used as a tradeoff between match score and other metrics. In order to quantify the number of overlapping c-Fos+ and eYFP+ cells, an automated algorithm was used to carry out pairwise comparisons between the pixels of each eYFP and c-Fos cell and the results were filtered to only include overlapping cells of a comparable size (within at least 25% of each-other's size) that were mostly overlapping (75% of smaller object). Automated counts were used for increased reproducibility.

### *Quantification and statistical analysis*

Independent and paired sample t-tests were used to compare effects across and within groups respectively. A mixed effects linear model with main effects of group and light condition was fit to the accuracy data in Figure 2A with coefficient tests. Error bars display +/- SEM, while shaded patches indicate 95% confidence intervals. Bonferroni-Holm corrected p-values are reported where multiple t-test and correlation tests are made. Correlations were run using Pearson's R. Test statistics, groups sizes, and p-values are reported in figures and legends. All tests were performed in Matlab using publicly available functions. For all figures, * = $p < 0.05$, ** = $p < 0.01$, *** = $p < 0.001$.

## Results

*Nonspecific activity-dependent ensemble tagging in a spatial working memory task*

To investigate the contribution of dentate gyrus (DG) to spatial working memory, we first trained mice in a Delayed-Non-Match-to-Position (DNMP) T-maze task (Fig 3.1A). Briefly, this task assesses spatial memory in mice by dividing memory encoding and retrieval into a Train and Test phase respectively. Water-restricted mice are required to traverse one arm of the maze in the Train phase to receive a sucrose solution reward and then must choose the opposite trajectory during the Test phase to earn a second sucrose solution reward. Separating these phases with a 15-second delay increases task difficulty and involves the hippocampus (Costa et al., 2005).

After initial training, we performed surgery to bilaterally inject the DG with the tet-tag activity-dependent viral labeling system and to insert fiber optic cannulae (Fig. 3.1B,C). Endogenous c-Fos arising from cellular activity or plasticity in virally transfected cells drives the expression of ChR2-eYFP or eYFP in the experimental and control groups respectively. This viral expression is temporally gated by the presence or absence of the antibiotic doxycycline (dox) in the subjects' chow. Due to very sparse labeling in a one-shot exposure tag paradigm used in pilot experiments (data not shown) we chose instead to leave the subjects off dox for the period of time after surgery, resulting in c-Fos activity-dependent labeling throughout the remainder of the experiment (Fig. 3.1C). This paradigm led to strong expression of viral constructs in many DG cells across repeated exposure to the maze and task (Fig. 3.1D and Fig. S3.1A,B). Instead of

random sparse expression, this paradigm ensured relevance of the ChR2-expressing ensembles to experiences post-surgery, including maze-learning experience We termed this temporally non-specific expression ‘nonspecific ensemble tagging.’

To disentangle effects of prior experience versus novel memory, we pre-trained the mice in one T-maze (labeled as Context T) and performed stimulation experiments in another T-maze (labeled as Context A), which differed in scent, texture, geometry, room location, and visual cues. For consistency and comparability with prior studies (Wilmerding et al., 2023), after pre-training we exposed them to a one-route maze task during a 20 minute behavioral session on Context A. During the following 5 days in Context A, 20Hz pulsatile optical stimulation of the DG was delivered during the entirety of pseudo-randomly chosen Train Phases in the DNMP task, counterbalanced for left and right turns (Fig. 3.1C). This manipulation was chosen based on prior work indicating the importance of hippocampal outputs during the Train Phase, but not the Delay or Test Phase (Spellman et al., 2015; Maisson et al., 2018). The mice remained off dox during this time, allowing nonspecific tagging of c-Fos expressing cells activated by learning and optical stimulation. This paradigm allowed us to examine the role of DG ensembles during individual memory encoding episodes and test for memory generalizability across contexts and learning time points.

On the final day, mice performed the task as on previous days, received a rest, and then were placed on a familiar, neutral platform for 5 minutes. During this time they received pulsatile stimulation to optogenetically reactivate the same ensembles outside

the maze context. Mice were sacrificed and perfused 90-min. after this 5min. optogenetic stimulation period to visualize the stimulation-evoked c-Fos expression.

*Nonspecific ensemble stimulation disrupts spatial working memory*

First, we examined the outcome of Train Phase stimulation on overall DNMP accuracy (Fig. 3.2). To test effects between groups and across stimulation conditions, we created a linear mixed effects model on the average of each mouse's performance across all days. We found a significant intercept coefficient ($F_{(1,20)} = 467.82$, $p < 0.0001$), no main effect of group ($F_{(1,20)} = 0.16$, $p = 0.69$) or light condition ($F_{(1,20)} = 0.060$, $p = 0.81$) but a significant interaction of group and light condition ($F_{(1,20)} = 6.05$, $p = 0.023$). We conclude that stimulation of nonspecific ensembles in DG reduced DNMP accuracy by 11% (linear model coefficient). This finding indicates that DG ensembles can be used to manipulate spatial working memory, extending previous activity-dependent labeling studies driving fear, place preference, and spatial reference memory in a water maze (Ramirez et al., 2013; Redondo et al., 2014; Lamothe-Molina et al., 2022).

The effect on accuracy was heterogeneous across days, with strongest accuracy impairment on Day 1, and minimal accuracy change on Days 2 and 3 (Fig. 3.2B). While the control group exhibited some variability in performance across days, they showed no light-induced performance impairment on Day 1, suggesting that the robust effect in the ChR2-eYFP group was not due to the novelty of the light stimulus on its own. To validate this finding, we analyzed the average number of light pulses delivered across groups and found no difference in aggregate or on any experimental day (Fig S2A,B). Furthermore, the number of pulses delivered did not correlate to task accuracy during

light-on trials (Fig. 3.S2C). Finally, while Day 1 performance off-stimulation was high in both groups, we confirmed that mice were successfully generalizing learning from Context T to Context A within the first 5 baseline trials on Day 1. All ChR2 experimental mice were above chance prior to any light-on experience, as were most eYFP control mice (Fig. S3.2D). Several animals developed seizure-like behavior and near complete c-Fos activation in the DG over the course of the experimental days and were therefore excluded from the main results (Fig. S3.5A). Nevertheless, on days prior to seizure development, these animals showed consistent performance impairment on most days, indicating a robust link between DG disruption and SWM (Fig. S3.5).

Because of the Day 0 behavioral experience, each mouse had an additional experience with either the left or right maze trajectory. We first examined overall biases in performance based on the Train Phase trajectory and found no sidedness difference in stimulation impairment for either group (Fig. 3.2C). However, averaging across days could have obscured an effect present only on Day 1, so we examined each mouse on the day after the Day 0 one-sided experience. Although we were underpowered to make formal comparisons, we observed almost no difference in performance impairment between mice with Day 0 experience on the Left (L) or Right (R) maze trajectory on experimental Day 1. Taken together, these results indicate that Train Phase stimulation of nonspecific ensembles in DG produces robust, transient impairment of spatial working memory regardless of maze trajectory and prior experience.

Lastly, we observed that several animals in each group exhibited some viral expression in the subiculum. We excluded the two ChR2-eYFP mice with prominent

subiculum labeling and performed the same accuracy comparisons. We observed a similar decrease in overall accuracy during light-on only, with similar accuracy changes across days and lack of sidedness bias (Fig. S3.3A,B,C). While we cannot rule out the possibility of the subiculum contributing to the accuracy impairment in some animals (see discussion), we confirmed that the DG was playing a role in our main effect.

*Nonspecific ensemble stimulation minimally affects other behavioral markers*

We next asked whether stimulation of nonspecific ensembles affected other behavioral metrics on the DNMP T-maze task, in case the manipulation globally affected decision making. Using DeepLabCut, we extracted mouse position on the maze relative to Train and Test Phase onsets and offsets to calculate lap time, time to choice point, choice point occupancy, and overall speed and distance (Mathis et al., 2018). Next, we normalized the on-stimulation score of each behavioral marker to the off-condition in the associated Train or Test phase and compared across groups. No difference was found in normalized lap time, time to choice point, or choice point occupancy across groups in either phase, although there was a trending difference in time to choice point in the Train Phase prior to correction for multiple comparisons (Fig. 3.3A,B,C). There was a small increase in overall distance traveled during Train phases and average velocity in both phases for the experimental group relative to control (Fig. 3.3D,E). Given that dorsal DG stimulation can increase exploratory drive we interpret this to mean that stimulation mildly increased overall locomotor activity without impacting deliberation times, lap completion times, or choice point dwell time (Kheirbek et al., 2013). We examined the evolution of behavior across days and found that mice in both groups became largely

more efficient, traversing less distance at higher speeds and improving lap times in both task phases (Fig. 3.3A-E).

While there were only minor differences in velocity and speed, we decided to rule out the possibility that differences in these behavioral markers drove the central effect on memory accuracy. We correlated the normalized on-stimulation scores of each behavioral metric to on-stimulation accuracy in each group and found no significant relationships (Fig. S3.4A-E). These results together suggest that the effect of nonspecific ensemble stimulation is largely specific to memory impairment in this paradigm, rather than simply increasing impulsivity or indecision. Our findings align with and extend previous work indicating that hippocampal engram stimulation evokes memory-like behavior, rather than inducing non-specific behavioral changes (Ramirez et al., 2013; Denny et al., 2014; Redondo et al., 2014; Chen et al., 2019).

*Tag strength does not correlate to accuracy impairment*

Lastly, we sought to correlate the strength of the nonspecific ensemble tag to the strength of the behavioral impairment on spatial working memory. Using automated cell counting methods, we extracted the average number of tagged nonspecific ensemble neurons in the DG granular layer, the number of c-Fos positive cells evoked by stimulation, and the overlap between these groups. We found a significantly higher number of overlap cells normalized to the total nonspecific tag population in the ChR2 group (Fig. 3.4A). This result confirmed the successful optogenetic reactivation of ensembles in the experimental group. We next asked whether the strength of the overlap in these populations showed a relationship to spatial working memory accuracy. We

found no significant relationship between overlap and accuracy in either light condition or group, even though the ChR2 group was on average lower in accuracy under stimulation (Fig. 3.4B-C). This analysis suggests that memory impairment is achieved regardless of the exact strength of the nonspecific ensemble stimulation.

## Discussion

We investigated the behavioral role of an upstream hippocampal subregion, the Dentate Gyrus (DG), during a delayed-non-match-to-position (DNMP) T-maze task (Fig. 3.1A). Employing an activity-dependent labeling approach (Fig. 3.1B), we tagged DG cells with eYFP or ChannelRhodopsin2 (ChR2) across an extended time window to create so-called 'nonspecific ensembles' representing learning across repeated task exposures in both a training Context T and experimental Context A (Fig. 3.1C,D). Stimulation of nonspecific ensembles during the memory encoding phase of the DNMP task in Context A resulted in acute accuracy impairments (Fig. 3.2A) that evolved across recording days (Fig. 3.2B) without altering lap times or decision times (Fig. 3.3). Finally, we found no relationship of accuracy to either the quantity of cells nonspecifically tagged or cells activated by the stimulation (Fig. 3.4). Together, these results suggest that the DG contributes to spatial working memory computations previously examined in manipulations of region CA1 (Siegle & Wilson, 2014; Spellman et al., 2015).

### *DG inputs to downstream HPC in spatial working memory computations*

The role of the DG in spatial memory is complex and has been dissected for decades (O'Reilly & McClelland, 1994; Treves & Rolls, 1994; I. Lee & Kesner, 2004;

Neunuebel & Knierim, 2012; Kesner, 2013; GoodSmith et al., 2017; Hainmueller & Bartos, 2020). The most parsimonious explanation of the observed DNMP accuracy impairment under nonspecific DG ensemble stimulation is that aberrant output from DG cells is sufficient to disrupt natural circuit behavior in CA3 and CA1 necessary for behavior. Even so, total silence of DG inputs to downstream HPC during normal working memory is unlikely. Colchicine lesion studies of the DG in DNMP T-maze and plus-maze tasks suggest that lack of granule cell input impairs DNMP memory at delays greater than 3 seconds, though performance can be recovered with extensive re-training (Emerich & Walsh, 1989; Costa et al., 2005; Xavier & Costa, 2009; but see Jeltsch et al., 2001). Further, loss of DG mossy fiber inputs to CA3 pyramidal cells degrades spatial tuning specificity and reduces sharp-wave ripple rate as well as task performance on an eight-arm radial maze (Sasaki et al., 2018). These findings of DG contributions to spatial memory tasks align with growing evidence for stable and specific spatial tuning of DG granule cells (M. W. Jung & McNaughton, 1993; J. K. Leutgeb et al., 2007; Neunuebel & Knierim, 2012, 2014; Diamantaki et al., 2016; GoodSmith et al., 2017; Hainmueller & Bartos, 2018; Cholvin et al., 2021). We hypothesize that coherent, decodable output from the upstream DG onto CA3 and subsequently to CA1 is used during normal spatial working memory encoding and retrieval in this task. While the mice had experience of one trajectory in Context A from the Day 0 behavioral experience (Fig. 3.1C), we observed no sidedness bias on the first day (Fig. 3.2D) or across all days (Fig. 3.2C). More temporally refined tagging and stimulation approaches, such as calcium integrators

and closed-loop stimulation, will be necessary to test the contribution of route-specific DG ensembles (Siegle & Wilson, 2014; C. K. Kim et al., 2020)

### *Pattern Separation vs Completion in the Dentate Gyrus*

Generalization of learning across contexts while maintaining a representation of trial-specific memory information in the absence of sensory input is a difficult cognitive task to which the prefrontal cortex (PFC) and hippocampus (HPC) contribute complimentary computations (Euston et al., 2012; Eichenbaum, 2017; Shin et al., 2019; Samborska et al., 2022; Tang et al., 2023). Our task design allowed investigation of both of these cognitive functions. Mice generalized learning between the training Context T and the experimental context A on the first experimental day in control subjects, even within the first 5 trials prior to stimulation in the experimental subjects (Fig. S3.2D). However, stimulation of cell ensembles recruited by experience in a different context was sufficient to strongly impair accuracy on the first experimental day (Fig. 3.2B), consistent with prior disruption of CA1 output to medial PFC (Spellman et al., 2015). At a time when the subjects could only rely on a task structure learned in another context, behavioral accuracy was acutely degraded by aberrant activation of ensembles which prior work has shown to be labeled by both turn directions and task phases (Wilmerding et al., 2023). On the following two days, mice showed no consistent impairment, possibly by relying on maze representations formed in Context A on the first day during unstimulated trials. It is unlikely the mice switched to a different strategy given the short timescales of artificial perturbation and without the extensive retraining required (Emerich & Walsh, 1989; Costa et al., 2005; Goshen et al., 2011). On the final two

experimental days, when mice were most familiar with Context A, stimulation lead to smaller but consistent performance impairment. We interpret this to mean that sufficient nonspecific ensembles from Context A had been recruited to consistently disrupt memory encoding in that context. We hypothesize that while some compensatory process of pattern separation recovered accuracy on Days 2 and 3, initial generalization across contexts was vulnerable to DG stimulation.

### *Cell ensemble recruitment*

We confirmed a higher overlap between the stimulation-induced c-Fos and nonspecific eYFP label in the ChR2 group, indicating successful optogenetic excitation (3.4A). Interestingly, less than 30% of nonspecific-tagged cells expressed c-Fos (Fig. 3.4). A number of mechanisms may account for this result. First, artificial activation of granule cells and mossy cells in the hilus could recruit disynaptic inhibition of DG interneurons back onto the granule cell layer, limiting the activated ensemble size (Buzsaki & Eidelberg, 1981; Amaral et al., 2007; Scharfman, 2007; Larimer & Strowbridge, 2008). Perhaps during aberrant stimulation a winners-take-all effect leads to a constrained c-Fos ensemble size, given that NMDA-R plasticity, not activity, is linked to IEG expression (Labiner et al., 1993). Indeed, somatostatin interneurons may control ensemble size in the DG by suppressing dendritic activity needed for plasticity of perforant-pathway synapses in DG (Stefanelli et al., 2016; S. Kim et al., 2018). Therefore, while stimulation may have driven spiking in a larger proportion of the DG ChR2-expressing neurons, only a subset were observable using the c-Fos marker.

Additionally, we found no correlation between cell counts and accuracy (Fig. 3.4B,C). Past work has shown little relationship between behavioral measures and memory ensemble reactivation in fear memories (Zaki et al., 2022), general locomotion (VanElzakker et al., 2008) or DNMP memories (Wilmerding et al., 2023). In some mice that were not included in the main analysis, we observed that nonspecific ensemble stimulation led to near complete ChR2-eYFP tagging and post-stimulation c-Fos expression in the DG (Fig. S3.5). These animals were excluded from the central results because they exhibited seizure-like behaviors at some point in the course of the experiment, but they also showed stronger accuracy impairments prior to seizure onsets, consistent with a relationship between excitatory:inhibitory balance and c-Fos expression levels. Our results are consistent with a hypothesis of tightly regulated memory ensemble size in DG under both natural and artificial network activation.

*Potential contribution of the nonspecific subiculum tag*

A limitation of our study was the non-specificity of injection targeting in several animals leading to off-target viral expression in the subiculum (Fig. S3.1A,B). While we repeated analysis and found similar results after excluding animals with prominent subiculum tag in the ChR2-eYFP group (Fig. S3.3), we cannot rule out some contribution of subiculum to our central findings. Disruption of subiculum function can impair accuracy in delayed-non-match-to-sample Skinner box tasks at delays of up to 15 seconds in rats (Hampson et al., 1999; Hampson & Deadwyler, 2003). Recordings of subiculum and CA1 suggest a complementary role for each region, with the subiculum accurately encoding task variables for delays up to 15 seconds, as in our task, and the CA1 encoding

trial outcomes for longer delays (Deadwyler & Hampson, 2004). There exists a dearth of studies specifically examining the role of the mouse subiculum in more spatially distributed DNMP tasks like the one used in the present study.

### *Conclusions*

We investigated the role of dentate gyrus outputs during spatial working memory using a Delayed-Non-Match-to-Position T-maze task. By labeling dentate gyrus neurons recruited during task learning across multiple days, we were able to stimulate these 'nonspecifically' tagged ensembles to generate aberrant dentate outputs during working memory computations. Stimulation in the experimental group only caused acute performance impairments that evolved across days. These deficits were largely confined to decision accuracy without impacting behavior around the choice itself, nor was the recruited ensemble size linearly correlated to memory ability. Our results are consistent with the hypothesis that the dentate contributes to spatial working memory while also demonstrating its broader function in pattern separation and completion.

## Acknowledgments

We thank the Hasselmo and Ramirez labs for thoughtful feedback and commentary on the work.

This work was supported by the National Institutes of Health [grant numbers: R01 MH052090, MH060013, MH120073, HD101402-02; and DP5 OD023106-01], and the Office of Naval Research [grant numbers: MURI N00014-16-1-2832, N00014-19-1-2571; and DURIP N00014-17-1-2304].

## Author Contributions

Conceptualization, L.K.W., S.R., and M.E.H.; Methodology, L.K.W., and I.K.; Investigation and data acquisition, L.K.W., W.B.S., and I.K.; Writing – Original Draft, L.K.W.; Writing – Review & Editing, L.K.W., W.B.S., I.K., S.R., and M.E.H.; Funding Acquisition, M.E.H. and S.R.; Formal Analysis, L.K.W.; Visualization, L.K.W.; Supervision, M.E.H. and S.R.

## Declaration of Competing Interests

The authors declare no competing interests

## Figures

**Figure 3.1**

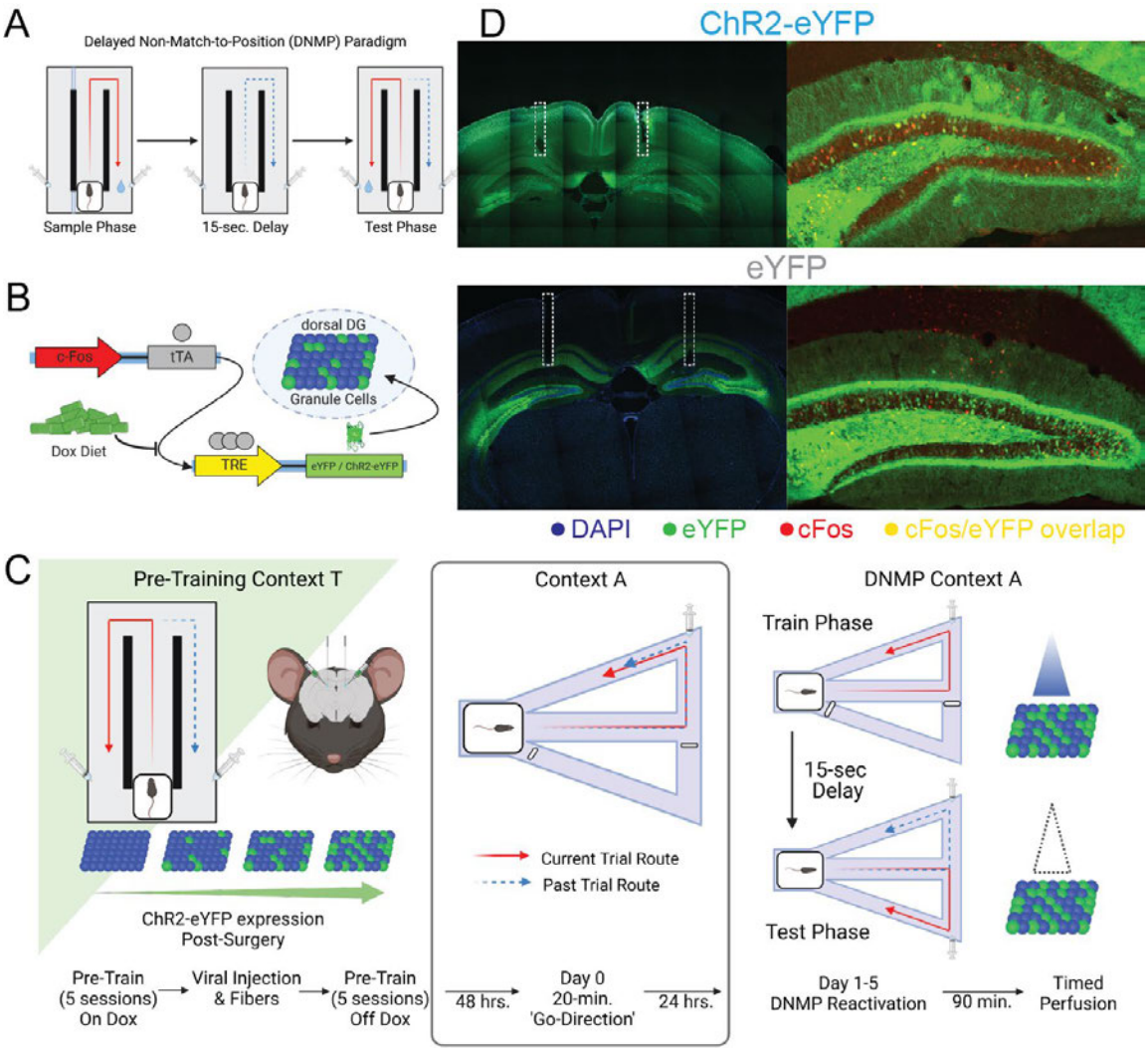


**Figure 3.1. Nonspecific activity-dependent ensemble tagging in spatial working memory task.**

**A)** DNMP paradigm. A-C created with BioRender.

**B)** Activity-dependent viral labeling strategy (see Methods).

**C)** Experimental timeline. Pre-training used Context T. On Day 0, mice were exposed to novel context A and ran one-sided laps. On experimental Days 1-5, mice performed the DNMP task on Context A with optogenetic stimulation in the Train phase on pseudo-randomly interleaved trials. On Day 5 mice were perfused 90 minutes after 5-min. of pulsatile stimulation on a familiar, neutral platform.

**D)** Example histology demonstrating fiber placement and nonspecific ensemble tagging in the experimental (ChR2-eYFP, blue) and control group (eYFP, grey). Red-labeled cells indicate c-Fos expression 90-min. after familiar neutral platform stimulation.

**Figure 3.2**

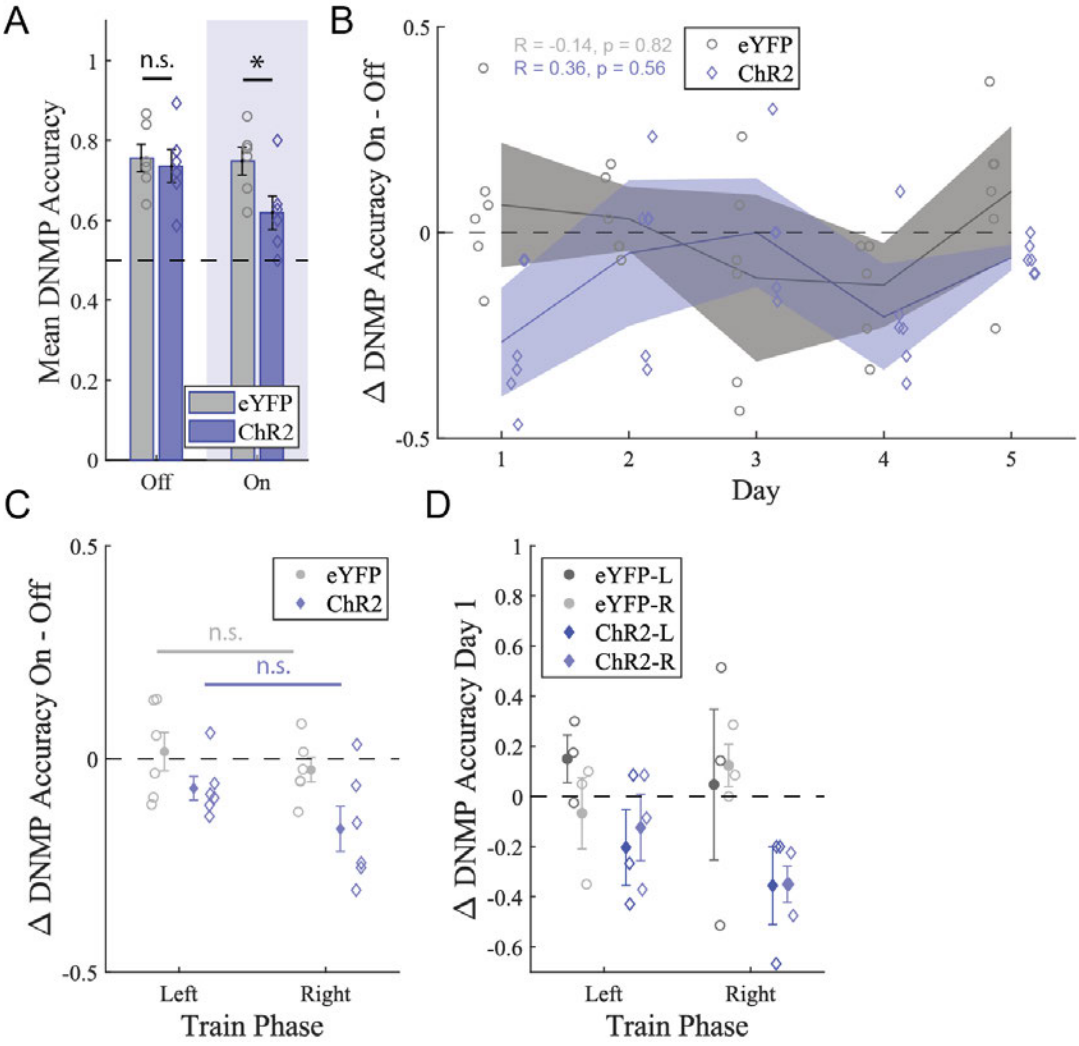


**Figure 3.2. Nonspecific ensemble stimulation disrupts spatial working memory.**
**A)** Mean DNMP accuracy was impaired in the ChR2 group during stimulation (Mixed effect linear model; group by light condition interaction coefficient test, t = 2.46, p = 0.023).
**B)** Difference in accuracy on versus off stimulation was heterogeneous in the ChR2 group.
**C)** There was no clear sidedness bias as the change in accuracy on stimulation versus off stimulation was not significantly different for the left versus right side training phases in the control (Paired t-test; t = 0.94, p = 0.39) or experimental group (t = 2.48, p = 0.11).
**D)** ChR2 animals displayed consistent impairment on both maze sides on Day 1 despite differential Day 0 experience on the Left (L) or Right (R) route of the maze. See Results text.

Error bars represent +/- SEM. Shaded patches represent 95% CI. Scatter plots denote individual subjects (circle = eYFP; diamond = ChR2). N = 6 mice in eYFP and ChR2 groups.

**Figure 3.3**

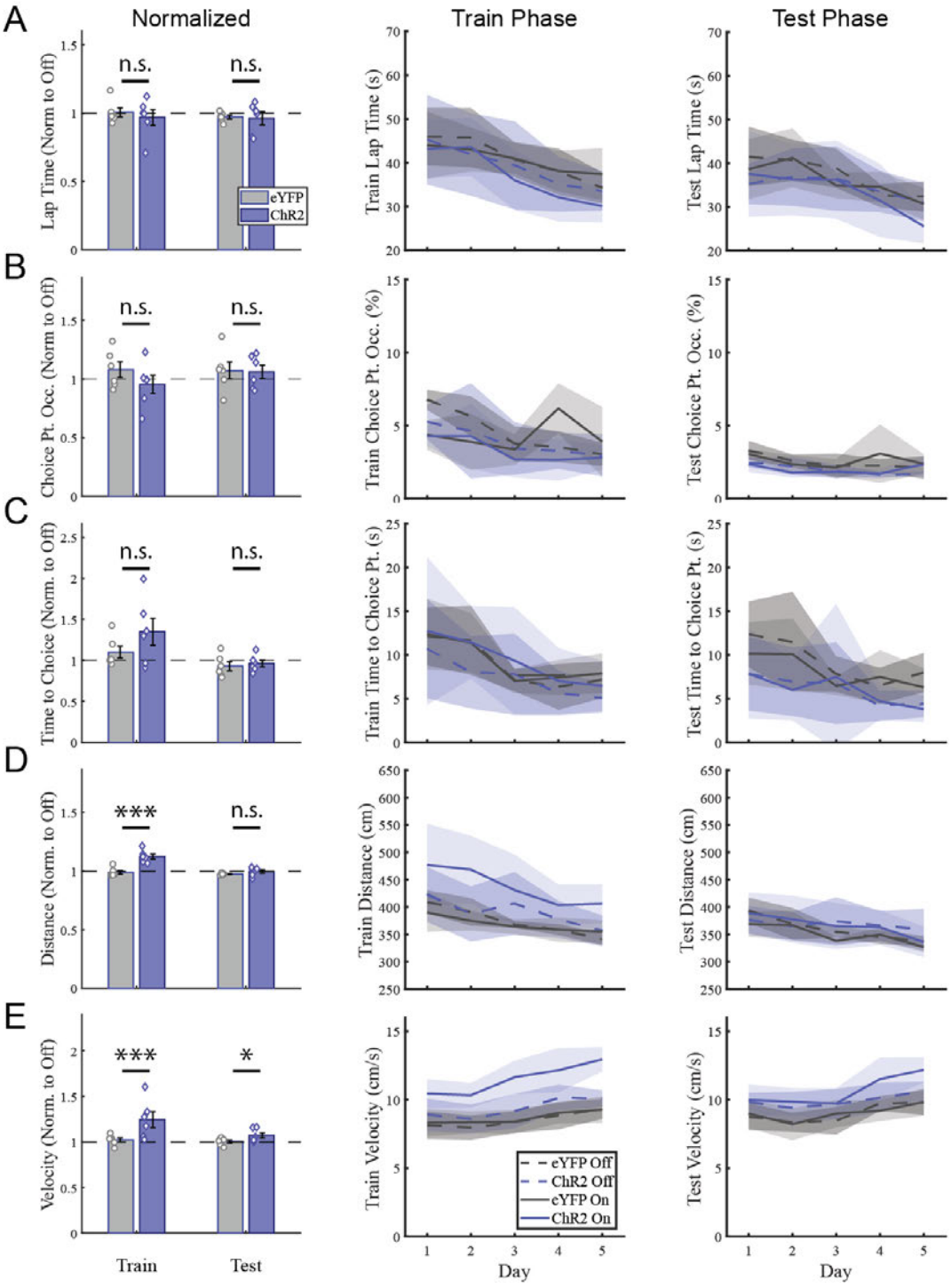


**Figure 3.3. Nonspecific ensemble stimulation minimally affects other behavioral markers.**

**A)** Left: On-stimulation lap time normalized to off condition shows no difference across groups in train phase (independent t-test; $t = 0.96$, $p = 0.68$) or test phase ($t = 0.24$, $p = 0.81$). Raw lap time (seconds) in Train Phase (middle) and Test Phase (right) across days split by stimulation light on (solid) or light off trials (dashed).
**B)** As in A, but for choice point occupancy, not differing across groups in train phase ($t = 0.94$, $p = 0.70$) or test phase ($t = 0.11$, $p = 0.91$)
**C)** As in A, but for time to choice point, not differing across groups in train phase ($t = 2.16$, $p = 0.07$) or test phase ($t = 0.40$, $p = 0.69$).
**D)** As in A, but for distance traveled, showing a difference across groups in train phase ($t = 5.40$, $p < 0.001$) but not test phase ($t = 1.22$, $p = 0.23$).
**E)** As in A, but for average velocity, showing a difference across groups in train phase ($t = 5.19$, $p < 0.001$) and test phase ($t = 2.30$, $p = 0.02$)
Error bars represent +/- SEM. Shaded patches represent 95% CI. Scatter plots denote individual subjects (circle = eYFP; diamond = ChR2). N = 6 mice in eYFP and ChR2 groups.

**Figure 3.4**

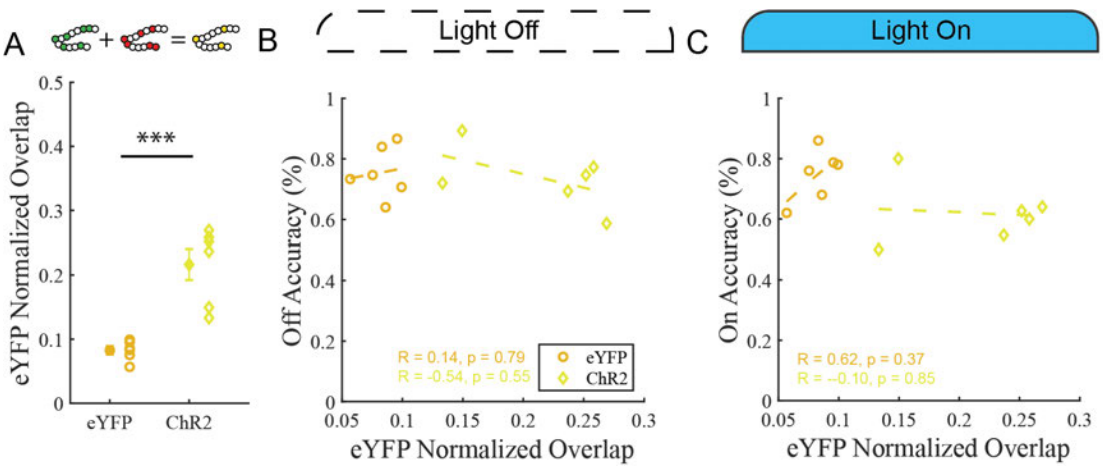


**Figure 3.4. Tag strength does not correlate to accuracy impairment**
**A)** Mouse-averaged nonspecific ensemble and c-Fos ensemble overlap normalized to eYFP population shows a difference in recruited population across groups ($t = 5.34$, $p < 0.001$).
**B)** No correlation between eYFP normalized overlap and accuracy in either group in the light off condition.
**C)** Same as B but for the light on condition. Note the overall lower accuracy in the ChR2 group, consistent with Fig. 3.2A.
Error bars represent +/- SEM. Scatter plots denote individual subjects (circle = eYFP; diamond = ChR2). N = 6 mice in eYFP and ChR2 groups.

*Supplemental Figures*

**Figure S3.1**

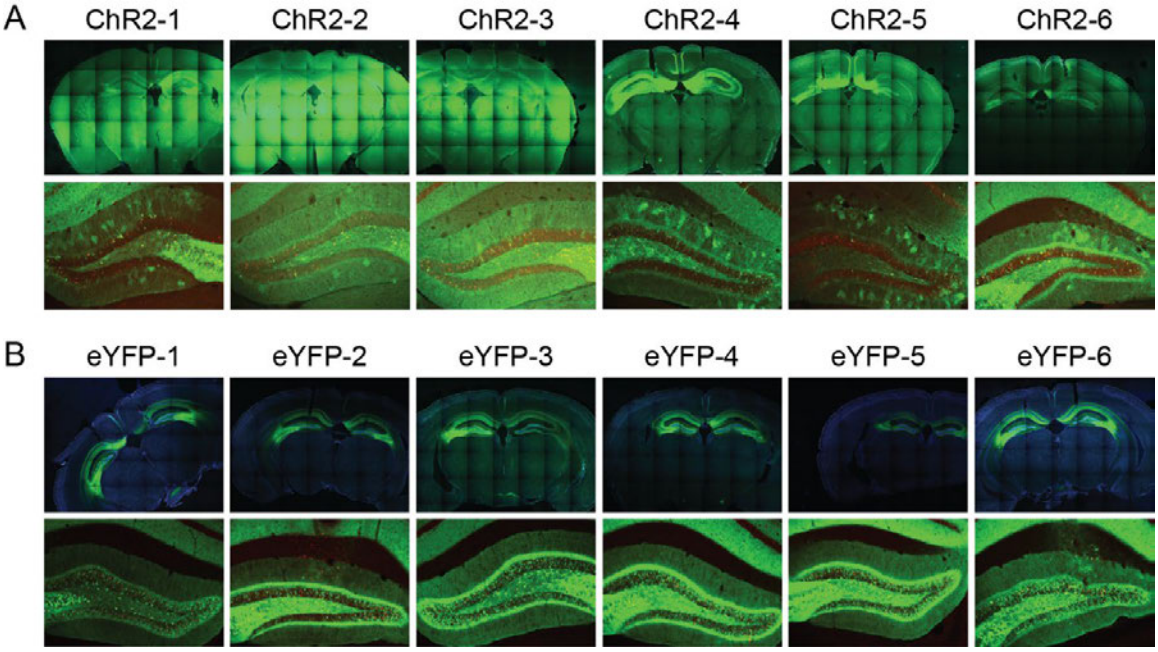


**Figure S3.1. Representative histology of nonspecific ensembles.**
Related to Figure 3.1.
**A)** Histology from all ChR2-eYFP experimental mice.
**B)** Histology from all eYFP control mice.

**Figure S3.2**

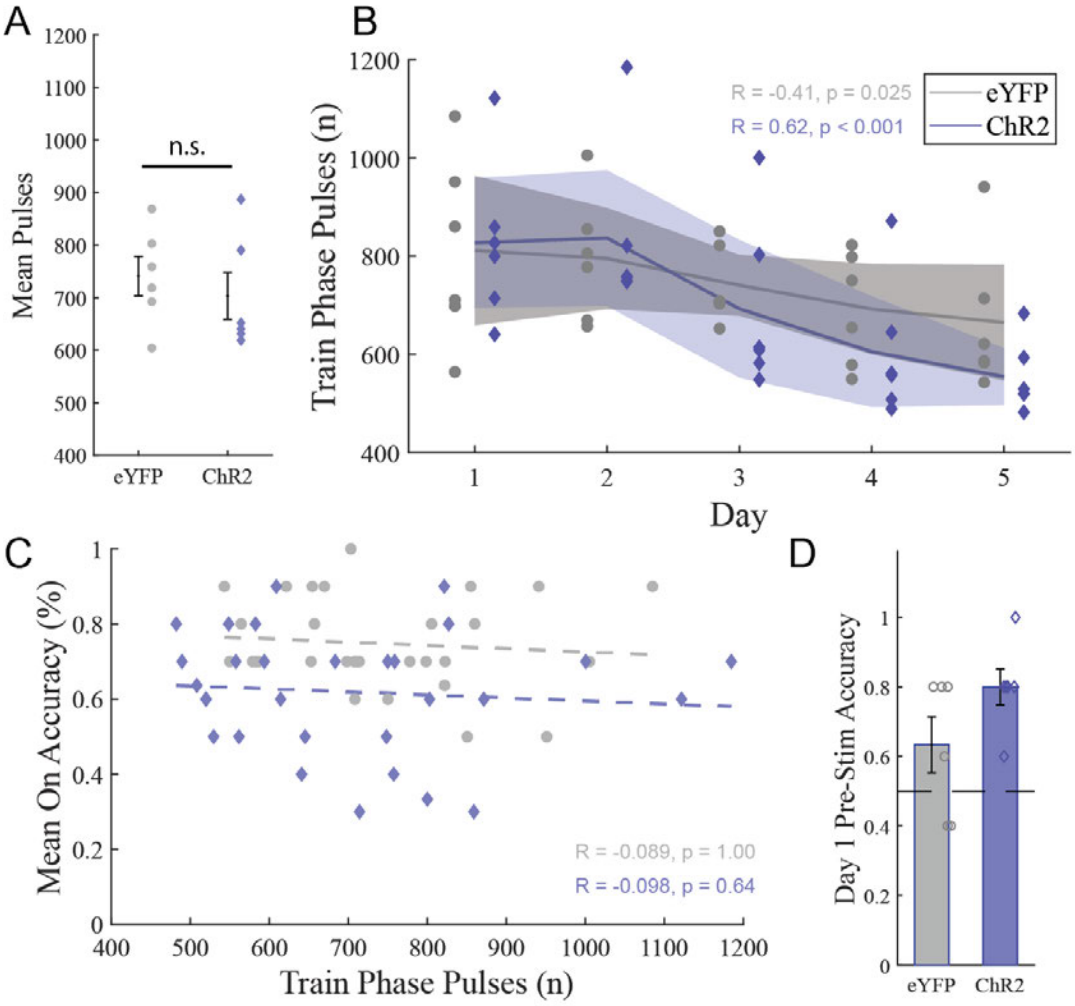


**Figure S3.2. Similar pulses delivered between groups does not correlate to task accuracy.**

Related to Figure 3.2.

**A)** No difference in average pulses between groups (Independent t-test, t = 0.64, p = 0.53).

**B)** Mean number of pulses delivered in the training phase dropped across days in both groups.

**C)** Mean number of train phase pulses did not correlate to DNMP accuracy.

**D)** All mice in the ChR2 group performed above chance on Day 1 during baseline trials prior to stimulation, as did most eYFP mice.

Error bars represent +/- SEM. Shaded patches represent 95% CI. Scatter plots denote individual subjects (circle = eYFP; diamond = ChR2). N = 6 mice in eYFP and ChR2 groups, n = 30 sessions in eYFP and ChR2 groups (panel C).

**Figure S3.3**

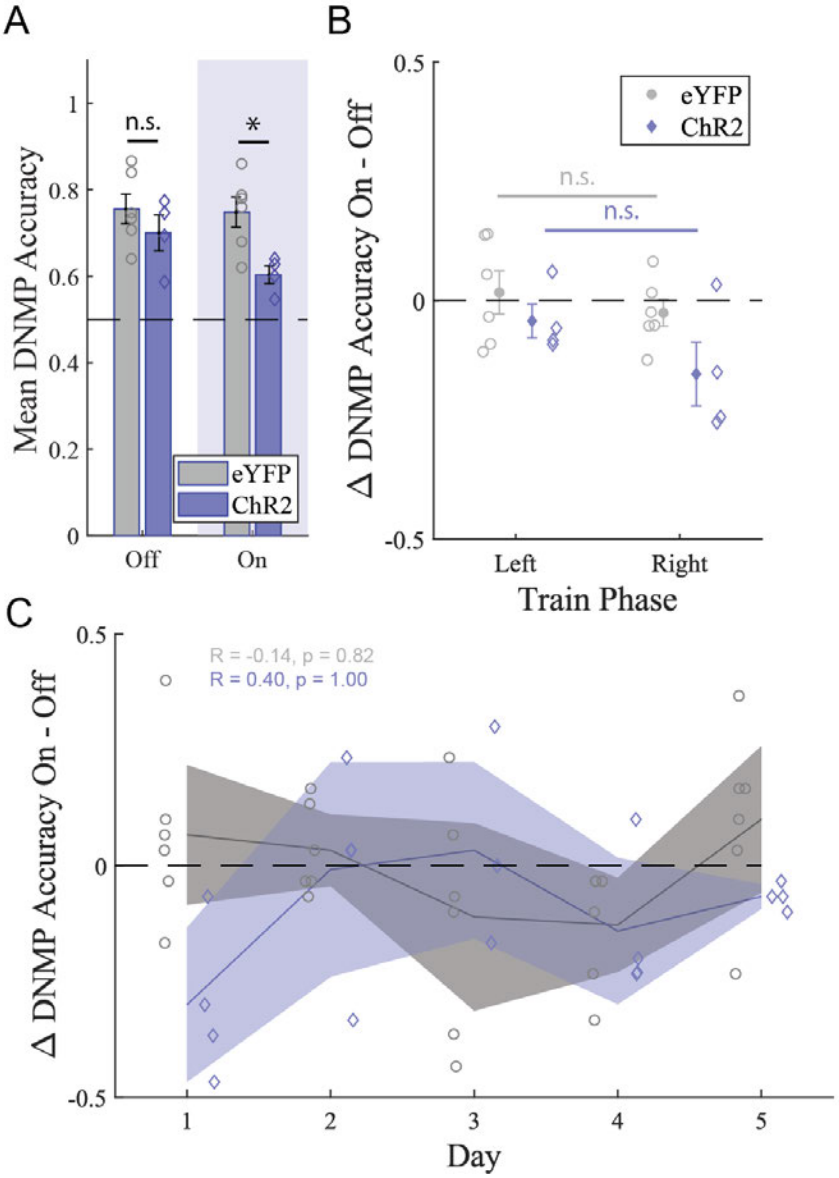


**Figure S3.3. Behavioral accuracy impairment is not solely mediated by subiculum output.**

Related to Figure 3.2.

**A)** Excluding 2 ChR2 mice with subiculum tag, no difference in accuracy between groups off stimulation (Independent t-test; $t = 1.03$, $p = 0.33$) but the ChR2 group decreases accuracy on stimulation ($t = 3.11$, $p = 0.029$).

**B)** No sidedness bias emerges in accuracy after exclusion of 2 ChR2 subiculum-tagged mice (Paired t-test; $t = 2.92$, $p = 0.12$).

**C)** Similar patterns in behavioral impairment emerge across days, with no correlation in either group.

Error bars represent +/- SEM. Shaded patches represent 95% CI. Scatter plots denote individual subjects (circle = eYFP; diamond = ChR2). N = 6 mice in eYFP and 4 mice in ChR2 group.

**Figure S3.4**

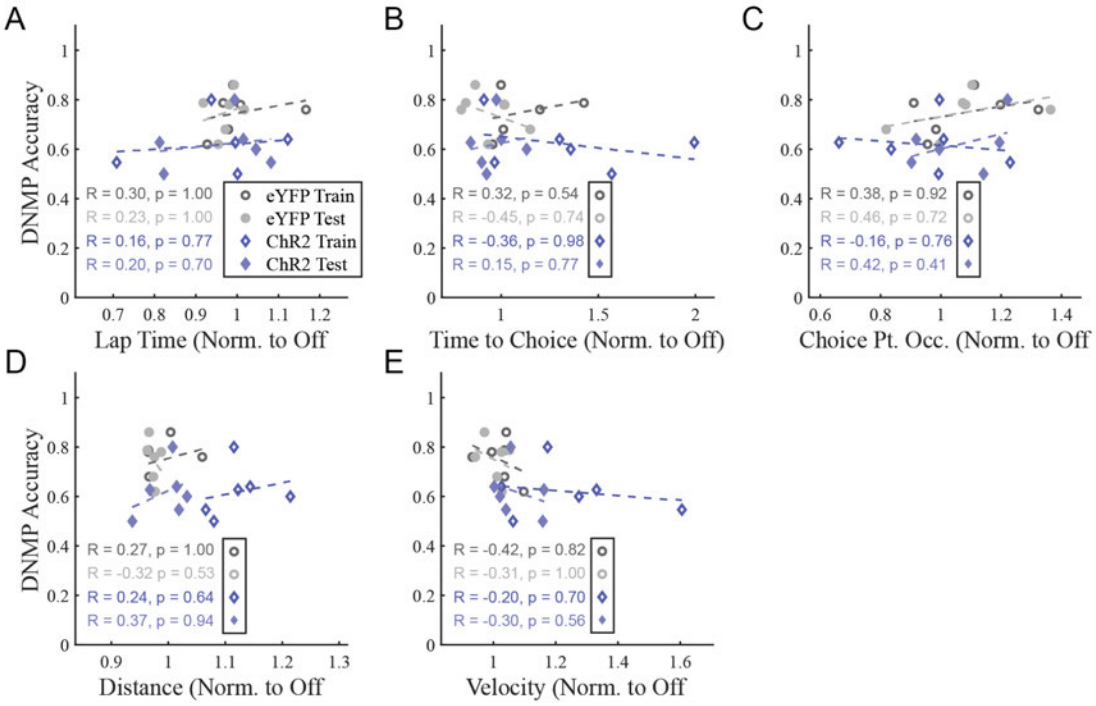


**Figure S3.4. Differences in granular behavioral metrics do not correlate to task performance.**

Related to Figure 3.3.

**A)** Accuracy on stimulation trials does not correlate to on-stimulation lap time (normalized to off-stimulation) in the train or test phase in either group.

**B)** Same as A but for normalized time to choice point.

**C)** Same as A but for normalized choice point occupancy.

**D)** Same as A but for normalized distance.

**E)** Same as A but for normalized velocity.

Scatter plots denote individual subjects (circle = eYFP; diamond = ChR2, open = train phase, closed = test phase). N = 6 mice in eYFP and ChR2 groups.

**Figure S3.5**

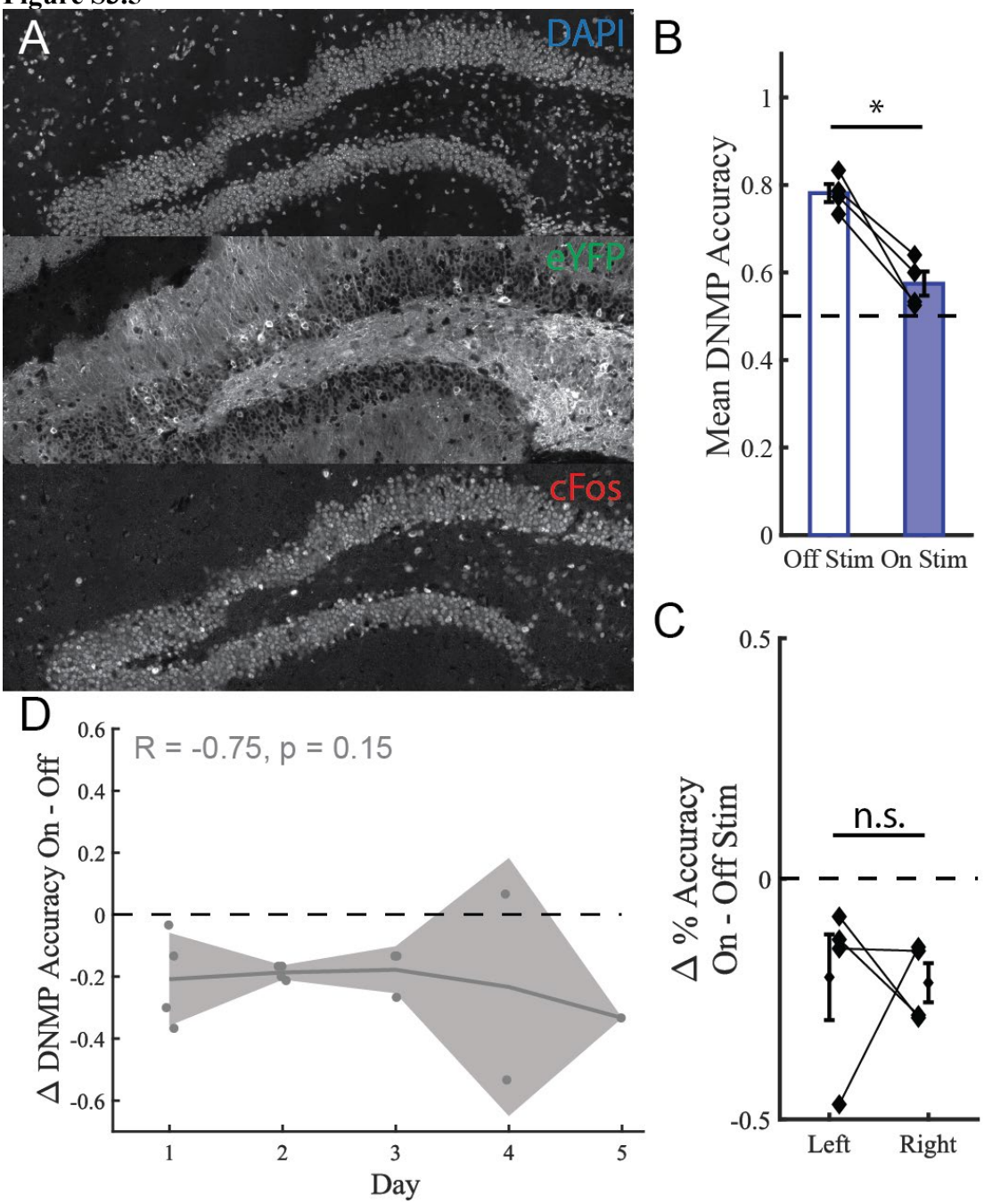


**Figure S3.5**. **Stronger labeling leads to larger spatial working memory impairment and seizure.**

**A)** Representative histology from a mouse which exhibited a seizure phenotype during behavior. Note that cFos-mCherry and ChR2-eYFP appear in most of the DAPI-labeled nuclei, confirming the seizure.

**B)** Nonspecific ensemble stimulation decreases spatial working memory accuracy relative to baseline (RM t-test; $t = 5.83$, $p = 0.01$).

**C)** No sidedness bias in working memory impairment (RM t-test; $t = 0.094$, $p = 0.93$).
**D)** Stimulation impairment relative to baseline does not increase or decrease across days (Spearman's $R = -0.75$, $p = 0.15$). Note some mice drop out across time due to seizures starting on day 3, 4, or 5.
N = 4 mice (2 male, 2 female). Data for each mouse averaged across completed sessions only (no seizure sessions).

# CHAPTER FOUR: PRELIMINARY ELECTROPHYSIOLOGICAL RECORDING OF HIPPOCAMPAL CIRCUIT RESPONSE TO FEAR ENGRAM STIMULATION

## Introduction

The advent of immediate early gene (IEG) driven technologies and targeted control of well-defined neuronal populations has given unprecedented insight into the "irritable substance" of memories, or engrams, proposed by Richard Semon (Semon, 1921; Ramirez et al., 2013; Josselyn & Tonegawa, 2020). However, care should be taken when interpreting the findings of engram manipulation studies claiming necessity and sufficiency of memory-related ensembles for memory-guided behavior in the absence of additional corroborating physiological evidence (Jou et al., 2023). In particular, the question remains whether artificial stimulation of memories eliciting behavioral responses occurs by generating new circuit responses or instead relies on activating innate circuit properties and dynamics, as suggested by a recent preprint (Jou et al., 2023). To date, relatively little physiological data has been reported on engram cells *in vivo*. During initial exposure to a neutral arena, optogenetically identified engram cells in the absence of stimulation were recorded to determine their physiological correlates and found to be relatively unstable place cells that nonetheless differentiated contexts effectively (Tanaka et al., 2018). In contrast, another group recorded the calcium dynamics of Fos-expressing cells and found that Fos-high, engram-like, neurons had higher spatial tuning stability within and across days than non-engram neurons and formed reliable functional ensembles (Pettit et al., 2022). Unifying these inconsistent

results and characterizing the physiological ramifications of perturbing these engram ensembles will be an important step toward a unified explanation of memory function.

To examine the circuit-level outcomes of engram reactivation, we recorded cells in the hippocampus using electrophysiology during artificial stimulation of a dentate gyrus (DG) mediated fear memory. A behavioral readout is a key component of identifying memory-related ensembles to which fear conditioning and the freezing response are well suited (Ramirez et al., 2013; Denny et al., 2014; Roy et al., 2016; Kitamura et al., 2017; Chen et al., 2019). We used contextual fear conditioning to induce temporally gated expression of the ChannelRhodopsin-2 construct in DG cells expressing the IEG c-Fos and tag a fear engram in mice. Subsequently, LFP was recorded from DG and CA1 and single units from CA1 during transient optogenetic reactivation in either a small arena mimicking the fear conditioning chamber or a large open field to detect place field activity. Preliminary evidence from four behavioral animals, two of which had confirmed hippocampal recordings, show a modest behavioral impact of CFC engram stimulation. Despite the lack of robust behavior change, engram stimulation acutely drove network oscillations at the stimulation frequency both within the target DG and downstream CA1 regions. Additionally, single unit analyses confirmed that upstream stimulation modulated the firing rate and reduced the spatial information of a subpopulation of recorded CA1 cells. Finally, a linear decoder successfully classified the presence or absence of stimulation based on the population firing rate. While these findings need further replication, the initial results suggest the DG strongly modulates

network oscillations in target regions and that artificial DG engram reactivation drives a partially replicable network state in CA1.

## Materials and Methods

### *Subjects*

4 wildtype (WT) C57B6J male mice (Jax) were group-housed prior to surgery and kept on a reverse 12 hour light-dark cycle throughout the study. Mice received food and water *ad libitum* and were placed on a diet containing 40 mg/kg doxycycline (dox; Bio-Serv) at least 1 week prior to surgery at the age of 16 weeks. They remained on dox diet except for a 48 hour window ending with the fear conditioning experiment described below. Post-surgically, the mice were housed singly. All procedures related to mouse care and treatment were in accordance with Boston University and National Institutes of Health guidelines for the Care and Use of Laboratory Animals.

### *Viral constructs and packaging*

The pAAV9-cFos-tTA and pAAV9-TRE-ChR2-eYFP were constructed as described previously (Ramirez et al., 2013) and sourced from the Gene Therapy Center and Vector Core at the University of Massachusetts Medical School. The viral titrations were $1.5*10^{13}$ genome copy per mL for the cFos-tTA virus and $1.0*10^{13}$ genome copy per mL for the TRE-ChR2-eYFP virus.

*Stereotactic injection and fiber placement*

Mice were surgically implanted with custom-made microdrives under aseptic conditions. Custom-designed, lightweight, enclosed, 3D printable microdrives with three independently moveable shuttles were fitted with eight nickel chromium tetrodes (12um, Kanthal-Sandvik). A polyimide guide cannula was glued to each shuttle and fed into a 3D printable guide array at the base of the drive. Each guide cannula housed two to three tetrodes pinned to a 32-channel EIB with omnetics connector (Open-Ephys). Tetrodes were plated with gold solution (Sifco ASC) to reduce impedance to ~250kOhm. Two optic fibers (NA 0.22, Doric Lenses) were inserted into the drive and fixed to the EIB with dental cement (Henry Schein). One fiber was positioned amidst the three tetrode guide cannulae in the guide array base, the other was contralateral and spaced 2.6mm away. The three tetrode cannulae and optic fiber spanned a region of ~0.8mm diameter.

All surgeries were performed under stereotactic guidance and all coordinates are reported relative to bregma. 5.0% isoflurane was used for anesthetic induction and maintained at a concentration of 1.5-2.0%. Two skull screws were inserted bilaterally above PFC, and a third screw posterior to the coronal suture contralateral to the drive craniotomy. A ground screw with soldered, insulated wire was implanted above the cerebellum. Viral injections were targeted to -2.2mm (AP), +/- 1.3 (ML) and -2.0 (DV) through bilateral burr holes made using a 0.5mm drill. The 300nL viral cocktail infusions (equal parts cFost-tTA construct with TRE-ChR2-eYFP or TRE-eYFP) were performed with a  pulled glass micropipette needle (Drummond Scientific, catalog no. 3-000-203 G/X) at a rate of 60nL/min controlled by a MicroSyringe Pump Controller (Drummond

Scientific, Nanoject III). The needle remained at the site for at least 3 minutes following the end of the infusion and was withdrawn slowly thereafter. Next, a larger craniotomy (1.5mm diameter) was made surrounding the right burr hole and dura was resected. The 32-channel microdrive with bilateral optic fibers was lowered to the skull surface, with fibers targeting -2.2 (AP), +/-1.3 (ML) and -1.6 (DV) to reach dorsal DG. Sterilized Vaseline was applied between the base of the implant and the skull and around the contralateral optic fiber and burr hole. The implant was fixed in place with C&B metabond (Parkell) and dental cement (Henry Schein). Finally, the ground wire was soldered to a connector on the microdrive EIB. Post-operative subcutaneous injections of Buprenorphine (0.1 mg/kg) and Ketoprofen (5 mg/kg) were administered for three days following surgery and Enrofloxacin (10 mg/kg) and 0.9% sterile saline (as needed) for five days. Targeting and viral expression was confirmed by histological assessment.

### *Electrophysiological Recording and Spike Sorting*

Neural signals were amplified by a 32-channel digitizing headstage connected to the microdrive EIB and acquired by a SpikeGadgets Main Control Unit (SpikeGadgets) via an electrical commutator. Continuous signal from all channels was recorded at 30kHz for spikes and 1500Hz for LFP. One tetrode in each drive with clean signal but no single units was designated a reference for each session.

After each experiment, data was imported to Plexon Offline Sorter 3 (Plexon Inc.) and spikes were detected above a threshold on any given electrode from each tetrode bundle. Spikes were manually clustered by the experimenter (LKW) into single units using the following features: peak, peak-valley, and principal components 1 to 3. Noisy

events were excluded based on the features of square root of energy and full-width half maximum. Clusters with >0.3% spikes within an inter-spike-interval of 2ms were excluded. Single units exhibiting significant drift were excluded by manual observation. Of the 125 single units, 82 hippocampal units were identified on the basis of histological verification of tetrode targeting and a combination of physiological signatures such as strong theta rhythm on the associated electrode or in the autocorrelogram, the presence of punctate place fields, or the absence of a strong head direction signal. Interneurons and pyramidal cells were separated on the basis of average firing rate above or below 10Hz respectively, or place field size greater or smaller than one half of the overall open field environment respectively.

### *Optogenetic methods*

During experimental days, 20Hz square pulsatile stimulation (15ms pulse width) was delivered during stimulation epochs of the behavioral sessions during ongoing electrophysiological recording, consistent with prior fear engram reactivation studies (Ramirez et al., 2013; Chen et al., 2019). Laser output was tested (Digital handheld optical power and energy meter console, ThorLabs) before each experiment to ensure at least 8mW power output at the end of a test fiber matching the implanted fibers. Implanted optic fibers were plugged into a branching patch-cable connected to a fiber optic rotary joint and a mono-fiber patch cable leading to a 473nm laser diode controlled by automated software (Doric Lenses). Laser onset and offset was controlled by custom programs made in the Doric Studio software (Doric Lenses).

*Behavioral assays and ensemble tagging*

Prior to onset of behavioral training and surgery, mice were handled for 2-5 minutes per day for at least two days and placed on dox diet. Mice performed behavioral assays during the light cycle of the day (7:00 - 18:00). Prior to surgery, mice were acclimated to foraging for chocolate sprinkles in two mazes with identical proportions to the ones used for experimental recording but made of a white plastic material. After surgical recovery, mice were acclimated to foraging for sprinkles in a 2ft square wooden arena (Context C) painted entirely in orange with 1ft high walls for 10-20 minute sessions daily (Fig. 4.1A). Mice were also habituated to plug-in of both the recording tether and optical patch cord. Short recordings were made to identify electrophysiological signatures of hippocampal activity and guide tetrodes to either the CA1 or DG on the basis of theta phase reversal and spatial tuning properties of recorded well-isolated single units (not included in experimental analyses).

Mice were also acclimated for one 10 minute period to a small, square wooden arena (Context B) painted entirely in blue with dimensions of 8in. x 8in. x 12in. tall mimicking the fear conditioning chamber dimensions. Immediately prior to opening the off-dox tagging window, mice were re-exposed to Context B while plugged into the optical patch-cord and underwent a pre-tagging stimulation and recording experiment (Fig. 4.1A). The stimulation protocol was 2 min. off, 2 min. 20Hz pulses on, 2 min. off, 2 min. 20Hz pulses on., 2 min. off for a total 10 minute exposure (Fig. 4.1D). After this pre-tagging session mice were returned to a clean cage with regular (non-Dox) chow.

Contextual Fear Conditioning (CFC) was performed in a metallic 8in. x 8in. x 11in. tall operant chamber (Context A) with shock grid floor (Coulborn Instruments). The grid floor was swabbed with a rag smelling of lemon (Lysol All Purpose Cleaner). The chamber was surrounded with a removable wall to limit distal cues. The implant was wrapped in a vet wrap adhesive bandage to minimize hard impact. Subjects were then placed in the chamber for 10 minutes during which they received 4 mild (1.0mA) foot shocks each of 2 second duration. After a baseline period of 210sec the first shock was delivered and the following shocks were separated by a 60sec. inter-shock-interval (Fig. 4.1D). After CFC, mice were returned to a clean home cage with Dox diet.

On the following day, mice were recorded in Context B for a post-tagging stimulation session with identical stimulation parameters as the pre-tagging session. After a four hour rest, and for the subsequent four days, mice performed the Open Field foraging task in Context C for 30 min. After a 10 min. baseline period, 30 sec on, 30 sec off trials of 20Hz optical stimulation were delivered for a total of 10x stimulation trials over 10 min (Fig. 4.1D). Recording was continued for 10 min post-stimulation. To minimize cable tangling, the recording was paused after 9 min, the optical patch cord was attached to the optic fibers, and the mice were given a short break. The mice were returned to the arena for the final minute of the baseline epoch before optical stimulation began. On the fifth experimental day mice underwent both the Context B and C paradigms, as on day 1 post-CFC.

After a short break following the Context C open field arena stimulation on Day 5, mice were briefly anesthetized and electrolytic lesions were made at the tip of each

tetrode (High Current Stimulus Isolator, World Precision Instruments inc.). The following day mice were returned to CFC Context A for 10 minutes and sacrificed 90 minutes later to match peak c-Fos expression timing (see Immunohistochemistry section).

Behavior was recorded by an overhead Mako G-131c GigE camera (35fps, Allied Vision) in Context B and C, or by an overhead Logitech C270 webcam (30fps, Logitech) in Context A. Position in all arenas was extracted using Deeplabcut (Mathis et al., 2018). DeepLabCut outputs were further refined by interpolating across occasional tracking jumps outside the arena caused by the superposition of the recording and stimulation cables over the mouse. Video, shock delivery TTL pulses, laser pulse timestamps, spatially scaled position, and neural timestamps were calculated and aligned using the CMBHome framework (https://github.com/hasselmonians/CMBHOME/wiki).

*Histology and immunohistochemistry*

On Day 6, 90 min after the final Context A fear extinction session, subjects were sacrificed with Euthasol (390 mg/kg) and Isoflurane to enable transcardial perfusion with 0.9% saline followed by 10% formalin. Tetrodes were withdrawn and then brains were extracted and soaked in formalin for 2-3 days at 4 ℃. Subsequently, brains were cryoprotected in 30% sucrose solution for another 2-3 days at 4 ℃ prior to slicing on a cryostat.

Immunohistochemistry was performed as previously described (Chen et al., 2019; Wilmerding et al., 2023). Briefly, 50μm slices were blocked for 2 hours at 4 ℃ in 1x phosphate-buffered-saline + 2% Triton (PBS-T) and 5% normal goat serum (NGS). Slices were then incubated for 48 hours at 4 ℃ with primary antibodies diluted in 5%

NGS in PBS-T as follows: rabbit anti-c-Fos (1:1000, Abcam, #190289) and chicken anti-GFP (1:1000, ThermoFisher, #A10262). After the primaries, slices underwent 3x 10 min washes in PBS-T, followed by a 2 hour incubation in the secondary antibodies diluted in 5% NGS in PBS-T as follows: Alexa 555 goat anti-rabbit (1:200; ThermoFihser, #A21429) and Alexa 488 goat anti-chicken (1:200, ThermoFisher, #A11039). Tissue was washed 3 more times for 10 min each in PBS-T. Slices were mounted, covered in a thin line of VECTASHIELD® Hardset™ Antifade Mounting Medium with DAPI (Vector Labs, #H-1500) and cover-slipped. Cover slips were sealed with nail polish 1 day later.

### *Quantification and statistical analysis*

#### *Cell counting*

Images of non-consecutive slices were acquired with an FV10i confocal laser-scanning microscope, using 10x magnification / 0.25 NA objective. DAPI was acquired at 405nm with laser power of 49.3%, eYFP at 473nm with laser power between 4 and 12% and c-Fos at 559nm with laser power of 19.7%.

Custom-trained StarDist neural networks were used to automatically count c-Fos+ and ChR2-eYFP+ cells in the DG granule cell layer (Schmidt et al., 2018; Weigert et al., 2020; Wilmerding et al., 2023). The overlap of each population was automatically calculated using an in-house pipeline (https://github.com/hasselmonians/ImageJ-Automated-Cell-Counter-Algorithm) that performed pair-wise pixel correlations between each cell ROI and excluded cells of vastly different size (<25% volume) and minimal

overlap (<75% of the smaller object) as previously used (Wilmerding et al., 2023). Automated counts were used for increased reproducibility.

### *Behavioral analysis*

Immobility (velocity < 0.5cm/sec) was used in lieu of freezing due to the lack of widely adopted freezing analysis packages for overhead video data with cable artifact. Previous fear conditioning studies employing electrophysiological recording tethers used a similar immobility threshold method (Moita et al., 2004). Immobility probability was calculated as the proportion of immobile frames for each behavioral epoch (e.g. the first stimulated 2min. period in Context B). In the fear chamber, 5x 60sec epochs were used starting one minute prior to the first shock and ending one minute after the final shock, with equivalent time points selected for the Day 6 fear extinction session. In the open field (Context C), the center dwell time (P(Center)) was calculated as the number of frames in which the mouse was within a 1-foot square box at the center of the arena divided by the total frames in that epoch.

### *Local field potential analysis*

Local field potential (LFP) was analyzed using the Spectral Connectivity package (https://github.com/Eden-Kramer-Lab/spectral_connectivity) and visualized in Matlab (Denovellis et al., 2022). A linear regression model on the LFP using the binarized laser state at 0msec time lag as a predictor was created in order to remove potential opto-electric artifact. The model residuals were used for subsequent analyses. Multitaper objects were constructed with a time half-bandwidth product of 3 and 60sec time window

durations. Spectra were averaged over time windows and tapers within epoch (off or on stimulation) for the purposes of calculating spectral power or within session for coherence. Model pulse trains of 15msec pulse width at 19Hz or 21Hz were generated for the purpose of comparing coherence magnitude and phase specificity to the true 20Hz pulse sequence (Fig. 4.2F,G). For visualization purposes, the spectrogram was calculated with 5 sec window durations and 2.5 sec overlap.

*Stimulation and spatial response analysis*

A nested GLM approach was taken to quantify the number of engram stimulation responsive cells using the Point Process Neuron package (https://github.com/hasselmonians/pippin) as previously described (Alexander et al., 2020). Briefly, head direction, velocity, spatial position and binarized laser state (1's in the laser-on time bins) were used as predictors of firing rate in 500 ms bins. A leave-one-out approach tested the difference in deviance of the reduced model against the full model using a Chi-squared distribution. A conservative threshold of $p < 0.01$ was used as a cutoff for models that performed significantly better with the laser state predictor included, indicating an opto+ cell. 10-fold cross validation was used to test each cell. For the purposes of correlation and statistical testing, the Z-scored firing rate of each unit was also calculated against the mean and standard deviation of that cell's firing rate in the pre- and post-stimulation epochs over 60sec intervals.

Spatial information was calculated by epoch after thresholding each cell for spikes occurring above a velocity of 2cm/sec. Spatial correlations were calculated

between the speed-thresholded, occupancy-normalized spatial firing rate maps across epochs on a bin-for-bin basis.

### *Population vector correlations*

Population vector correlations (PVCs) were calculated using the binned firing rates (500msec bins) of pyramidal units. The mean rate of each bin was removed from the matrix of firing rates and the resulting matrix correlated to itself with a Spearman correlation for both the full matrix and trial-averaged matrix.

### *Linear discriminant analysis (decoding)*

Linear classifiers were trained on 500 ms bin size population firing rate vectors using the classify function in Matlab. For the first set of decoders, a random 50% of the laser-on time bins (spanning trials) were selected and an equivalent number of bins from the laser-off time periods (spanning epochs) were used as training data. A random set of hippocampal neurons (Pyrs and INs) were drawn for each shuffle and used in both the training and testing of that decoder. Different numbers of neurons, up to n-1 of the whole population, were used to show the improvement of the classifier with additional network size. For the cell tuning specific classifiers, n = 25 random high Z-score magnitude (top 20%), low Z-score magnitude (bottom 20%) and high pre to post-stim spatial correlation (top 20%)  cells were chosen per shuffle. Next, n = 25 cells were randomly drawn per shuffle from the top and bottom 20% of the sorted raw Z-scores to compare the contribution of positively and negatively stimulation responsive cells, respectively. Lastly, for the cross-epoch generalizing decoders, classifiers were trained on a

combination of 5/6ths of the data from one or more randomly selected stimulation trials and 60 randomly chosen laser-off time bins (spanning epochs; equivalent to one full laser-on trial). Decoding accuracy was tested on the $1/6^{th}$ held-out data from the trained trials and on all bins from the held-out, untrained trials and equivalent random bins from the laser-off epochs. Equivalent control shuffles were created for the increasing cell # and epoch # classifiers using matched cell or epoch numbers but randomly shuffled bin labels. Prediction accuracy is reported as the mean of the true positive and true negative rate, with proportions of laser-on and off test data chosen such that chance stands at 0.5 or 50%. 500 shuffles were performed for each decoder.

### *Statistics*

One and two way repeated measures ANOVA models were run for behavioral analyses in Contexts A, B and C, for spatial information and spatial correlation tests, and for linear decoders with increasing cell counts and training trials. One way independent ANOVA models were made for the population vectors and for linear decoders using different subsets of cells. Pearson's rank correlations were used for the spatial correlations and between the spatial correlation and Z-score values. Bonferroni corrected or Tukey's HSD p-values are reported for all post-hoc tests. Throughout all figures, error bars indicate +/- SEM as do the shaded patches on the spike rasters in Fig. 4.3B. Test statistics, groups sizes, and p-values are reported in figures or legends. All tests were performed in Matlab 2019b using publicly available functions. For all figures, n.s. = $p > 0.05$, * = $p < 0.05$, ** = $p < 0.01$, *** = $p < 0.001$.

## Results

*Experimental paradigm and histology of recording HPC fear engram ensembles*

To examine the circuit effects of artificial engram reactivation, we context fear conditioned (CFC) mice in a small fear chamber, and then optogenetically reactivated the fear ensembles in dentate gyrus (DG) while the mice explored other environments (Fig. 4.1A). Mice were implanted with 8-tetrode custom microdrives with unilateral electrode targeting to right HPC and bilateral optic fibers to stimulate DG (Fig. 4.1B). In order to limit the temporal expression of the ChannelRhodopsin-2 (ChR2) construct to the CFC experience, we used the c-Fos-tTA immediate-early-gene tagging paradigm inhibited by doxycycline (Dox) in the subjects' diet (Ramirez et al., 2013; Redondo et al., 2014; Chen et al., 2019). While on Dox, subjects were acclimated to an open field foraging task appropriate to detect place cells during which time bundles of tetrodes were advanced into hippocampal CA1 or DG based on local field potential (LFP) characteristics and preliminary analyses of spatial tuning property in single-units. Removal of the Dox diet opened a short window during which endogenous c-Fos produced by cellular activity or plasticity in virally transfected DG cells induced the expression of ChR2-eYFP (Fig. 4.1C). Further expression was inhibited by reintroduction of dox diet during subsequent stimulation and recording experiments. Finally, mice underwent a final fear extinction session for 10 min in Context A and were sacrificed 90 min later to optimally visualize c-Fos expression. Histological staining and visualization confirmed the recording location of the tetrode bundles and successful viral expression of ChR2-eYFP in a sparse cell

population limited to DG (Fig. 4.1E-G). Figure 4.1D summarizes the CFC and optogenetic methods used during the behavioral tasks.

*Fear engram reactivation drives slight freezing and robust network synchrony*

We first examined the outcomes of CFC and fear engram reactivation in the small box. Mice spent more time immobile (speed < 0.5cm/s) as a function of shock delivery during conditioning, indicating successful fear acquisition (Fig. 4.2A). During the fear extinction session, mice exhibited a high amount of immobility during baseline which modestly decreased across time, confirming an aversive memory for the Context A chamber (Fig. 4.2A). Prior to CFC engram tagging, laser pulse delivery did not increase immobility relative to baseline (Fig. 4.2B). After engram tagging, optogenetic reactivation of DG-mediated CFC fear ensembles in Context B drove a slight increase in immobility across the whole session, although there was no difference in freezing between laser-on and off epochs (Fig. 4.2B). The effect size and lack of laser epoch specificity were surprising and may be a result of the low number of subjects included relative to prior engram studies (Ramirez et al., 2013; Chen et al., 2019), or the use of contextual fear conditioning in lieu of tone-shock conditioning (Liu et al., 2012).

After verifying the behavioral relevance of the artificial engram ensemble reactivation, we examined the effects on the hippocampal network during engram stimulation. We observed an increase in 20Hz (and its harmonics) power during Context B stimulation sessions after Day 0 CFC which matched the timing of stimulation epochs (Fig 4.2C). An opto-electric artifact could have driven the increase in 20Hz spectral

power, so the pulse sequence was regressed out of the LFP signal. We noted some remaining artifact at 20Hz during stimulation epochs prior to tagging on Day -1, suggesting leakiness of the Dox inhibitor labeling cells prior to the tag day (Fig. 4.2D). However, 20Hz spectral power strongly increased above this level after CFC in both the DG and CA1, suggesting that stimulation of DG engram ensembles promotes network oscillatory synchrony within region and downstream (Fig. 4.2D,E). As a comparison, the change in theta power in laser-on epochs relative to laser-off remained largely consistent across days (Fig. 4.2E). No formal hypothesis tests were made due to the confound of sampling individual electrodes from the same mice and region. To confirm this result, we compared the phase coherence between each electrode and a signal composed of the 20Hz pulses and found a low coherence magnitude prior to CFC which increased strongly after tagging (Fig. 4.2F). No increase was observed for neighboring 19Hz or 21Hz frequencies. The coherence phase also shifted to be largely consistent at an average of 69 degrees lagged to the 20Hz pulses (Days 1 and 5), although there was some heterogeneity between electrodes and across sessions (Fig. 4.2G). Together, these results suggest that artificial engram reactivation drives frequency-specific, phase coherent network synchrony within and across regions.

*Fear engram reactivation reduces spatial tuning in a downstream reader*

We next analyzed the effects of fear engram reactivation in the open field environment split across the three 10 min epochs of pre-stimulation (pre), stimulation (stim), and post-stimulation (post). Distance traveled, average run speed, and time spent in the center of the arena decreased slightly across epochs, suggesting an effect of

satiation on the foraging task (Fig. 4.3A). Curiously, the time spent immobile also decreased with time, perhaps as the animals shifted from a more ballistic start-and-stop strategy to a slower continuous exploration strategy. Arena exploration remained sufficiently broad to observe place fields during the stim and post-stim epochs, enabling further investigation (Fig. 4.3B example spatial coverage maps).

To understand the effect of artificial engram stimulation of an upstream region on downstream dynamics, we explored the spatial firing and peri-stimulus spiking of CA1 pyramidal cells. Many cells exhibited spatially-tuned firing properties, or place fields, as described previously (O'Keefe & Dostrovsky, 1971; O'Keefe, 1976; Muller et al., 1987) some with multiple firing fields as is more common in mouse than rat (Mou et al., 2018). While some cells were spatially stable across epochs (Fig. 4.3B unit 4), others increased their firing in a spatially non-specific manner (Fig. 4.3B unit 5), or spatially remapped (Fig. 4.3B unit 3) during engram stimulation. Stimulation trial-aligned rasters and average firing rate plots confirmed the effect of DG engram stimulation on acutely driving or suppressing single unit firing (Fig. 4.3B raster plots, see also 4.4A,B). Peri-pulse histograms verified the consistent timing of spikes relative to individual pulses in responsive cells as compared to spikes in the baseline period or spikes in non-responsive cells (Fig. 4.3B). To quantify the proportions of engram stimulation-responsive cells in the CA1, each cell was fit with a generalized linear model (GLM) including spatial and laser-state predictors. Cells were classified as optogenetic stimulation-responsive (opto+) if the GLM outperformed a version of the model without the laser-state predictor (see Methods) or non-responsive (opto-) if not. Roughly 59% (45 cells) were opto+ across

both mice with HPC units (Fig. 4.3C). Note that while many cells were opto+, the changes in firing rate were indirectly driven by upstream stimulation in the DG acting on the CA3 and CA1 cells which were not virally transfected with ChR2-eYFP (Fig. 4.1E). These initial observations suggested a heterogeneous response of the CA1 network to external perturbation of a memory-associated DG population.

We next quantified the outcome of engram stimulation on spatial tuning in opto+ and opto- units across epochs. Spatial information decreased during the stim and post-stim epochs, with opto+ cells losing more spatial information during the stim epoch than opto- cells (Fig. 4.3D). While some drop in SI might relate to the decrease in distance traveled during the stim and post epochs (Fig. 4.3A), the specific decrease in the opto+ population represents an additional disruption of spatial coding. We built on this finding by examining the correlation of spatial firing maps across epochs, as it appeared that even strongly opto+ cells could have consistent place fields between the pre and post-stim epochs (Fig. 4.3B units 3 & 5). Indeed, there was no main effect of epoch on spatial correlation but an interaction effect such that opto+ cells specifically had higher spatial correlation between the unstimulated epochs (Fig. 4.3E). Lastly we correlated the spatial correlation value of all the cells to their Z-scored firing rate change during stimulation. No relationship was found for the pre to stim comparison (Fig. 4.3F) but the pre to post comparison showed a linear relationship with strength of engram responsiveness (Fig. 4.3G). Taken together, these results reveal that the CA1 loses spatial specificity during engram stimulation but that opto+ cells can recover their pre-existing location tuning after acute artificial perturbation.

*Population activity decorrelates during stimulation*

We then investigated the effects of engram modulation at the CA1 population level. The self-normalized firing rate of all HPC units across mice and sessions, including INs, was sorted based on each cell's Z-scored stimulation responsiveness relative to baseline to create a "mega-mouse" firing raster (Fig. 4.4A). While subtle increases or decreases of firing rate during individual 30 sec stimulation trials could be seen, the response became clearer when the same map was created from a trial-averaged firing rate for each neuron, with matched averaged time periods from the pre and post epochs (Fig. 4.4B). To confirm that this was not merely a gestalt effect of trial-averaging, the firing rate of the top 10% of opto+ cells was averaged to show trial-specific increases in spiking for each trial (Fig. 4.4C left). The same was done for the bottom 10% of Z-scored cells (which were also opto+) to show a decrease in firing rate during most stimulation trials and a modest rebound effect between trials (Fig. 4.4C right). Finally, we correlated the activity vector of the network for each time bin against all other time bins to create a population vector correlation (PVC) for the full firing rate matrix (Fig. 4.4D) and the trial-averaged matrix (Fig. 4.4E; S. Leutgeb et al., 2005; Jou et al., 2023). Comparison against the baseline epoch showed a slight 'checkerboard' effect of alternating high and low correlation during the stim period, although there were only minor differences in overall PVC across time (Fig. 4.4F,G). To tease out the effect of stimulation, we next examined the trial-averaged PVC which exhibited more obvious within-epoch synchrony and found the stim epoch to be most strongly decorrelated from baseline compared to the adjacent laser-off and post-stimulation periods (Fig. 4.4G). The network state partially

recovered during the post-stim period (Fig. 4.4G). In summary, fear engram stimulation drives a change in network state which is partially reversible.

*CA1 firing rate decodes a consistent network state during engram reactivation*

Lastly, we sought to determine whether single unit activity from the open field sessions could be used to reliably decode the presence or absence of optogenetic modulation. A linear classifier was trained on random samples of half the binned firing rate data from the stim epoch and an equal amount of data from all the laser-off epochs (see Methods). The decoder was able to predict the presence or absence of optogenetic stimulation above chance using even as few as 2 neurons (Fig. 4.5A). Increasing the number of neurons used by the classifier increased decoding accuracy significantly. Next, various subsets of HPC cells defined by their spatial or engram modulation responses were used to train new decoders. Matching for numbers of cells used, stimulation responsive units decoded significantly better than all other tested cell types (Fig. 4.5B). Furthermore, cells with high spatial correlation between the pre and post-stim epochs decoded at higher levels than non-responders or random pyramidal cells, corroborating the previous finding relating degree of engram modulation and spatial stability before and after stimulation (Fig. 4.5B, 4.3E,G). The increase in decoding accuracy was largely driven by cells that increased firing rate during stimulation, rather than decreasing it (Fig. 4.5C).

Finally, we trained another set of decoders using data from a subset of stimulation trials to test whether the network was repeatably modulated by engram reactivation.

Training on even a single trial (e.g. the fifth 30-sec laser-on period) yielded classification accuracy of other trials and laser-off periods above chance (Fig. 4.5D). Prediction of held out data from within each training trial confirmed the performance of the classifier (Fig. 4.5D green line). Increasing the number of training periods used improved prediction accuracy. In sum, these results indicate the network state could be reliably decoded at the level of single units and that this artificially driven state was repeatable across stimulation periods given that data from one trial could accurately decode the network state during other trials.

## Discussion

We present preliminary evidence exploring the outcome of artificial memory reactivation within the dentate gyrus of hippocampus on single unit and network dynamics in downstream CA1. Our early findings show a number of effects including the frequency-specific entrainment of multiple HPC regions during engram stimulation (Fig. 4.2). Additionally, stimulation drove a reduction in spatially specific firing in a subset of CA1 neurons responsive to upstream engram stimulation (Fig. 4.3). Curiously, this same population exhibited more consistent spatial firing before and after the stimulation (Fig. 4.3). Lastly, we showed that in the absence of a strong overt behavioral phenotype during stimulation, the internal network dynamic nevertheless shifted to a partially replicable and readily-decodable state reflecting the stimulation (Fig. 4.5). These results are consistent with the hypothesis that engram stimulation drives pre-configured network

dynamics (Jou et al., 2023) but also suggest that uncommon rhythms (i.e. 20Hz) could support changes in behavior.

*Network dynamics bridging memories to behavior*

Early work on stimulating engram ensembles demonstrated marked effects on memory-guided freezing behavior and stimulus-driven spiking in anesthetized and *ex vivo* brains (Ramirez et al., 2013; Cowansage et al., 2014; Denny et al., 2014; Redondo et al., 2014) but the question remains how artificial memory stimulation alters networks during awake, freely-moving behavior. Fear conditioning, especially contextual fear conditioning (CFC), drives place field and rate remapping in CA1, especially around the shock location (Moita et al., 2004; Schuette et al., 2020). While our data do show some example cells transiently remapping their field location (Fig. 4.3B unit 1), these changes in firing pattern were largely limited to the stimulation epoch given the high rate of pre and post-stimulation map stability in engram stimulation responsive (opto+) cells. This transient disruption is consistent with a preprint study which altered CA1 network activity specifically during the period of stimulation of a CA1 engram (Jou et al., 2023). Furthermore, CA1 cells responded to transient perturbation by heterogeneously changing firing rate (Fig. 4.4A,B) and reducing spatial information (Fig. 4.3D), rather than largely decreasing firing rate but increasing spatial information as seen during CFC (Schuette et al., 2020). We did not observe a specific reduction in interneuron firing rate during engram stimulation as might be expected during novel experiences (M. A. Wilson & McNaughton, 1993), although very few HPC interneurons were recorded. Prior false memory creation studies stimulated engrams of a novel neutral context during shock

conditioning which allowed behavioral expression at later time points, suggesting a more permanent remapping (Garner et al., 2012; Ramirez et al., 2013). Behaviorally, mice continued to show extensive pre-stim behavioral exploration across sessions in line with the transient network effects of DG engram reactivation (Fig. 4.3A). The maintenance of exploratory behavior even after negative memory recall is consistent with the ability for the HPC to support multiple maps of the same environment (Sheintuch et al., 2020). These preliminary findings suggest that short retrievals of negative memories in familiar, safe environments do not 'overwrite' the existing hippocampal map of that environment, which may be of interest in interpreting clinical treatment of anxiety and post-traumatic stress disorders involving negative memories.

*Memory or map? Between a Fos and a hard place cell*

The relationship between engram neurons and the cognitive map is still murky, especially given the ambiguity of immediate-early genes like c-Fos for neural activity. Individual action potentials do not monotonically relate to the quantity of c-Fos expression (Labiner et al., 1993). Indeed, a recent preprint study suggests c-Fos may be induced not by cellular action potentials but in response to slow (0.1Hz) or fast synaptic input (50Hz) but not intermediate frequencies (Anisimova et al., 2023). The presence of c-Fos in CA1 pyramidal cells may drive functional ensemble formation via peptidergic signaling with interneuron populations (Yap et al., 2021) and contribute to place field formation, spatial stability, and reliable spatial maps (Pettit et al., 2022). Yet, prior electrophysiological evidence suggests that in novel environments c-Fos negative place cells are more reliable spatial anchors while c-Fos expressing place cells contribute more

to memory discrimination than navigation (Tanaka et al., 2018). The present study did not specifically address this debate, but the question of how sparse DG populations influence downstream CA1 spatial maps is relevant. We found that artificial stimulation reduced spatial information in a subpopulation of CA1 cells that nevertheless exhibited a stable spatial code outside of the memory recall epoch (Fig. 4.3D,E). Prior to stimulation, these cells were indistinguishable from non-responders in terms of spatial information, perhaps due to much more extensive experience with the arena, similar to Pettit et al. It is possible that the opto+ CA1 subpopulation constituted its own c-Fos expressing engram population, though chronic *in vivo* imaging methods would be needed to adequately investigate the relationship to c-Fos expression and spatial mapping.

*Considerations for neural outcomes of engram reactivation*

What are the consequences of artificial memory stimulation? Optogenetic reactivation entrained multiple HPC regions from the DG to CA1, consistent with a previous study demonstrating enhancement of theta power during 8Hz DG engram stimulation (Rahsepar et al., 2023). Interestingly, some studies were able to drive behavior by stimulating a CA1 engram at 20Hz (Ohkawa et al., 2015) while others were not (Ramirez et al., 2013) or had to rely on 4 or 8Hz stimulation (Rahsepar et al., 2023; Ryan et al., 2015). Both frequency and pulse shape are important to driving spiking (Padilla-Coreano et al., 2019; Wilmerding et al., 2022), which our paradigm circumvented by leveraging upstream regions to drive 20Hz spiking in CA1 pyramidal units (Fig. 4.3B). One preprint found that stimulation of a behaviorally verified CA1 active place avoidance engram transiently drove cell firing for ~30sec and decorrelated

the population activity from baseline (Jou et al., 2023), similar to our findings (Fig. 4.4G). During this time, however, Jou et al. found pre-existing spike relationships between individual cells were preserved as were low-dimensional population activity measures, suggesting that engram reactivation relies on pre-existing network architecture and functional connectivity (Dragoi & Tonegawa, 2013; Villette et al., 2015). The presence of engram modulation on the CA1 network state was readily decodable, even when training classifiers on a small subset of the stimulation trials suggesting a stable underlying circuit (Fig. 4.5). though it remains to be demonstrated whether pre-existing spike relationships between cells existed before the onset of stimulation in our data.

*Limitations and conclusions*

Further recordings will be needed to confirm the initial results discussed above. Additionally, the relationship of engram stimulation to sharp-wave ripples and replay would be valuable for understanding how specific contextual memories may be broadcast to the neocortex during memory consolidation. Analysis of the spike timing relationships between active CA1 cells before, during and after engram stimulation in DG would be informative for resolving the question of how simultaneous activation of sparse DG populations can lead to the expression of memory-guided behaviors, perhaps via meaningful sequence generation in the downstream CA3 and CA1 regions (Stark et al., 2015). Our current results support the hypothesis that DG engram stimulation entrains downstream hippocampal regions at the network and single cell level by engaging an existing network of spatially tuned cells.

## Acknowledgments

We thank the Hasselmo and Ramirez labs for thoughtful feedback and commentary on the work, in particular Bill Chapman, Lucas Carstensen, and Andy Alexander.

This work was supported by the National Institutes of Health [grant numbers: R01 MH052090, MH060013, MH120073, HD101402-02; and DP5 OD023106-01], and the Office of Naval Research [grant numbers: MURI N00014-16-1-2832, N00014-19-1-2571; and DURIP N00014-17-1-2304].

## Author Contributions

Conceptualization, L.K.W., S.R., and M.E.H.; Methodology, L.K.W., and W.B.S.; Investigation and data acquisition, L.K.W., W.B.S.; Writing – Original Draft, L.K.W.; Writing – Review & Editing, L.K.W.; Funding Acquisition, M.E.H. and S.R.; Formal Analysis, L.K.W.; Visualization, L.K.W.; Supervision, M.E.H. and S.R.

## Declaration of Competing Interests

The authors declare no competing interests

## Figures

**Figure 4.1**

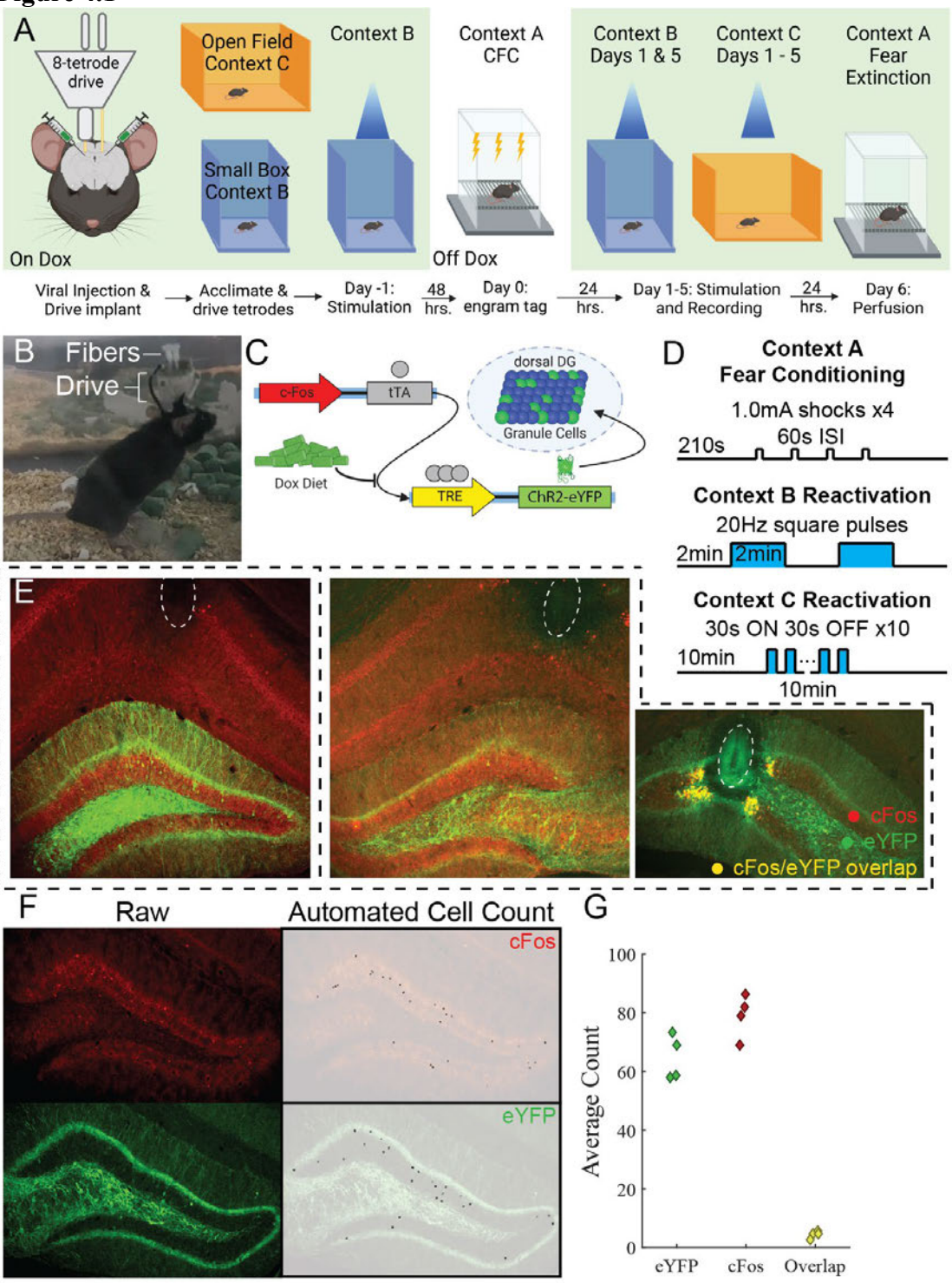

**Figure 4.1. Experimental paradigm and histology of recording HPC fear engram ensembles.**

**A)** Experimental timeline. N = 4 mice underwent bilateral viral injections in DG and surgical implantation of a microdrive containing unilateral tetrodes and bilateral fibers. Mice were acclimated to foraging in an open field (many exposures) and small box (1 exposure) during tetrode lowering. Day -1: 1x pre-tagging stimulation session in Context B (see E) served as a behavioral and physiological recording control. Day 0: Contextual Fear Conditioning (CFC) and engram tagging in Context A (see E). Days 1-5: daily recording and stimulation session in Context C (see E). Days 1 and 5 included a Context B recording and stimulation session. Electrolytic lesions performed after final experiment on Day 5. Day 6: 10 min fear extinction 90 min prior to perfusion. Presence or absence of Dox inhibitor noted by green or white background, respectively. A & C created with BioRender.

**B)** Example microdrive implant.

**C)** Viral approach for ChR2-eYFP expression in DG cells temporally gated by absence of doxycycline (Dox) inhibitor in diet (see Methods).

**D)** Shock and stimulation protocols. Context A (CFC): 4x moderate, 2-sec 1.0mA foot shocks administered at 60 sec intervals after a 210 sec acclimation period. Context B (small box): 2x 2 min optogenetic stimulation periods between 3x 2 min laser-off periods. Context C (open field): 3x 10 min epochs including pre-stimulation, stimulation and post-stimulation. Stimulation comprised 10x 30 sec laser on, 30 sec laser off trials.

**E)** Example histology demonstrating tetrode lesions (dark halos) in 2 mice delineated by dashed borders. One mouse had simultaneous CA1 and DG targeting.

**F)** Cell counting example using automated neural network identification of c-Fos and eYFP positive cell bodies in DG granule cell layer.

**G)** Visualization of average eYFP (engram) and c-Fos-mCherry (Context A re-exposure) populations and the overlap between them demonstrating similar quantities in N = 4 mice.

**Figure 4.2**

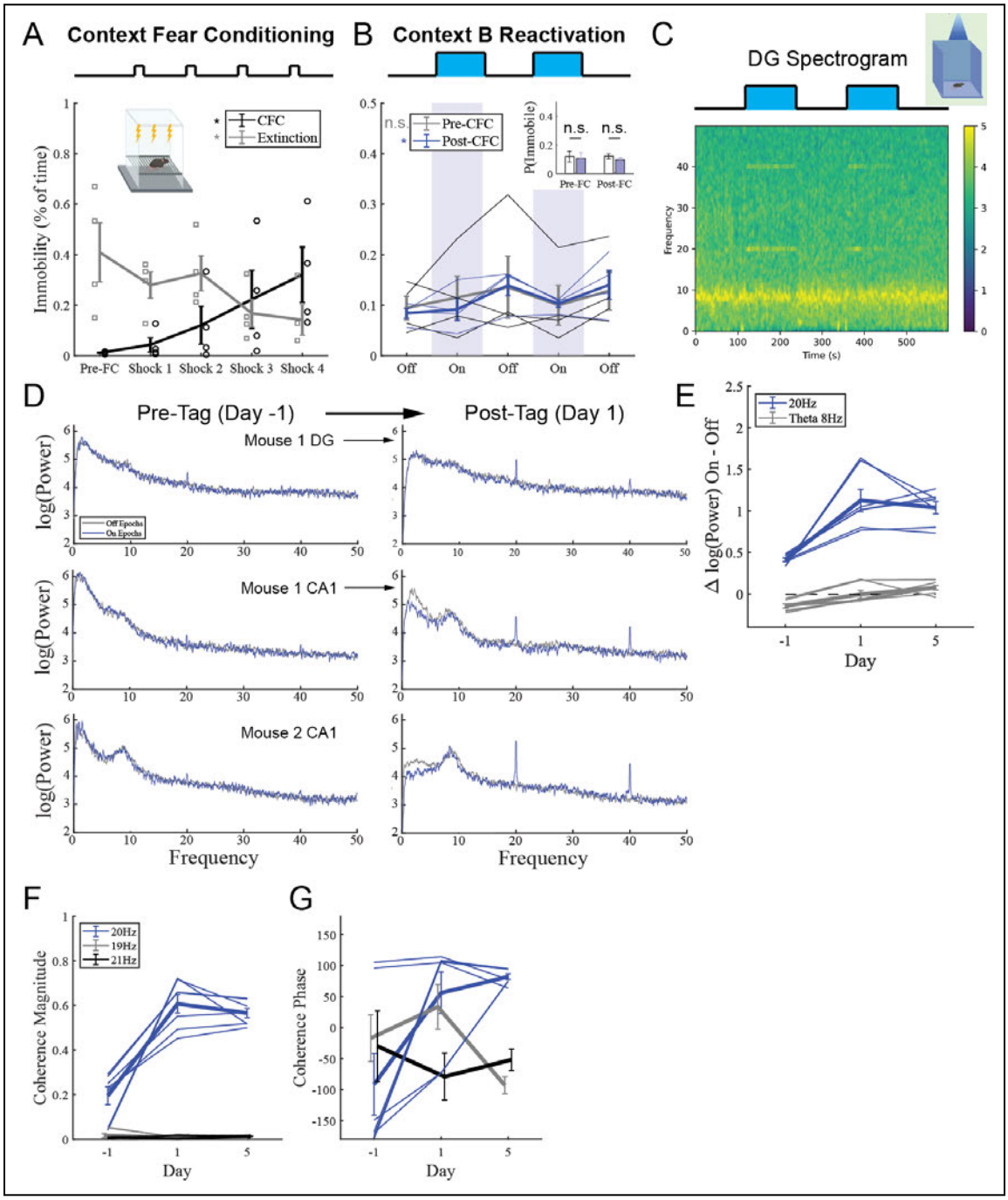


**Figure 4.2. Fear engram reactivation drives slight freezing and robust network synchrony.**

**A)** Contextual fear conditioning (CFC) increases immobility as a function of shock ($F_{(4,12)}$ = 5.02, p = 0.013). Fear extinction reduces immobility across equivalent non-shocked time points ($F_{(4,12)}$ = 3.65, p = 0.036).

**B)** Pulsatile stimulation does not increase freezing across time prior to CFC (grey lines; $F_{(4,12)} = 0.66$, $p = 0.63$) but slightly increases freezing across the session after CFC (blue lines; $F_{(4,12)} = 4.29$, $p = 0.022$). Inset: No difference was found in mean immobility between on and off epochs before or after CFC (RM t-test; Pre: $t = 0.81$, $p = 0.48$; Post: $t = 2.18$, $p = 0.12$).
**C)** Spectrogram of DG LFP during Context B fear engram reactivation. Note the increase in 20Hz power at 2 and 6 minutes corresponding to the stimulation onset.
**D)** Power spectra of three example electrodes (rows) from two regions and two mice before (left) and after tagging (right). Grey indicates average power during laser-off epochs, blue for laser-on.
**E)** Difference in 20Hz power between laser off and on epochs increases after tagging and remains high across days. Change in theta power across epochs is largely identical pre and post tagging. No formal comparisons made for E-G due to confounded electrodes within the same region and mouse.
**F)** Coherence magnitude between 20Hz LFP and 20Hz optogenetic pulse sequence, but not a 19Hz or 21Hz sequence, increases after tagging and remains high across days.
**G)** Coherence phase offset between the LFP and 20Hz optogenetic pulses, but not 19Hz or 21Hz pulses, becomes more consistent across time. Individual electrodes plotted for 20Hz only to improve readability.
N = 4 mice for A-B. n = 7 electrodes for E-G

**Figure 4.3**

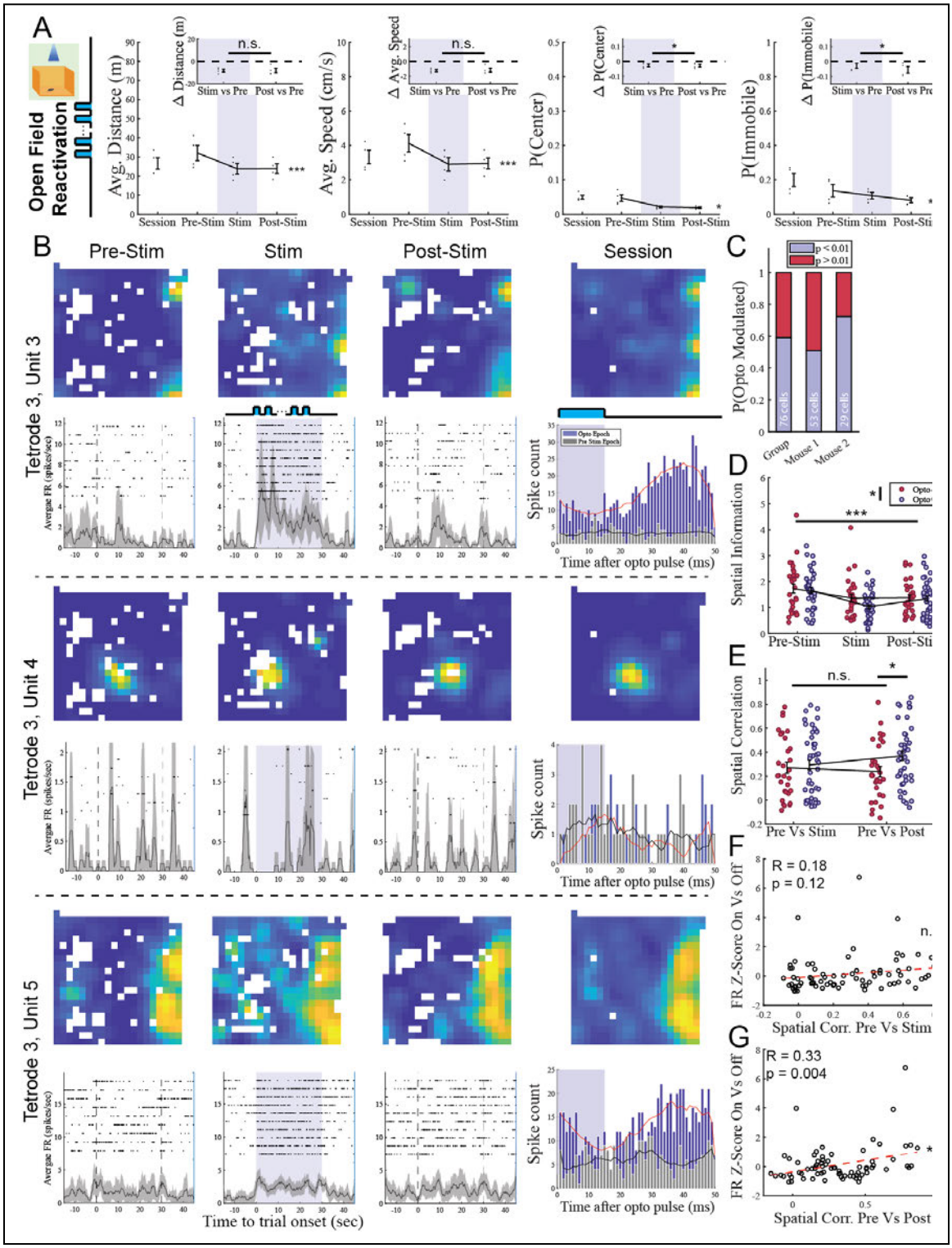
A
Open Field Reactivation
Avg. Distance (m)
Δ Distance (m)
n.s.
Stim vs Pre
Post vs Pre
Avg. Speed (cm/s)
Δ Avg. Speed
P(Center)
Δ P(Center)
P(Immobile)
Δ P(Immobile)
Session
Pre-Stim
Stim
Post-Stim
B
Pre-Stim
Stim
Post-Stim
Session
Tetrode 3, Unit 3
Tetrode 3, Unit 4
Tetrode 3, Unit 5
Average FR (spikes/sec)
Spike count
Opto Epoch
Pre Stim Epoch
Time after opto pulse (ms)
Time to trial onset (sec)
C
P(Opto Modulated)
p < 0.01
p > 0.01
76 cells
53 cells
19 cells
Group
Mouse 1
Mouse 2
D
Spatial Information
Pre-Stim
Stim
Post-Sti
E
Spatial Correlation
Pre Vs Stim
Pre Vs Post
F
FR Z-Score On Vs Off
R = 0.18
p = 0.12
Spatial Corr. Pre Vs Stim
G
FR Z-Score On Vs Off
R = 0.33
p = 0.004
Spatial Corr. Pre Vs Post

**Figure 4.3. Fear engram reactivation reduces spatial tuning in a downstream reader.**

**A)** The average distance traveled, speed, immobility and arena center exploration decreased across time during open field foraging (Distance: $F_{(2,6)} = 17.56$, $p = 0.0031$; Speed: $F_{(2,6)} = 19.60$, $p = 0.0023$; Immobility: $F_{(2,6)} = 5.50$, $p = 0.044$; Center: $F_{(2,6)} = 8.61$, $p = 0.017$). The change in behavior relative to baseline was not different between the stimulation and post-stimulation epochs for distance and speed (RM t-test; Distance: $t = -0.041$, $p = 0.97$; Speed: $t = -0.20$, $p = 0.85$) but slightly differed on immobility and center dwell time (RM t-test; Immobility: $t = 4.25$, $p = 0.024$; Center: $t = 3.25$, $p = 0.048$). N = 4 mice.

**B)** Example speed-thresholded spatial rate maps (upper panels, $3cm^2$ bin size) and trial-aligned firing rasters (lower panels, 60-sec windows) for three CA1 cells during the same open field recording session. Whole session rate map displayed to the right of the post-stim rate map. The first and third unit exhibit stable spatial tuning pre- and post-stimulation and a marked increase in firing rate during the stimulation block. The second unit is unresponsive to stimulation and maintains a stable field across epochs. Below the session rate map, the laser pulse-timed spike histogram is shown as a 50 ms window after the onset of every pulse in the stimulation epoch (blue) and equivalent time points in the baseline epoch (grey) with smoothed average in red and black respectively.

**C)** Visualization of the proportion of stimulation responsive/non-responsive pyramidal units determined by a GLM (see Methods) split by total population and N = 2 mice. Total number of cells per group included in each bar.

**D)** Spatial information (SI) decreases during stimulation and post-stimulation ($F_{(2,120)} = 28.59$, $p < 0.001$) with a significant interaction between higher SI stimulation non-responsive cells than responsive cells ($F_{(2,120)} = 3.34$, $p = 0.034$). n = 31 non-responsive pyrs, 45 responsive pyrs.

**E)** No main effect of epoch on correlation between spatial rate maps relative to baseline ($F_{(1,71)} = 0.35$, $p = 0.56$) but a significant interaction between stimulation responsive cells which showed higher correlation than non-responsive cells ($F_{(1,71)} = 4.12$, $p = 0.046$). n = 31 non-responsive pyrs, 45 responsive pyrs.

**F-G)** Spatial correlation between the pre-stim and stim epoch (F) did not correlate to the Z-scored firing rate modulation by stimulation (Pearson's $R = 0.18$, $p = 0.12$) but did correlate between the pre-stim and post-stim epoch (G) and Z-scored firing rate modulation ($R = 0.33$, $p = 0.004$). n = 76 pyrs.

**Figure 4.4**

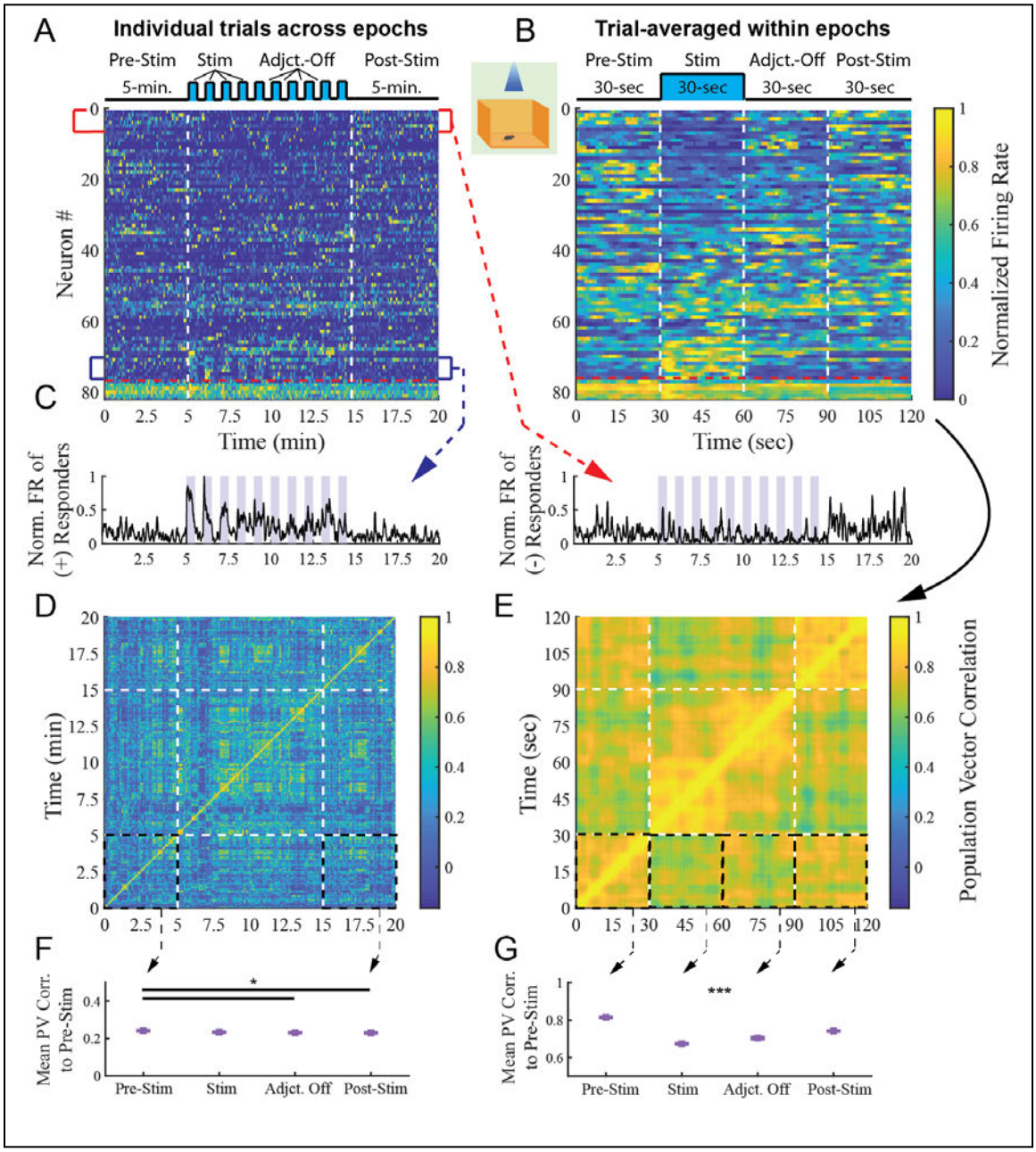


**Figure 4.4. Population activity decorrelates during stimulation.**

**A)** Normalized firing rate (500 ms bins) of all HPC units sorted by Z-scored stimulation response across 5 min pre-stim, 10x 30 sec stim trials interleaved with 10x 30-sec adjacent off periods and 5-min post-stim. Interneurons separated below the red dashed line. n = 82 cells.

**B)** The same as A but with trial-averaged data of 10x 30 sec trials from within each epoch. Adjacent off stim period between stim trials shown to the right of the stim bins.

**C)** Average of the normalized firing rate of the top (left) and bottom (right) 10% Z-scored stimulation responsive units across the same time periods depicted in A. n = 8 units each.
**D)** Population vector correlation (PVC) of pyramidal units across the same time periods depicted in A. Black dashed boxes mark example comparisons used in F. Individual demarcation of stim trials not shown to improve readability
**E)** Trial-averaged PVC of pyramidal units across the same time periods depicted in B. Black dashed boxes mark all comparisons made in G.
**F)** The average PVC to baseline differed across epochs ($F_{(3,2394)} = 3.61$, $p = 0.013$) with post-hoc tests revealing a minor difference in the pre-stim and adjacent groups ($p = 0.034$) and pre-stim and post-stim groups ($p = 0.016$) but no other differences. n = 600 bins per group.
**G)** Same as F but for the trial-averaged PVC to baseline differing across epochs ($F_{(3,236)} = 272.24$, $p = < 0.001$) with post-hoc tests revealing differences between all groups at the level of $p < 0.001$. n = 240 bins per group.

**Figure 4.5**

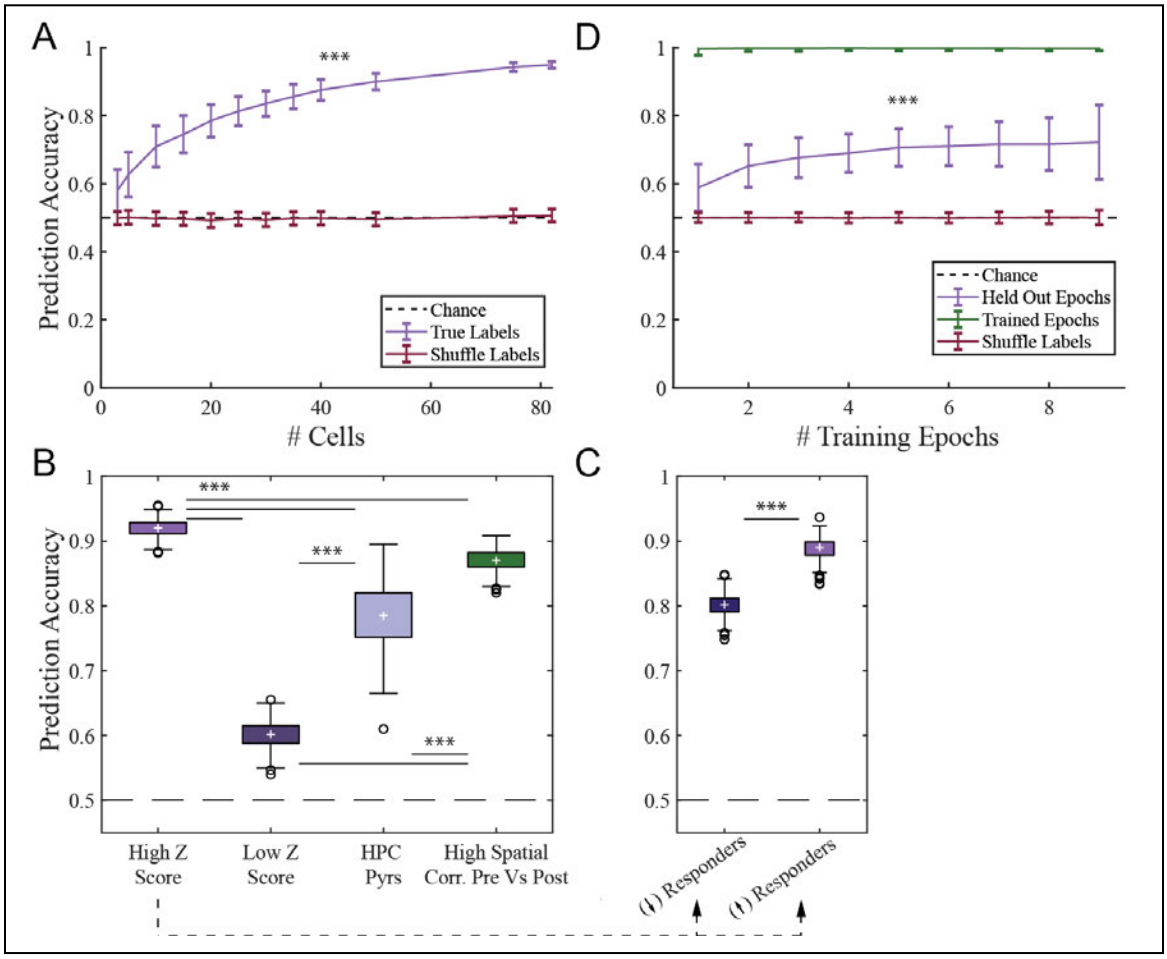


**Figure 4.5. CA1 firing rate decodes a consistent network state during engram reactivation.**

**A)** Linear decoder predicts laser state based on single unit firing rates, improving with more cells ($F_{(11,10978)} = 3037.1$, $p < 0.001$). There was an interaction between # of cells and label type ($F_{(11,10978)} = 2944.7$, $p < 0.001$), and the true labels outperformed the shuffled labels in all cases (Bonferroni-corrected $p < 0.001$ for all comparisons). n = 2, 4, 9, 14, 19, 24, 29, 34, 39, 49, 74, or 81 cells per shuffle.

**B)** Classification accuracy differed based on subsets of hippocampal cell types ($F_{(3,1996)} = 13,053$, $p < 0.001$). Post-hoc comparisons revealed significant differences between all ($p < 0.001$). n = 25 cells per shuffle.

**C)** Stimulation-responsive cells that increased firing rate contributed more than cells that decreased firing rate ($t = -87.61$, $p < 0.001$). n = 25 cells per shuffle.

**D)** Prediction of laser state in untrained, held-out epochs increased as a function of the number of included training epochs ($F_{(8,7984)} = 182.55$, $p < 0.001$). There was an interaction between # of epochs and label type ($F_{(8,7984)} = 180.82$, $p < 0.001$) and the true

labels outperformed the shuffled labels in all cases (Bonferroni-corrected $p < 0.001$ for all comparisons). Prediction accuracy was near 100% on held-out data from trained epochs (green). n = 1 – 9 training epochs per shuffle, 81 cells per shuffle.
n = 500 shuffles per group in all cases.

# CHAPTER FIVE: SUMMARY AND DISCUSSION

The work contained in this dissertation sought to explore contributions of the dentate gyrus to memory and navigation with an emphasis on the recruitment and reactivation of sparse, experience-associated cellular ensembles, or engrams. Landmark studies manipulating such ensembles in the DG and other regions to drive or suppress learned behavior motivated the present work (Ramirez et al., 2013; Denny et al., 2014; Cowansage et al., 2014; Ryan et al., 2015; Kitamura et al., 2017). The data here represent a logical extension of the use of immediate-early-gene dependent tagging technologies (Radulovic et al., 1998; Guzowski et al., 1999; Reijmers et al., 2007; Tayler et al., 2013) to study sparse hippocampal populations involved in spatial memory and the cognitive map hypothesis (Tolman, 1948). Recent functional recording of DG cell responses offered evidence of stable spatial tuning within environments and across days (GoodSmith et al., 2017; Hainmueller & Bartos, 2018; Cholvin et al., 2021) which further informed the experimental design used to investigate key aspects of DG populations in spatial memory and navigational representation. The above experiments examined 1) the encoding of specific routes by IEG-defined DG populations, 2) the importance of the DG population subserving spatial working memory and learning transfer across environments, and 3) the functional outcomes of reactivating a DG-mediated fear engram on downstream regions during navigation.

The unique architecture and loss of function studies in the hippocampus, outlined in Chapter 1, led to specific roles assigned for individual hippocampal subregions including pattern separation (DG), completion (CA3), and comparison (CA1; Marr, 1971;

McNaughton & Morris, 1987; O'Reilly & McClelland, 1994; Treves & Rolls, 1994; M. Hasselmo et al., 1995). On its face, these delineations seem reasonable, especially given the evidence of functional specialization within regions (Nakazawa et al., 2002; J. K. Leutgeb et al., 2007; Neunuebel & Knierim, 2014). In Chapter 2 we examined the ability for two sparse DG populations to separate a specific sub-route within a larger maze context. The results revealed that while the DG separated two dissimilar contexts to the degree expected by statistical chance, visiting a single familiar sub-route produced pattern overlap above chance but below the maximum overlap expected by repeated exposure to the full maze. Surprisingly, therefore, the DG performed a role of both pattern separation and completion in this navigational task.

Should the apparent pattern separation / completion dichotomy be revisited? The initial theoretical work detailing hippocampal function (Marr, 1971) defined the following rules for a memory system: 1) the storage of events by "memorizer" cells, 2) the recognition of subevents (separation), and 3) the completion of "simple" representations. While Marr identified the CA pyramidals as natural memorizers due to modifiable synapses and low event rates, and noted the obvious recurrent anatomy of the CA3 pyramidals as supporting a completion function, the job of subevent recognition was largely assigned to the inhibitory population. This last hypothesis is supported by a recent engram tagging study demonstrating multiple engram populations within DG for the same event defined by different IEGs (Sun et al., 2020). One population received excitatory input from entorhinal cortex, the other from DG interneurons and they played a functional role in fear memory generalization or separation respectively. Marr also

classified the granule cells of DG as memorizers which form an extended collateral network with the CA regions, thus including them in the role of pattern completion. Subsequent anatomical observation of the DG to CA3/hilus to DG connectivity strengthens this case further (Ribak et al., 1985; Frotscher et al., 1991; X.-G. Li et al., 1994; Scharfman, 2007). Other theorists also remained region-agnostic in their interpretation of the principles of hetero-associativity (feedforward excitatory loops such as DG to CA3 to DG) as merely a variant of the broader concept of auto-associativity (feedforward self-excitation such as CA3 to CA3) leading to synaptic weight modification necessary for memory storage (McNaughton & Morris, 1987; Lisman, 1999). Some authors merely required the CA3 to arrive at a pattern separated representation of the EC input, with aid from DG (O'Reilly & McClelland, 1994).

One of the primary computational arguments in favor of the DG acting as a pattern separator is Marr-Albus theory or "expansion coding:" the principle of divergent feedforward excitation from a small input region onto a much larger output region leading to minimally-overlapping representations in the downstream reader (Marr, 1969; Albus, 1971; Cayco-Gajic & Silver, 2019). The enlargement in DG granule cells relative to the number of EC input cells led to the hypothesis that separable representations of similar events would arise in DG (Treves & Rolls, 1994; Cayco-Gajic & Silver, 2019). However, the DG population is only one order of magnitude larger than EC (Amaral et al., 1990), whereas the ratio of all cerebellar to *all* cerebral cortex neurons is 3.6 to 1 across multiple mammalian species and in rats the roughly 140 million cerebellar cells must necessarily receive input from regions several orders of magnitude less populous

(Herculano-Houzel & Lent, 2005; Herculano-Houzel et al., 2006; Herculano-Houzel, 2010). While expansion coding may play a role in pattern separation from the EC to DG, other mechanisms such as sparse coding and decorrelation of firing pattern may also contribute (Cayco-Gajic & Silver, 2019).

Chapter 3 revealed insight on pattern separation and completion by manipulating nonspecific, IEG-defined populations in the DG during spatial working memory in novel and familiar environments. Stimulation of nonspecific ensembles tagged by exposure to both training maze routes disrupted performance, likely due to a failure of pattern separation of the current trajectory during the memory encoding phase of the task. Interestingly, during the initial learning transfer from the training context to the experimental context mice performed the task well, but were also most impaired by subsequent disruption of the DG, suggesting an initial dependence on this region for learning generalization (completion). Leutgeb et al. found that cells in the DG (or hilus, see Chapter 1) were shown to exhibit immediate decorrelation during subtle shifts in environmental cues, while CA3 cells demonstrated more gradual remapping to more obvious environmental differences (J. K. Leutgeb et al., 2007). However, the DG/hilus cells performed less rate remapping when the rats were placed in another room, whereas an entirely different population of CA3 cells were recruited, leading to pattern separation by this region and not the DG. The observation of CA2/3 and CA1 place cells discriminating across contexts via global remapping while the DG place map remains stable has been repeated with large scale calcium imaging (Hainmueller & Bartos, 2018; Cholvin et al., 2021). These distinctions could also explain why the use of firing rate

correlations, not field stability, demonstrated obvious pattern separation in the DG but not CA3 within a single environment with altered cues (Neunuebel & Knierim, 2014). If a similar population of task-related cells were recruited in DG by both training and experimental mazes, perhaps with decorrelated firing rates but not spatial maps, then the effects of learning transfer and disruption vulnerability would be well explained (Chapter 3).

While lesion and KO studies certainly indicate a role of CA3 in pattern completion (Nakazawa et al., 2002; Gold & Kesner, 2005), this does not preclude the possibility that DG also contributes to this process (Hainmueller & Bartos, 2018) nor that CA3 simultaneously contributes to pattern separation. Nor do the lesion and NMDA receptor KO studies in DG (Gilbert et al., 2001; McHugh et al., 2007; Sasaki et al., 2018) that show errors in spatial and contextual discrimination rule out that CA3 neurons participate in pattern separation (O'Reilly & McClelland, 1994; J. K. Leutgeb et al., 2007; Hainmueller & Bartos, 2018). Other cell types such as mossy cells and interneurons may serve specific roles in this computational process (Andrews-Zwilling et al., 2012; Jinde et al., 2012; GoodSmith et al., 2019). For example, lesion of mature but not adult-born GCs actually increases behavioral context discrimination while irradiation of the newborn GC population impairs discrimination (Nakashiba et al., 2012). Despite near total ablation of mature GC outputs to CA3, spatial discrimination within a radial arm maze task was preserved, suggesting pattern separation could be accomplished by adult-born GCs and CA3 together. Lastly, hidden platform escape latency was slower in mature GC KO mice indicating that rapid pattern completion relies on these cell types.

Ultimately, the debate of pattern separation vs completion is hampered by the lack of key empirical data. First, there is a need for studies employing identical behavioral tests alongside cell-type or connection specific lesion of both DG and CA3 together and separately (Senzai, 2019). Second, the ability to record large populations of cells in all the relevant regions simultaneously – EC, DG, and CA3 – during behavioral tests of context discrimination or transfer learning would do much to reconcile inconsistencies inherent to assessing this cognitive process in only one region at a time (Santoro, 2013). Calcium imaging with prism lenses or multi-site pixel probes would be appropriate methods for addressing this last point. We propose that such studies would reveal, in addition to joint pattern separation and completion across the DG and CA3, that both phenomena would evolve not merely across the circuit, but also across time. This is suggested by the anatomy of HPC itself, with a tri-synaptic loop connected at both ends to the EC and the proposed need for a comparator function to align memory patterns to input cues (O'Reilly & McClelland, 1994; Hasselmo et al., 1995; Lisman, 1999). This comparison would necessarily involve a difference in time for the first instance as EC-DG-CA3-CA1 requires more processing than EC-CA1, but may also involve iterative updating of the retrieved representation to better match the cue from EC. More formally, the Similarity, S, of two patterns, A and B, decreases across regions such that: $S_{EC}$ (A,B) > $S_{DG}$ (A,B) > $S_{CA3}$ (A,B) and across time, t, such that: $S_{DG}$ ($At_1$,$At_2$) > $S_{DG}$ ($At_2$,$At_3$). This process is likely to evolve rapidly in time, on the order of tens or hundreds of milliseconds as with theta sweeps (Johnson & Redish, 2007), to enable rapid decision making at the level of behavior.

What then, are the neural consequences of a separated, completed pattern arriving in downstream target regions? Our final set of experiments lacked single unit readout from DG and CA3, so we must focus instead on the outcome of specific memory stimulation on altering ongoing behavior and spatial map representation in CA1. In Chapter 4 we found that DG engram stimulation altered the firing rates and spatial information content of a subpopulation of CA1 cells that were otherwise stable navigational anchors. The CA1 contains pre-existing connectivity biasing certain populations to fire together in reliable sequences or "syllables" prior to new experiences or even in the absence of experience (Dragoi & Tonegawa, 2011, 2013; Villette et al., 2015; Grosmark & Buzsaki, 2016; McKenzie et al., 2021). Excitable cells become incorporated into engrams according to the allocation hypothesis, hinting at the nature of existing circuit architecture to which novel experiences becomes mapped (Han et al., 2009; J. Kim et al., 2014; Cai et al., 2016). Our data fit with these observations, given that the network took on a repeated state other than baseline across different stimulation trials. Whether these cells exhibit pre-existing functional correlation (Jou et al., 2023) or if new ensembles are recruited by this artificial reactivation of memory remains to be demonstrated. New place fields can be formed in DG and CA1 during awake behavior by artificial stimulation of dendritic plateau potentials (Diamantaki et al., 2016; Bittner et al., 2017) and naturalistically by target signals from EC onto CA1 (Grienberger & Magee, 2022). The theory of Hebbian experience-dependent plasticity (Hebb, 1949), and evidence of HPC engrams stabilized by post-learning synaptic plasticity (Ryan et al., 2015; Choi et al., 2018) argues in favor of a balance between existing architecture and

updated connectivity following learning. We suggest a refinement of the hippocampal indexing theory (Teyler & DiScenna, 1986; Teyler & Rudy, 2007) such that unique activations of cortical modules map onto and update preconfigured cell ensembles in HPC creating new chains of sub-ensemble "syllables" (Malvache et al., 2016) which involve both inhibitory/discriminatory and excitatory/generalizing components (Sun et al., 2020). During recall, evolving pattern separation and completion is accomplished by these complimentary sub-ensembles which reactivate sequentially to regenerate the broader representation across cortical modules and actively construct the memory.

## Limitations

Throughout the optogenetic experiments conducted, only a single stimulation frequency was used (20Hz). While this allowed consistent comparison within study and with prior DG engram reactivation literature (Ramirez et al., 2013, 2015; Chen et al., 2019), other stimulation patterns may be more effective for driving neural and behavioral outcomes. Stimulation of the basolateral amygdala at 4Hz or 8Hz can differentially drive or suppress freezing behavior in a context dependent manner (Ozawa et al., 2020). In CA1, 4Hz engram stimulation effectively drives freezing while 20Hz may not (Ryan et al., 2015). Similarly, stimulation of vHPC terminals in PFC at 8Hz, but not 2, 4, or 20Hz, drove place avoidance (Padilla-Coreano et al., 2019). Phase specific stimulation, especially the trough of theta, improves memory recall generally (Siegle & Wilson, 2014) and with DG engram-specific reactivation (Rahsepar et al., 2023). These results are in keeping with models of specific theta phases of memory encoding versus retrieval at the

peak or trough of the CA1 theta phase respectively (Hasselmo et al., 2002; Hasselmo & Stern, 2014). Thus, driving DG engrams at the trough of theta, or at another stimulation frequency such as 6-8Hz to match and entrain the theta rhythm, might have elicited stronger behavioral response during CFC engram reactivation (Chapter 4). During spatial working memory, theta trough-specific stimulation of a one-route maze engram might have been more effective in biasing behavior in the limited number of cells tagged by a single neutral context exposure (Chapter 3 Discussion section).

Lastly, it should not escape notice that the brains and behavior of rodents differ conspicuously from those of humans. While pains were taken to assess multiple forms of episodic memory – navigational and fear conditioning – the behavioral affordances of rodents and reductive nature of the experimental conditions limit generalizability to humans and other mammals.

## Conclusion

We began by asking how the architecture and activity of our brains could support the evolutionarily adaptive phenomenon of memory. Early researchers defined strict functional roles for memory-associated brain regions such as pattern separation within the dentate gyrus and completion within the CA3. While such models beneficially drove the testing of falsifiable hypotheses, the evidence accumulated from experiments testing those ideas has mounted to the point that the theories must be re-examined and revised. We present empirical and theoretical evidence for the role of the dentate gyrus as a single node of an extended separation/completion circuit distributed anatomically and

temporally as a neural mechanism supporting episodic memory. Finally, we offer preliminary evidence of the outcome of dentate gyrus-mediated episodic memory recall (albeit artificially induced) on entraining specific downstream populations in a decodable manner.

## BIBLIOGRAPHY

Albus, J. S. (1971). A theory of cerebellar function. *Mathematical Biosciences*, *10*(1), 25–61. https://doi.org/10.1016/0025-5564(71)90051-4

Alexander, A. S., Carstensen, L. C., Hinman, J. R., Raudies, F., Chapman, G. W., & Hasselmo, M. E. (2020). Egocentric boundary vector tuning of the retrosplenial cortex. *Science Advances*, *6*(8), eaaz2322. https://doi.org/10.1126/sciadv.aaz2322

Alexander, A. S., Rangel, L. M., Tingley, D., & Nitz, D. A. (2018). Neurophysiological signatures of temporal coordination between retrosplenial cortex and the hippocampal formation. *Behavioral Neuroscience*, *132*(5), 453–468. https://doi.org/10.1037/bne0000254

Alzheimer, A. (1911). Über eigenartige Krankheitsfälle des späteren Alters. *Zeitschrift für die gesamte Neurologie und Psychiatrie*, *4*(1), 356–385. https://doi.org/10.1007/BF02866241

Amaral, D. G., Ishizuka, N., & Claiborne, B. (1990). Chapter 1 Chapter Neurons, numbers and the hippocampal network. In J. Storm-Mathisen, J. Zimmer, & O. P. Ottersen (Eds.), *Progress in Brain Research* (Vol. 83, pp. 1–11). Elsevier. https://doi.org/10.1016/S0079-6123(08)61237-6

Amaral, D. G., Scharfman, H. E., & Lavenex, P. (2007). The dentate gyrus: Fundamental neuroanatomical organization (dentate gyrus for dummies). *Progress in Brain Research*, *163*, 3–22. https://doi.org/10.1016/S0079-6123(07)63001-5

Amaral, D. G., & Witter, M. P. (1989). The three-dimensional organization of the hippocampal formation: A review of anatomical data. *Neuroscience*, *31*(3), 571–591. https://doi.org/10.1016/0306-4522(89)90424-7

Andrews-Zwilling, Y., Gillespie, A. K., Kravitz, A. V., Nelson, A. B., Devidze, N., Lo, I., Yoon, S. Y., Bien-Ly, N., Ring, K., Zwilling, D., Potter, G. B., Rubenstein, J. L. R., Kreitzer, A. C., & Huang, Y. (2012). Hilar GABAergic Interneuron Activity Controls Spatial Learning and Memory Retrieval. *PLoS ONE*, *7*(7), e40555. https://doi.org/10.1371/journal.pone.0040555

Anisimova, M., Lamothe-Molina, P. J., Franzelin, A., Aberra, A. S., Hoppa, M. B., Gee, C. E., & Oertner, T. G. (2023). *Neuronal FOS reports synchronized activity of presynaptic neurons* [Preprint]. Neuroscience. https://doi.org/10.1101/2023.09.04.556168

Armbruster, B. N., Li, X., Pausch, M. H., Herlitze, S., & Roth, B. L. (2007). Evolving the lock to fit the key to create a family of G protein-coupled receptors potently activated by an inert ligand. *Proceedings of the National Academy of Sciences of the United States of America*, *104*(12), 5163–5168. https://doi.org/10.1073/pnas.0700293104

Bartus, R. T., Dean, R. L., Beer, B., & Lippa, A. S. (1982). The Cholinergic Hypothesis of Geriatric Memory Dysfunction. *Science*, *217*(4558), 408–414. https://doi.org/10.1126/science.7046051

Bear, M. F., & Kirkwood, A. (1993). Neocortical long-term potentiation. *Current Opinion in Neurobiology*, *3*(2), 197–202. https://doi.org/10.1016/0959-4388(93)90210-P

Bertoni-Freddari, C., Fattoretti, P., Casoli, T., Caselli, U., & Meier-Ruge, W. (1996). Deterioration threshold of synaptic morphology in aging and senile dementia of Alzheimer's type. *Analytical and Quantitative Cytology and Histology*, *18*(3), 209–213.

Bimonte, H. A., & Denenberg, V. H. (2000). Sex differences in vicarious trial-and-error behavior during radial arm maze learning. *Physiology & Behavior*, *68*(4), 495–499. https://doi.org/10.1016/S0031-9384(99)00201-2

Bittner, K. C., Milstein, A. D., Grienberger, C., Romani, S., & Magee, J. C. (2017). Behavioral time scale synaptic plasticity underlies CA1 place fields. *Science*, *357*(6355), 1033–1036. https://doi.org/10.1126/science.aan3846

Bliss, T. V. P., & Lømo, T. (1973). Long-lasting potentiation of synaptic transmission in the dentate area of the anaesthetized rabbit following stimulation of the perforant path. *The Journal of Physiology*, *232*(2), 331–356.

Bobinski, M., Wegiel, J., Tarnawski, M., Bobinski, M., Reisberg, B., de Leon, M. J., Miller, D. C., & Wisniewski, H. M. (1997). Relationships between Regional Neuronal Loss and Neurofibrillary Changes in the Hippocampal Formation and Duration and Severity of Alzheimer Disease. *Journal of Neuropathology & Experimental Neurology*, *56*(4), 414–420. https://doi.org/10.1097/00005072-199704000-00010

Boss, B. D., Turlejski, K., Stanfield, B. B., & Cowan, W. M. (1987). On the numbers of neurons on fields CA1 and CA3 of the hippocampus of Sprague-Dawley and Wistar rats. *Brain Research*, *406*(1), 280–287. https://doi.org/10.1016/0006-8993(87)90793-1

Boyden, E. S., Zhang, F., Bamberg, E., Nagel, G., & Deisseroth, K. (2005). Millisecond-timescale, genetically targeted optical control of neural activity. *Nature Neuroscience*, *8*(9), 1263–1268. https://doi.org/10.1038/nn1525

Braak, H., & Braak, E. (1991). Neuropathological stageing of Alzheimer-related changes. *Acta Neuropathologica*, *82*(4), 239–259. https://doi.org/10.1007/BF00308809

Bragin, A., Engel Jr, J., Wilson, C. L., Fried, I., & Buzsáki, G. (1999). High-frequency oscillations in human brain. *Hippocampus*, *9*(2), 137–142. https://doi.org/10.1002/(SICI)1098-1063(1999)9:2<137::AID-HIPO5>3.0.CO;2-0

Buzsaki & Eidelberg. (1981). Commissural projection to the dentate gyrus of the rat: Evidence for feed-forward inhibition. *Brain Research*, *230*(1–2), 346–350. https://doi.org/10.1016/0006-8993(81)90413-3

Buzsáki, G. (2015). Hippocampal sharp wave-ripple: A cognitive biomarker for episodic memory and planning. *Hippocampus*, *25*(10), 1073–1188. https://doi.org/10.1002/hipo.22488

Buzsáki, G., Lai-Wo S., L., & Vanderwolf, C. H. (1983). Cellular bases of hippocampal EEG in the behaving rat. *Brain Research Reviews*, *6*(2), 139–171. https://doi.org/10.1016/0165-0173(83)90037-1

Cai, D. J., Aharoni, D., Shuman, T., Shobe, J., Biane, J., Song, W., Wei, B., Veshkini, M., La-Vu, M., Lou, J., Flores, S., Kim, I., Sano, Y., Zhou, M., Baumgaertel, K., Lavi, A., Kamata, M., Tuszynski, M., Mayford, M., … Silva, A. J. (2016). A shared neural ensemble links distinct contextual memories encoded close in time. *Nature*, *534*(7605), 115–118. https://doi.org/10.1038/nature17955

Cayco-Gajic, N. A., & Silver, R. A. (2019). Re-evaluating Circuit Mechanisms Underlying Pattern Separation. *Neuron*, *101*(4), 584–602. https://doi.org/10.1016/j.neuron.2019.01.044

Chalfie, M., Tu, Y., Euskirchen, G., Ward, W. W., & Prasher, D. C. (1994). Green Fluorescent Protein as a Marker for Gene Expression. *Science*, *263*(5148), 802–805. https://doi.org/10.1126/science.8303295

Chen, B. K., Murawski, N. J., Cincotta, C., McKissick, O., Finkelstein, A., Hamidi, A. B., Merfeld, E., Doucette, E., Grella, S. L., Shpokayte, M., Zaki, Y., Fortin, A., & Ramirez, S. (2019). Artificially Enhancing and Suppressing Hippocampus-Mediated Memories. *Current Biology*, *29*(11), 1885-1894.e4. https://doi.org/10.1016/j.cub.2019.04.065

Choi, S. H., Bylykbashi, E., Chatila, Z. K., Lee, S. W., Pulli, B., Clemenson, G. D., Kim, E., Rompala, A., Oram, M. K., Asselin, C., Aronson, J., Zhang, C., Miller, S. J., Lesinski, A., Chen, J. W., Kim, D. Y., van Praag, H., Spiegelman, B. M., Gage, F. H., & Tanzi, R. E. (2018). Combined adult neurogenesis and BDNF mimic exercise effects on cognition in an Alzheimer's mouse model. *Science*, *361*(6406), eaan8821. https://doi.org/10.1126/science.aan8821

Cholvin, T., Hainmueller, T., & Bartos, M. (2021). The hippocampus converts dynamic entorhinal inputs into stable spatial maps. *Neuron*, *109*(19), 3135-3148.e7. https://doi.org/10.1016/j.neuron.2021.09.019

Conklin, B. R., Hsiao, E. C., Claeysen, S., Dumuis, A., Srinivasan, S., Forsayeth, J. R., Guettier, J.-M., Chang, W. C., Pei, Y., McCarthy, K. D., Nissenson, R. A., Wess, J., Bockaert, J., & Roth, B. L. (2008). Engineering GPCR signaling pathways with RASSLs. *Nature Methods*, *5*(8), 673–678. https://doi.org/10.1038/nmeth.1232

Costa, V. C. I., Bueno, J. L. O., & Xavier, G. F. (2005). Dentate gyrus-selective colchicine lesion and performance in temporal and spatial tasks. *Behavioural Brain Research*, *160*(2), 286–303. https://doi.org/10.1016/j.bbr.2004.12.011

Cowansage, K. K., Shuman, T., Dillingham, B. C., Chang, A., Golshani, P., & Mayford, M. (2014). Direct Reactivation of a Coherent Neocortical Memory of Context. *Neuron*, *84*(2), 432–441. https://doi.org/10.1016/j.neuron.2014.09.022

Dannenberg, H., Young, K., & Hasselmo, M. E. (2017). Modulation of Hippocampal Circuits by Muscarinic and Nicotinic Receptors. *Frontiers in Neural Circuits*, *11*. https://www.frontiersin.org/articles/10.3389/fncir.2017.00102

Davies, C. A., Mann, D. M. A., Sumpter, P. Q., & Yates, P. O. (1987). A quantitative morphometric analysis of the neuronal and synaptic content of the frontal and temporal cortex in patients with Alzheimer's disease. *Journal of the Neurological Sciences*, *78*(2), 151–164. https://doi.org/10.1016/0022-510X(87)90057-8

Davis, C. D., Jones, F. L., & Derrick, B. E. (2004). Novel Environments Enhance the Induction and Maintenance of Long-Term Potentiation in the Dentate Gyrus. *The Journal of Neuroscience*, *24*(29), 6497–6506. https://doi.org/10.1523/JNEUROSCI.4970-03.2004

Deadwyler, S. A., & Hampson, R. E. (2004). Differential but Complementary Mnemonic Functions of the Hippocampus and Subiculum. *Neuron*, *42*(3), 465–476. https://doi.org/10.1016/S0896-6273(04)00195-3

Denny, C. A., Kheirbek, M. A., Alba, E. L., Tanaka, K. F., Brachman, R. A., Laughman, K. B., Tomm, N. K., Turi, G. F., Losonczy, A., & Hen, R. (2014). Hippocampal Memory Traces Are Differentially Modulated by Experience, Time, and Adult Neurogenesis. *Neuron*, *83*(1), 189–201. https://doi.org/10.1016/j.neuron.2014.05.018

Denovellis, E. L., Myroshnychenko, M., Sarmashghi, M., & Stephen, E. P. (2022). Spectral Connectivity: A python package for computingmultitaper spectral estimates and frequency-domain brain connectivitymeasures on the CPU and GPU. *Journal of Open Source Software*, *7*(80), 4840. https://doi.org/10.21105/joss.04840

Diamantaki, M., Frey, M., Preston-Ferrer, P., & Burgalossi, A. (2016). Priming Spatial Activity by Single-Cell Stimulation in the Dentate Gyrus of Freely Moving Rats. *Current Biology*, *26*(4), 536–541. https://doi.org/10.1016/j.cub.2015.12.053

Diba, K., & Buzsáki, G. (2007). Forward and reverse hippocampal place-cell sequences during ripples. *Nature Neuroscience*, *10*(10), 1241–1242. https://doi.org/10.1038/nn1961

Dong, H.-W., Swanson, L. W., Chen, L., Fanselow, M. S., & Toga, A. W. (2009). Genomic–anatomic evidence for distinct functional domains in hippocampal field CA1. *Proceedings of the National Academy of Sciences of the United States of America*, *106*(28), 11794–11799. https://doi.org/10.1073/pnas.0812608106

Doucette, E., Merfeld, E., Leblanc, H., Monasterio, A., Cincotta, C., Grella, S. L., Logan, J., & Ramirez, S. (2020). Social behavior in mice following chronic optogenetic stimulation of hippocampal engrams. *Neurobiology of Learning and Memory*, *176*, 107321. https://doi.org/10.1016/j.nlm.2020.107321

Dragoi, G., & Tonegawa, S. (2011). Preplay of future place cell sequences by hippocampal cellular assemblies. *Nature*, *469*(7330), Article 7330. https://doi.org/10.1038/nature09633

Dragoi, G., & Tonegawa, S. (2013). Distinct preplay of multiple novel spatial experiences in the rat. *Proceedings of the National Academy of Sciences*, *110*(22), 9100–9105. https://doi.org/10.1073/pnas.1306031110

Edelmann, E., & Lessmann, V. (2018). Dopaminergic innervation and modulation of hippocampal networks. *Cell and Tissue Research*, *373*(3), 711–727. https://doi.org/10.1007/s00441-018-2800-7

Ego-Stengel, V., & Wilson, M. A. (2010). Disruption of ripple-associated hippocampal activity during rest impairs spatial learning in the rat. *Hippocampus*, *20*(1), 1–10. https://doi.org/10.1002/hipo.20707

Eichenbaum, H. (2017). On the integration of space, time, and memory. *Neuron*, *95*(5), 1007–1018. https://doi.org/10.1016/j.neuron.2017.06.036

Eichenbaum, H., Sauvage, M., Fortin, N., Komorowski, R., & Lipton, P. (2012). Towards a functional organization of episodic memory in the medial temporal lobe. *Neuroscience & Biobehavioral Reviews*, *36*(7), 1597–1608. https://doi.org/10.1016/j.neubiorev.2011.07.006

Einstein, G., Buranosky, R., & Crain, B. (1994). Dendritic pathology of granule cells in Alzheimer's disease is unrelated to neuritic plaques. *The Journal of Neuroscience*, *14*(8), 5077–5088. https://doi.org/10.1523/JNEUROSCI.14-08-05077.1994

Emerich, D. F., & Walsh, T. J. (1989). Selective working memory impairments following intradentate injection of colchicine: Attenuation of the behavioral but not the neuropathological effects by gangliosides GM1 and AGF2. *Physiology & Behavior*, *45*(1), 93–101. https://doi.org/10.1016/0031-9384(89)90170-4

Emerich, D. F., & Walsh, T. J. (1990). Cholinergic cell loss and cognitive impairments following intraventricular or intradentate injection of colchicine. *Brain Research*, *517*(1–2), 157–167. https://doi.org/10.1016/0006-8993(90)91021-8

Euston, D. R., Gruber, A. J., & McNaughton, B. L. (2012). The Role of Medial Prefrontal Cortex in Memory and Decision Making. *Neuron*, *76*(6), 1057–1070. https://doi.org/10.1016/j.neuron.2012.12.002

Fanselow, M. S., & Dong, H.-W. (2010). Are the Dorsal and Ventral Hippocampus Functionally Distinct Structures? *Neuron*, *65*(1), 7–19. https://doi.org/10.1016/j.neuron.2009.11.031

Felix-Ortiz, A. C., Beyeler, A., Seo, C., Leppla, C. A., Wildes, C. P., & Tye, K. M. (2013). BLA to vHPC Inputs Modulate Anxiety-Related Behaviors. *Neuron*, *79*(4), 658–664. https://doi.org/10.1016/j.neuron.2013.06.016

Fenno, L., Yizhar, O., & Deisseroth, K. (2011). The Development and Application of Optogenetics. *Annual Review of Neuroscience*, *34*, 389–412. https://doi.org/10.1146/annurev-neuro-061010-113817

Ferbinteanu, J., & Shapiro, M. L. (2003). Prospective and Retrospective Memory Coding in the Hippocampus. *Neuron*, *40*(6), 1227–1239. https://doi.org/10.1016/S0896-6273(03)00752-9

Fernández-Ruiz, A., Oliva, A., Fermino de Oliveira, E., Rocha-Almeida, F., Tingley, D., & Buzsáki, G. (2019). Long-duration hippocampal sharp wave ripples improve memory. *Science*, *364*(6445), 1082–1086. https://doi.org/10.1126/science.aax0758

Fernández-Ruiz, A., Oliva, A., Soula, M., Rocha-Almeida, F., Nagy, G. A., Martin-Vazquez, G., & Buzsáki, G. (2021). Gamma rhythm communication between entorhinal cortex and dentate gyrus neuronal assemblies. *Science*, *372*(6537). https://doi.org/10.1126/science.abf3119

Foster, D. J., & Wilson, M. A. (2006). Reverse replay of behavioural sequences in hippocampal place cells during the awake state. *Nature*, *440*(7084), Article 7084. https://doi.org/10.1038/nature04587

Freund, & Buzsáki, G. (1996). Interneurons of the hippocampus. *Hippocampus*, *6*(4), 347–470. https://doi.org/10.1002/(SICI)1098-1063(1996)6:4<347::AID-HIPO1>3.0.CO;2-I

Frey, U., Krug, M., Reymann, K. G., & Matthies, H. (1988). Anisomycin, an inhibitor of protein synthesis, blocks late phases of LTP phenomena in the hippocampal CA1 region in vitro. *Brain Research*, *452*(1–2), 57–65. https://doi.org/10.1016/0006-8993(88)90008-X

Frotscher, M., & Léránth, C. (1985). Cholinergic innervation of the rat hippocampus as revealed by choline acetyltransferase immunocytochemistry: A combined light and electron microscopic study. *Journal of Comparative Neurology*, *239*(2), 237–246. https://doi.org/10.1002/cne.902390210

Frotscher, M., Seress, L., Schwerdtfeger, W. K., & Buhl, E. (1991). The mossy cells of the fascia dentata: A comparative study of their fine structure and synaptic connections in rodents and primates. *Journal of Comparative Neurology*, *312*(1), 145–163. https://doi.org/10.1002/cne.903120111

Fuller, S. C. (1907). A study of the neurofibrils in dementia paralytica, dementia senilis, chronic alcoholism, cerebral lues and microcephalic idiocy. *American Journal of Psychiatry*, *63*(4), 415-468–13. https://doi.org/10.1176/ajp.63.4.415

Fuller, S. C. (1911). A study of the miliary plaques found in brains of the aged. *American Journal of Psychiatry*, *68*(2), 147-220–16. https://doi.org/10.1176/ajp.68.2.147

Fyhn, M., Molden, S., Witter, M. P., Moser, E. I., & Moser, M.-B. (2004). Spatial Representation in the Entorhinal Cortex. *Science*, *305*(5688), 1258–1264. https://doi.org/10.1126/science.1099901

Garner, A. R., Rowland, D. C., Hwang, S. Y., Baumgaertel, K., Roth, B. L., Kentros, C., & Mayford, M. (2012). Generation of a Synthetic Memory Trace. *Science*, *335*(6075), 1513–1516. https://doi.org/10.1126/science.1214985

Gilbert, P. E., Kesner, R. P., & Lee, I. (2001). Dissociating hippocampal subregions: A double dissociation between dentate gyrus and CA1. *Hippocampus*, *11*(6), 626–636. https://doi.org/10.1002/hipo.1077

Gillespie, A. K., Maya, D. A. A., Denovellis, E. L., Liu, D. F., Kastner, D. B., Coulter, M. E., Roumis, D. K., Eden, U. T., & Frank, L. M. (2021). Hippocampal replay reflects specific past experiences rather than a plan for subsequent choice. *Neuron*, *0*(0). https://doi.org/10.1016/j.neuron.2021.07.029

Girardeau, G., Benchenane, K., Wiener, S. I., Buzsáki, G., & Zugaro, M. B. (2009). Selective suppression of hippocampal ripples impairs spatial memory. *Nature Neuroscience*, *12*(10), 1222–1223. https://doi.org/10.1038/nn.2384

Gold, A. E., & Kesner, R. P. (2005). The role of the CA3 subregion of the dorsal hippocampus in spatial pattern completion in the rat. *Hippocampus*, *15*(6), 808–814. https://doi.org/10.1002/hipo.20103

Gomperts, S. N., Kloosterman, F., & Wilson, M. A. (2015). VTA neurons coordinate with the hippocampal reactivation of spatial experience. *eLife*, *4*, e05360. https://doi.org/10.7554/eLife.05360

GoodSmith, D., Chen, X., Wang, C., Kim, S. H., Song, H., Burgalossi, A., Christian, K. M., & Knierim, J. J. (2017). Spatial representations of granule cells and mossy cells of the dentate gyrus. *Neuron*, *93*(3), 677-690.e5. https://doi.org/10.1016/j.neuron.2016.12.026

GoodSmith, D., Kim, S. H., Puliyadi, V., Ming, G., Song, H., Knierim, J. J., & Christian, K. M. (2022). Flexible encoding of objects and space in single cells of the dentate gyrus. *Current Biology*, *0*(0). https://doi.org/10.1016/j.cub.2022.01.023

GoodSmith, D., Lee, H., Neunuebel, J. P., Song, H., & Knierim, J. J. (2019). Dentate Gyrus Mossy Cells Share a Role in Pattern Separation with Dentate Granule Cells and Proximal CA3 Pyramidal Cells. *The Journal of Neuroscience*, *39*(48), 9570–9584. https://doi.org/10.1523/JNEUROSCI.0940-19.2019

Goshen, I., Brodsky, M., Prakash, R., Wallace, J., Gradinaru, V., Ramakrishnan, C., & Deisseroth, K. (2011). Dynamics of Retrieval Strategies for Remote Memories. *Cell*, *147*(3), 678–689. https://doi.org/10.1016/j.cell.2011.09.033

Grienberger, C., & Magee, J. C. (2022). Entorhinal cortex directs learning-related changes in CA1 representations. *Nature*, *611*(7936), Article 7936. https://doi.org/10.1038/s41586-022-05378-6

Griffin, A. L. (2015). Role of the thalamic nucleus reuniens in mediating interactions between the hippocampus and medial prefrontal cortex during spatial working

memory. *Frontiers in Systems Neuroscience*, *9*. https://www.frontiersin.org/articles/10.3389/fnsys.2015.00029

Griffin, A. L., Eichenbaum, H., & Hasselmo, M. E. (2007). Spatial Representations of Hippocampal CA1 Neurons Are Modulated by Behavioral Context in a Hippocampus-Dependent Memory Task. *Journal of Neuroscience*, *27*(9), 2416–2423. https://doi.org/10.1523/JNEUROSCI.4083-06.2007

Grosmark, A. D., & Buzsaki, G. (2016). Diversity in neural firing dynamics supports both rigid and learned hippocampal sequences. *Science*, *351*(6280), 1440–1443. https://doi.org/10.1126/science.aad1935

Gupta, A. S., van der Meer, M. A. A., Touretzky, D. S., & Redish, A. D. (2012). Segmentation of spatial experience by hippocampal theta sequences. *Nature Neuroscience*, *15*(7), 1032–1039. https://doi.org/10.1038/nn.3138

Guzowski, J. F., McNaughton, B. L., Barnes, C. A., & Worley, P. F. (1999). Environment-specific expression of the immediate-early gene Arc in hippocampal neuronal ensembles. *Nature Neuroscience*, *2*(12), 1120–1124. https://doi.org/10.1038/16046

Hafting, T., Fyhn, M., Molden, S., Moser, M.-B., & Moser, E. I. (2005). Microstructure of a spatial map in the entorhinal cortex. *Nature*, *436*(7052), Article 7052. https://doi.org/10.1038/nature03721

Hagena, H., & Manahan-Vaughan, D. (2017). The serotonergic 5-HT4 receptor: A unique modulator of hippocampal synaptic information processing and cognition.

*Neurobiology of Learning and Memory*, *138*, 145–153. https://doi.org/10.1016/j.nlm.2016.06.014

Hainmueller, T., & Bartos, M. (2018). Parallel emergence of stable and dynamic memory engrams in the hippocampus. *Nature*, *558*(7709), 292–296. https://doi.org/10.1038/s41586-018-0191-2

Hainmueller, T., & Bartos, M. (2020). Dentate gyrus circuits for encoding, retrieval and discrimination of episodic memories. *Nature Reviews Neuroscience*, *21*(3), 153–168. https://doi.org/10.1038/s41583-019-0260-z

Hampson, R. E., & Deadwyler, S. A. (2003). Temporal firing characteristics and the strategic role of subicular neurons in short-term memory. *Hippocampus*, *13*(4), 529–541. https://doi.org/10.1002/hipo.10119

Hampson, R. E., Jarrard, L. E., & Deadwyler, S. A. (1999). Effects of ibotenate hippocampal and extrahippocampal destruction on delayed-match and -nonmatch-to-sample behavior in rats. *The Journal of Neuroscience: The Official Journal of the Society for Neuroscience*, *19*(4), 1492–1507. https://doi.org/10.1523/JNEUROSCI.19-04-01492.1999

Han, J.-H., Kushner, S. A., Yiu, A. P., Hsiang, H.-L., Buch, T., Waisman, A., Bontempi, B., Neve, R. L., Frankland, P. W., & Josselyn, S. A. (2009). Selective Erasure of a Fear Memory. *Science*, *323*(5920), 1492–1496. https://doi.org/10.1126/science.1164139

Hargreaves, E. L., Rao, G., Lee, I., & Knierim, J. J. (2005). Major Dissociation Between Medial and Lateral Entorhinal Input to Dorsal Hippocampus. *Science*, *308*(5729), 1792–1794. https://doi.org/10.1126/science.1110449

Harris, J. C., Martinez, J. M., Grozdanov, P. N., Bergeson, S. E., Grammas, P., & MacDonald, C. C. (2016). The Cstf2t Polyadenylation Gene Plays a Sex-Specific Role in Learning Behaviors in Mice. *PLoS ONE*, *11*(11), e0165976. https://doi.org/10.1371/journal.pone.0165976

Harvey, R. E., Robinson, H. L., Liu, C., Oliva, A., & Fernandez-Ruiz, A. (2023). Hippocampo-cortical circuits for selective memory encoding, routing, and replay. *Neuron*, *111*(13), 2076-2090.e9. https://doi.org/10.1016/j.neuron.2023.04.015

Hasselmo, M. E. (1993). Acetylcholine and Learning in a Cortical Associative Memory. *Neural Computation*, *5*(1), 32–44. https://doi.org/10.1162/neco.1993.5.1.32

Hasselmo, M. E. (2006). The Role of Acetylcholine in Learning and Memory. *Current Opinion in Neurobiology*, *16*(6), 710–715. https://doi.org/10.1016/j.conb.2006.09.002

Hasselmo, M. E., Bodelón, C., & Wyble, B. P. (2002). A Proposed Function for Hippocampal Theta Rhythm: Separate Phases of Encoding and Retrieval Enhance Reversal of Prior Learning. *Neural Computation*, *14*(4), 793–817. https://doi.org/10.1162/089976602317318965

Hasselmo, M. E., & Eichenbaum, H. (2005). Hippocampal mechanisms for the context-dependent retrieval of episodes. *Neural Networks*, *18*(9), 1172–1190. https://doi.org/10.1016/j.neunet.2005.08.007

Hasselmo, M. E., & Schnell, E. (1994). Laminar selectivity of the cholinergic suppression of synaptic transmission in rat hippocampal region CA1: Computational modeling and brain slice physiology. *The Journal of Neuroscience*, *14*(6), 3898–3914. https://doi.org/10.1523/JNEUROSCI.14-06-03898.1994

Hasselmo, M. E., Schnell, E., & Barkai, E. (1995). Dynamics of learning and recall at excitatory recurrent synapses and cholinergic modulation in rat hippocampal region CA3. *The Journal of Neuroscience*, *15*(7), 5249–5262. https://doi.org/10.1523/JNEUROSCI.15-07-05249.1995

Hasselmo, M. E., & Stern, C. E. (2014). Theta rhythm and the encoding and retrieval of space and time. *NeuroImage*, *85*, 656–666. https://doi.org/10.1016/j.neuroimage.2013.06.022

Hasselmo, M. E., & Wyble, B. P. (1997). Free recall and recognition in a network model of the hippocampus: Simulating effects of scopolamine on human memory function. *Behavioural Brain Research*, *89*(1–2), 1–34. https://doi.org/10.1016/S0166-4328(97)00048-X

Hebb, D. O. (1949). *The Organization of Behavior: A Neuropsychological Theory*. Psychology Press.

Herculano-Houzel, S. (2010). Coordinated scaling of cortical and cerebellar numbers of neurons. *Frontiers in Neuroanatomy*, *4*. https://www.frontiersin.org/articles/10.3389/fnana.2010.00012

Herculano-Houzel, S., & Lent, R. (2005). Isotropic Fractionator: A Simple, Rapid Method for the Quantification of Total Cell and Neuron Numbers in the Brain. *Journal of Neuroscience*, *25*(10), 2518–2521. https://doi.org/10.1523/JNEUROSCI.4526-04.2005

Herculano-Houzel, S., Mota, B., & Lent, R. (2006). Cellular scaling rules for rodent brains. *Proceedings of the National Academy of Sciences*, *103*(32), 12138–12143. https://doi.org/10.1073/pnas.0604911103

Heroux, N. A., Osborne, B. F., Miller, L. A., Kawan, M., Buban, K. N., Rosen, J. B., & Stanton, M. E. (2018). Differential expression of the immediate early genes c-Fos, Arc, Egr-1, and Npas4 during long-term memory formation in the context preexposure facilitation effect (CPFE). *Neurobiology of Learning and Memory*, *147*, 128–138. https://doi.org/10.1016/j.nlm.2017.11.016

Hyman, J. M., Zilli, E. A., Paley, A. M., & Hasselmo, M. E. (2010). Working Memory Performance Correlates with Prefrontal-Hippocampal Theta Interactions but not with Prefrontal Neuron Firing Rates. *Frontiers in Integrative Neuroscience*, *4*, 2. https://doi.org/10.3389/neuro.07.002.2010

Insausti, R., Herrero, M. T., & Witter, M. P. (1997). Entorhinal cortex of the rat: Cytoarchitectonic subdivisions and the origin and distribution of cortical efferents. *Hippocampus*, *7*(2), 146–183. https://doi.org/10.1002/(SICI)1098-1063(1997)7:2<146::AID-HIPO4>3.0.CO;2-L

Ishizuka, N., Weber, J., & Amaral, D. G. (1990). Organization of intrahippocampal projections originating from CA3 pyramidal cells in the rat. *Journal of Comparative Neurology*, *295*(4), 580–623. https://doi.org/10.1002/cne.902950407

Jacobsen, J. S., Wu, C.-C., Redwine, J. M., Comery, T. A., Arias, R., Bowlby, M., Martone, R., Morrison, J. H., Pangalos, M. N., Reinhart, P. H., & Bloom, F. E. (2006). Early-onset behavioral and synaptic deficits in a mouse model of Alzheimer's disease. *Proceedings of the National Academy of Sciences*, *103*(13), 5161–5166. https://doi.org/10.1073/pnas.0600948103

Jadhav, S. P., Kemere, C., German, P. W., & Frank, L. M. (2012). Awake Hippocampal Sharp-Wave Ripples Support Spatial Memory. *Science*, *336*(6087), 1454–1458. https://doi.org/10.1126/science.1217230

Jadhav, S. P., Rothschild, G., Roumis, D. K., & Frank, L. M. (2016). Coordinated Excitation and Inhibition of Prefrontal Ensembles During Awake Hippocampal Sharp-Wave Ripple Events. *Neuron*, *90*(1), 113–127. https://doi.org/10.1016/j.neuron.2016.02.010

Jaeger, B. N., Linker, S. B., Parylak, S. L., Barron, J. J., Gallina, I. S., Saavedra, C. D., Fitzpatrick, C., Lim, C. K., Schafer, S. T., Lacar, B., Jessberger, S., & Gage, F. H. (2018). A novel environment-evoked transcriptional signature predicts reactivity in single dentate granule neurons. *Nature Communications*, *9*, 3084. https://doi.org/10.1038/s41467-018-05418-8

Jankowsky, J. L., Fadale, D. J., Anderson, J., Xu, G. M., Gonzales, V., Jenkins, N. A., Copeland, N. G., Lee, M. K., Younkin, L. H., Wagner, S. L., Younkin, S. G., &

Borchelt, D. R. (2004). Mutant presenilins specifically elevate the levels of the 42 residue β-amyloid peptide in vivo: Evidence for augmentation of a 42-specific γ secretase. *Human Molecular Genetics*, *13*(2), 159–170. https://doi.org/10.1093/hmg/ddh019

Jeltsch, H., Bertrand, F., Lazarus, C., & Cassel, J.-C. (2001). Cognitive Performances and Locomotor Activity Following Dentate Granule Cell Damage in Rats: Role of Lesion Extent and Type of Memory Tested. *Neurobiology of Learning and Memory*, *76*(1), 81–105. https://doi.org/10.1006/nlme.2000.3986

Jiang, Y., & VanDongen, A. M. J. (2021). Selective Increase of Correlated Activity in Arc-Positive Neurons after Chemically Induced Long-Term Potentiation in Cultured Hippocampal Neurons. *eNeuro*, *8*(6), ENEURO.0540-20.2021. https://doi.org/10.1523/ENEURO.0540-20.2021

Jinde, S., Zsiros, V., Jiang, Z., Nakao, K., Pickel, J., Kohno, K., Belforte, J. E., & Nakazawa, K. (2012). Hilar Mossy Cell Degeneration Causes Transient Dentate Granule Cell Hyperexcitability and Impaired Pattern Separation. *Neuron*, *76*(6), 1189–1200. https://doi.org/10.1016/j.neuron.2012.10.036

Jinno, S., & Kosaka, T. (2010). Stereological estimation of numerical densities of glutamatergic principal neurons in the mouse hippocampus. *Hippocampus*, *20*(7), 829–840. https://doi.org/10.1002/hipo.20685

Johnson, A., & Redish, A. D. (2007). Neural Ensembles in CA3 Transiently Encode Paths Forward of the Animal at a Decision Point. *Journal of Neuroscience*, *27*(45), 12176–12189. https://doi.org/10.1523/JNEUROSCI.3761-07.2007

Josselyn, S. A., & Tonegawa, S. (2020). Memory engrams: Recalling the past and imagining the future. *Science*, *367*(6473), eaaw4325. https://doi.org/10.1126/science.aaw4325

Jou, C., Hurtado, J. R., Carrillo-Segura, S., Park, E. H., & Fenton, A. A. (2023). *On the results of causal optogenetic engram manipulations* [Preprint]. Neuroscience. https://doi.org/10.1101/2023.05.15.540888

Jung, M. W., & McNaughton, B. L. (1993). Spatial selectivity of unit activity in the hippocampal granular layer. *Hippocampus*, *3*(2), 165–182. https://doi.org/10.1002/hipo.450030209

Jung, M., Wiener, S., & McNaughton, B. (1994). Comparison of spatial firing characteristics of units in dorsal and ventral hippocampus of the rat. *The Journal of Neuroscience*, *14*(12), 7347–7356. https://doi.org/10.1523/JNEUROSCI.14-12-07347.1994

Kandel, E. R., Dudai, Y., & Mayford, M. R. (2014). The Molecular and Systems Biology of Memory. *Cell*, *157*(1), 163–186. https://doi.org/10.1016/j.cell.2014.03.001

Kandel, E. R., & Tauc, L. (1964). Mechanism of Prolonged Heterosynaptic Facilitation. *Nature*, *202*(4928), Article 4928. https://doi.org/10.1038/202145a0

Karlsson, M. P., & Frank, L. M. (2009). Awake replay of remote experiences in the hippocampus. *Nature Neuroscience*, *12*(7), 913–918. https://doi.org/10.1038/nn.2344

Kerr, K. M., Agster, K. L., Furtak, S. C., & Burwell, R. D. (2007). Functional neuroanatomy of the parahippocampal region: The lateral and medial entorhinal areas. *Hippocampus*, *17*(9), 697–708. https://doi.org/10.1002/hipo.20315

Kesner, R. P. (2013). An analysis of the dentate gyrus function. *Behavioural Brain Research*, *254*, 1–7. https://doi.org/10.1016/j.bbr.2013.01.012

Kheirbek, M. A., Drew, L. J., Burghardt, N. S., Costantini, D. O., Tannenholz, L., Ahmari, S. E., Zeng, H., Fenton, A. A., & Hen, R. (2013). Differential Control of Learning and Anxiety along the Dorsoventral Axis of the Dentate Gyrus. *Neuron*, *77*(5), 955–968. https://doi.org/10.1016/j.neuron.2012.12.038

Kim, C. K., Sanchez, M. I., Hoerbelt, P., Fenno, L. E., Malenka, R. C., Deisseroth, K., & Ting, A. Y. (2020). A Molecular Calcium Integrator Reveals a Striatal Cell Type Driving Aversion. *Cell*, *183*(7), 2003-2019.e16. https://doi.org/10.1016/j.cell.2020.11.015

Kim, J., Kwon, J.-T., Kim, H.-S., Josselyn, S. A., & Han, J.-H. (2014). Memory recall and modifications by activating neurons with elevated CREB. *Nature Neuroscience*, *17*(1), Article 1. https://doi.org/10.1038/nn.3592

Kim, S., Kim, Y., Lee, S.-H., & Ho, W.-K. (2018). Dendritic spikes in hippocampal granule cells are necessary for long-term potentiation at the perforant path synapse. *eLife*, *7*, e35269. https://doi.org/10.7554/eLife.35269

Kinsky, N. R., Mau, W., Sullivan, D. W., Levy, S. J., Ruesch, E. A., & Hasselmo, M. E. (2020). Trajectory-modulated hippocampal neurons persist throughout memory-

guided navigation. *Nature Communications*, *11*, 2443. https://doi.org/10.1038/s41467-020-16226-4

Kitamura, T., Ogawa, S. K., Roy, D. S., Okuyama, T., Morrissey, M. D., Smith, L. M., Redondo, R. L., & Tonegawa, S. (2017). Engrams and circuits crucial for systems consolidation of a memory. *Science*, *356*(6333), 73–78. https://doi.org/10.1126/science.aam6808

Kitchigina, V., Vankov, A., Harley, C., & Sara, S. J. (1997). Novelty-elicited, Noradrenaline-dependent Enhancement of Excitability in the Dentate Gyrus. *European Journal of Neuroscience*, *9*(1), 41–47. https://doi.org/10.1111/j.1460-9568.1997.tb01351.x

Kjelstrup, K. B., Solstad, T., Brun, V. H., Hafting, T., Leutgeb, S., Witter, M. P., Moser, E. I., & Moser, M.-B. (2008). Finite Scale of Spatial Representation in the Hippocampus. *Science*, *321*(5885), 140–143. https://doi.org/10.1126/science.1157086

Klausberger, T., & Somogyi, P. (2008). Neuronal Diversity and Temporal Dynamics: The Unity of Hippocampal Circuit Operations. *Science*, *321*(5885), 53–57. https://doi.org/10.1126/science.1149381

Korczyn, A. D. (2008). The amyloid cascade hypothesis. *Alzheimer's & Dementia*, *4*(3), 176–178. https://doi.org/10.1016/j.jalz.2007.11.008

Kupfermann, I., & Kandel, E. R. (1969). Neuronal Controls of a Behavioral Response Mediated by the Abdominal Ganglion of *Aplysia*. *Science*, *164*(3881), 847–850. https://doi.org/10.1126/science.164.3881.847

Labiner, D., Butler, L., Cao, Z., Hosford, D., Shin, C., & McNamara, J. (1993). Induction of c-fos mRNA by kindled seizures: Complex relationship with neuronal burst firing. *The Journal of Neuroscience*, *13*(2), 744–751. https://doi.org/10.1523/JNEUROSCI.13-02-00744.1993

Lamothe-Molina, P. J., Franzelin, A., Beck, L., Li, D., Auksutat, L., Fieblinger, T., Laprell, L., Alhbeck, J., Gee, C. E., Kneussel, M., Engel, A. K., Hilgetag, C. C., Morellini, F., & Oertner, T. G. (2022). ΔFosB accumulation in hippocampal granule cells drives cFos pattern separation during spatial learning. *Nature Communications*, *13*(1), Article 1. https://doi.org/10.1038/s41467-022-33947-w

Lane, R. M., Potkin, S. G., & Enz, A. (2005). Targeting acetylcholinesterase and butyrylcholinesterase in dementia. *The International Journal of Neuropsychopharmacology*, *9*(01), 101. https://doi.org/10.1017/S1461145705005833

Lansink, C. S., Goltstein, P. M., Lankelma, J. V., McNaughton, B. L., & Pennartz, C. M. A. (2009). Hippocampus Leads Ventral Striatum in Replay of Place-Reward Information. *PLOS Biology*, *7*(8), e1000173. https://doi.org/10.1371/journal.pbio.1000173

Larimer, P., & Strowbridge, B. W. (2008). Nonrandom Local Circuits in the Dentate Gyrus. *The Journal of Neuroscience*, *28*(47), 12212–12223. https://doi.org/10.1523/JNEUROSCI.3612-08.2008

Lashley, K. S. (1931). Mass Action in Cerebral Function. *Science*, *73*(1888), 245–254. https://doi.org/10.1126/science.73.1888.245

Lee, A. K., & Wilson, M. A. (2002). Memory of Sequential Experience in the Hippocampus during Slow Wave Sleep. *Neuron*, *36*(6), 1183–1194. https://doi.org/10.1016/S0896-6273(02)01096-6

Lee, I., & Kesner, R. P. (2004). Encoding versus retrieval of spatial memory: Double dissociation between the dentate gyrus and the perforant path inputs into CA3 in the dorsal hippocampus. *Hippocampus*, *14*(1), 66–76. https://doi.org/10.1002/hipo.10167

Leutgeb, J. K., Leutgeb, S., Moser, M.-B., & Moser, E. I. (2007). Pattern Separation in the Dentate Gyrus and CA3 of the Hippocampus. *Science*, *315*(5814), 961–966. https://doi.org/10.1126/science.1135801

Leutgeb, S., Leutgeb, J. K., Barnes, C. A., Moser, E. I., McNaughton, B. L., & Moser, M.-B. (2005). Independent Codes for Spatial and Episodic Memory in Hippocampal Neuronal Ensembles. *Science*, *309*(5734), 619–623. https://doi.org/10.1126/science.1114037

Levy, S. J., Kinsky, N. R., Mau, W., Sullivan, D. W., & Hasselmo, M. E. (2021). Hippocampal spatial memory representations in mice are heterogeneously stable. *Hippocampus*, *31*(3), 244–260. https://doi.org/10.1002/hipo.23272

Li, B., Yamamori, H., Tatebayashi, Y., Shafit-Zagardo, B., Tanimukai, H., Chen, S., Iqbal, K., & Grundke-Iqbal, I. (2008). Failure of Neuronal Maturation in Alzheimer Disease Dentate Gyrus. *Journal of Neuropathology & Experimental Neurology*, *67*(1), 78–84. https://doi.org/10.1097/nen.0b013e318160c5db

Li, X.-G., Somogyi, P., Ylinen, A., & Buzsáki, G. (1994). The hippocampal CA3 network: An in vivo intracellular labeling study. *Journal of Comparative Neurology*, *339*(2), 181–208. https://doi.org/10.1002/cne.903390204

Lisman, J. E. (1999). Relating Hippocampal Circuitry to Function: Recall of Memory Sequences by Reciprocal Dentate–CA3 Interactions. *Neuron*, *22*(2), 233–242. https://doi.org/10.1016/S0896-6273(00)81085-5

Liu, X., Ramirez, S., Pang, P. T., Puryear, C. B., Govindarajan, A., Deisseroth, K., & Tonegawa, S. (2012). Optogenetic stimulation of a hippocampal engram activates fear memory recall. *Nature*, *484*(7394), 381–385. https://doi.org/10.1038/nature11028

Louie, K., & Wilson, M. A. (2001). Temporally Structured Replay of Awake Hippocampal Ensemble Activity during Rapid Eye Movement Sleep. *Neuron*, *29*(1), 145–156. https://doi.org/10.1016/S0896-6273(01)00186-6

Lowenstein, D., Thomas, M., Smith, D., & McIntosh, T. (1992). Selective vulnerability of dentate hilar neurons following traumatic brain injury: A potential mechanistic link between head trauma and disorders of the hippocampus. *The Journal of Neuroscience*, *12*(12), 4846–4853. https://doi.org/10.1523/JNEUROSCI.12-12-04846.1992

Maisson, D. J.-N., Gemzik, Z. M., & Griffin, A. L. (2018). Optogenetic suppression of the nucleus reuniens selectively impairs encoding during spatial working memory. *Neurobiology of Learning and Memory*, *155*, 78–85. https://doi.org/10.1016/j.nlm.2018.06.010

Malenka, R. C., & Bear, M. F. (2004). LTP and LTD: An Embarrassment of Riches. *Neuron*, *44*(1), 5–21. https://doi.org/10.1016/j.neuron.2004.09.012

Malvache, A., Reichinnek, S., Villette, V., Haimerl, C., & Cossart, R. (2016). Awake hippocampal reactivations project onto orthogonal neuronal assemblies. *Science*, *353*(6305), 1280–1283. https://doi.org/10.1126/science.aaf3319

Margerison, J. H., & Corsellis, J. A. N. (1966). EPILEPSY AND THE TEMPORAL LOBES: A CLINICAL, ELECTROENCEPHALOGRAPHIC AND NEUROPATHOLOGICAL STUDY OF THE BRAIN IN EPILEPSY, WITH PARTICULAR REFERENCE TO THE TEMPORAL LOBES. *Brain*, *89*(3), 499–530. https://doi.org/10.1093/brain/89.3.499

Marr, D. (1969). A theory of cerebellar cortex. *The Journal of Physiology*, *202*(2), 437–470. https://doi.org/10.1113/jphysiol.1969.sp008820

Marr, D. (1971). Simple memory: A theory for archicortex. *Philosophical Transactions of the Royal Society of London. B, Biological Sciences*, *262*(841), 23–81. https://doi.org/10.1098/rstb.1971.0078

Marucci, G., Buccioni, M., Ben, D. D., Lambertucci, C., Volpini, R., & Amenta, F. (2021). Efficacy of acetylcholinesterase inhibitors in Alzheimer's disease. *Neuropharmacology*, *190*, 108352. https://doi.org/10.1016/j.neuropharm.2020.108352

Mathis, A., Mamidanna, P., Cury, K. M., Abe, T., Murthy, V. N., Mathis, M. W., & Bethge, M. (2018). DeepLabCut: Markerless pose estimation of user-defined

body parts with deep learning. *Nature Neuroscience*, *21*(9), 1281–1289. https://doi.org/10.1038/s41593-018-0209-y

McHugh, T. J., Jones, M. W., Quinn, J. J., Balthasar, N., Coppari, R., Elmquist, J. K., Lowell, B. B., Fanselow, M. S., Wilson, M. A., & Tonegawa, S. (2007). Dentate Gyrus NMDA Receptors Mediate Rapid Pattern Separation in the Hippocampal Network. *Science*, *317*(5834), 94–99. https://doi.org/10.1126/science.1140263

McKenzie, S., Huszár, R., English, D. F., Kim, K., Christensen, F., Yoon, E., & Buzsáki, G. (2021). Preexisting hippocampal network dynamics constrain optogenetically induced place fields. *Neuron*, *109*(6), 1040-1054.e7. https://doi.org/10.1016/j.neuron.2021.01.011

McLamb, R. L., Mundy, W. R., & Tilson, H. A. (1988). Intradentate colchicine disrupts the acquisition and performance of a working memory task in the radial arm maze. *Neurotoxicology*, *9*(3), 521–528.

McNaughton, B. L., Barnes, C. A., Meltzer, J., & Sutherland, R. J. (1989). Hippocampal granule cells are necessary for normal spatial learning but not for spatially-selective pyramidal cell discharge. *Experimental Brain Research*, *76*(3), 485–496. https://doi.org/10.1007/BF00248904

McNaughton, B. L., & Morris, R. G. M. (1987). Hippocampal synaptic enhancement and information storage within a distributed memory system. *Trends in Neurosciences*, *10*(10), 408–415. https://doi.org/10.1016/0166-2236(87)90011-7

Merrill, D. A., Chiba, A. A., & Tuszynski, M. H. (2001). Conservation of neuronal number and size in the entorhinal cortex of behaviorally characterized aged rats.

*Journal of Comparative Neurology*, *438*(4), 445–456. https://doi.org/10.1002/cne.1327

Moita, M. A. P., Rosis, S., Zhou, Y., LeDoux, J. E., & Blair, H. T. (2004). Putting Fear in Its Place: Remapping of Hippocampal Place Cells during Fear Conditioning. *Journal of Neuroscience*, *24*(31), 7015–7023. https://doi.org/10.1523/JNEUROSCI.5492-03.2004

Moosmang, S., Haider, N., Klugbauer, N., Adelsberger, H., Langwieser, N., Müller, J., Stiess, M., Marais, E., Schulla, V., Lacinova, L., Goebbels, S., Nave, K.-A., Storm, D. R., Hofmann, F., & Kleppisch, T. (2005). Role of Hippocampal Cav1.2 Ca2+ Channels in NMDA Receptor-Independent Synaptic Plasticity and Spatial Memory. *Journal of Neuroscience*, *25*(43), 9883–9892. https://doi.org/10.1523/JNEUROSCI.1531-05.2005

Morris, R. G. M., Garrud, P., Rawlins, J. N. P., & O'Keefe, J. (1982). Place navigation impaired in rats with hippocampal lesions. *Nature*, *297*(5868), Article 5868. https://doi.org/10.1038/297681a0

Moser, M.-B., & Moser, E. I. (1998). Functional differentiation in the hippocampus. *Hippocampus*, *8*(6), 608–619. https://doi.org/10.1002/(SICI)1098-1063(1998)8:6<608::AID-HIPO3>3.0.CO;2-7

Mou, X., Cheng, J., Yu, Y. S. W., Kee, S. E., & Ji, D. (2018). Comparing Mouse and Rat Hippocampal Place Cell Activities and Firing Sequences in the Same Environments. *Frontiers in Cellular Neuroscience*, *12*. https://doi.org/10.3389/fncel.2018.00332

Muller, R., Kubie, J., & Ranck, J. (1987). Spatial firing patterns of hippocampal complex-spike cells in a fixed environment. *The Journal of Neuroscience*, *7*(7), 1935–1950. https://doi.org/10.1523/JNEUROSCI.07-07-01935.1987

Mumby, D. G., & Pinel, J. P. J. (1994). Rhinal cortex lesions and object recognition in rats. *Behavioral Neuroscience*, *108*(1), 11–18. https://doi.org/10.1037/0735-7044.108.1.11

Naber, P. A., Lopes da Silva, F. H., & Witter, M. P. (2001). Reciprocal connections between the entorhinal cortex and hippocampal fields CA1 and the subiculum are in register with the projections from CA1 to the subiculum. *Hippocampus*, *11*(2), 99–104. https://doi.org/10.1002/hipo.1028

Nakashiba, T., Cushman, J. D., Pelkey, K. A., Renaudineau, S., Buhl, D. L., McHugh, T. J., Barrera, V. R., Chittajallu, R., Iwamoto, K. S., McBain, C. J., Fanselow, M. S., & Tonegawa, S. (2012). Young Dentate Granule Cells Mediate Pattern Separation whereas Old Granule Cells Contribute to Pattern Completion. *Cell*, *149*(1), 188–201. https://doi.org/10.1016/j.cell.2012.01.046

Nakazawa, K., Quirk, M. C., Chitwood, R. A., Watanabe, M., Yeckel, M. F., Sun, L. D., Kato, A., Carr, C. A., Johnston, D., Wilson, M. A., & Tonegawa, S. (2002). Requirement for Hippocampal CA3 NMDA Receptors in Associative Memory Recall. *Science (New York, N.Y.)*, *297*(5579), 211–218. https://doi.org/10.1126/science.1071795

Nanry, K. P., Mundy, W. R., & Tilson, H. A. (1989). Colchicine-induced alterations of reference memory in rats: Role of spatial versus non-spatial task components.

*Behavioural Brain Research*, *35*(1), 45–53. https://doi.org/10.1016/S0166-4328(89)80007-5

Neunuebel, J. P., & Knierim, J. J. (2012). Spatial Firing Correlates of Physiologically Distinct Cell Types of the Rat Dentate Gyrus. *The Journal of Neuroscience*, *32*(11), 3848–3858. https://doi.org/10.1523/JNEUROSCI.6038-11.2012

Neunuebel, J. P., & Knierim, J. J. (2014). CA3 Retrieves Coherent Representations from Degraded Input: Direct Evidence for CA3 Pattern Completion and Dentate Gyrus Pattern Separation. *Neuron*, *81*(2), 416–427. https://doi.org/10.1016/j.neuron.2013.11.017

O'Dell, T. J., Connor, S. A., Guglietta, R., & Nguyen, P. V. (2015). β-Adrenergic receptor signaling and modulation of long-term potentiation in the mammalian hippocampus. *Learning & Memory*, *22*(9), 461–471. https://doi.org/10.1101/lm.031088.113

Ohkawa, N., Saitoh, Y., Suzuki, A., Tsujimura, S., Murayama, E., Kosugi, S., Nishizono, H., Matsuo, M., Takahashi, Y., Nagase, M., Sugimura, Y. K., Watabe, A. M., Kato, F., & Inokuchi, K. (2015). Artificial Association of Pre-stored Information to Generate a Qualitatively New Memory. *Cell Reports*, *11*(2), 261–269. https://doi.org/10.1016/j.celrep.2015.03.017

Ohm, T. G. (2007). The dentate gyrus in Alzheimer's disease. In H. E. Scharfman (Ed.), *Progress in Brain Research* (Vol. 163, pp. 723–740). Elsevier. https://doi.org/10.1016/S0079-6123(07)63039-8

O'Keefe, J. (1976). Place units in the hippocampus of the freely moving rat. *Experimental Neurology*, *51*(1), 78–109. https://doi.org/10.1016/0014-4886(76)90055-8

O'Keefe, J., & Dostrovsky, J. (1971). The hippocampus as a spatial map. Preliminary evidence from unit activity in the freely-moving rat. *Brain Research*, *34*(1), 171–175. https://doi.org/10.1016/0006-8993(71)90358-1

O'Keefe, J., & Nadel, L. (1978). *The hippocampus as a cognitive map*. Clarendon Press ; Oxford University Press.

Oliva, A., Fernández-Ruiz, A., Buzsáki, G., & Berényi, A. (2016). Role of Hippocampal CA2 Region in Triggering Sharp-Wave Ripples. *Neuron*, *91*(6), 1342–1355. https://doi.org/10.1016/j.neuron.2016.08.008

Olton, D. S., Branch, M., & Best, P. J. (1978). Spatial correlates of hippocampal unit activity. *Experimental Neurology*, *58*(3), 387–409. https://doi.org/10.1016/0014-4886(78)90096-1

O'Reilly, R. C., & McClelland, J. L. (1994). Hippocampal conjunctive encoding, storage, and recall: Avoiding a trade-off. *Hippocampus*, *4*(6), 661–682. https://doi.org/10.1002/hipo.450040605

Ozawa, M., Davis, P., Ni, J., Maguire, J., Papouin, T., & Reijmers, L. (2020). Experience-dependent resonance in amygdalo-cortical circuits supports fear memory retrieval following extinction. *Nature Communications*, *11*(1), Article 1. https://doi.org/10.1038/s41467-020-18199-w

Padilla-Coreano, N., Canetta, S., Mikofsky, R. M., Alway, E., Passecker, J., Myroshnychenko, M. V., Garcia-Garcia, A. L., Warren, R., Teboul, E., Blackman, D. R., Morton, M. P., Hupalo, S., Tye, K. M., Kellendonk, C., Kupferschmidt, D. A., & Gordon, J. A. (2019). Hippocampal-Prefrontal Theta Transmission Regulates Avoidance Behavior. *Neuron*, *104*(3), 601-610.e4. https://doi.org/10.1016/j.neuron.2019.08.006

Palacios-Filardo, J., & Mellor, J. R. (2019). Neuromodulation of hippocampal long-term synaptic plasticity. *Current Opinion in Neurobiology*, *54*, 37–43. https://doi.org/10.1016/j.conb.2018.08.009

Park, A. (2023, January 6). *FDA Approves Lecanemab, a New Alzheimer's Drug*. Time. https://time.com/6244798/fda-approves-lecanemab-alzheimers-drug/

Parra, P., Gulyás, A. I., & Miles, R. (1998). How Many Subtypes of Inhibitory Cells in the Hippocampus? *Neuron*, *20*(5), 983–993. https://doi.org/10.1016/S0896-6273(00)80479-1

Patil, M. M., & Hasselmo, M. E. (1999). Modulation of Inhibitory Synaptic Potentials in the Piriform Cortex. *Journal of Neurophysiology*, *81*(5), 2103–2118. https://doi.org/10.1152/jn.1999.81.5.2103

Perusini, J. N., Cajigas, S. A., Cohensedgh, O., Lim, S. C., Pavlova, I. P., Donaldson, Z. R., & Denny, C. A. (2017). Optogenetic stimulation of dentate gyrus engrams restores memory in Alzheimer's disease mice. *Hippocampus*, *27*(10), 1110–1122. https://doi.org/10.1002/hipo.22756

Pettit, N. L., Yap, E.-L., Greenberg, M. E., & Harvey, C. D. (2022). Fos ensembles encode and shape stable spatial maps in the hippocampus. *Nature*, 1–8. https://doi.org/10.1038/s41586-022-05113-1

Peyrache, A., Khamassi, M., Benchenane, K., Wiener, S. I., & Battaglia, F. P. (2009). Replay of rule-learning related neural patterns in the prefrontal cortex during sleep. *Nature Neuroscience*, *12*(7), 919–926. https://doi.org/10.1038/nn.2337

Pfeiffer, B. E., & Foster, D. J. (2013). Hippocampal place cell sequences depict future paths to remembered goals. *Nature*, *497*(7447), 74–79. https://doi.org/10.1038/nature12112

Pikkarainen, M., Rönkkö, S., Savander, V., Insausti, R., & Pitkänen, A. (1999). Projections from the lateral, basal, and accessory basal nuclei of the amygdala to the hippocampal formation in rat. *Journal of Comparative Neurology*, *403*(2), 229–260. https://doi.org/10.1002/(SICI)1096-9861(19990111)403:2<229::AID-CNE7>3.0.CO;2-P

Poppenk, J., Evensmoen, H. R., Moscovitch, M., & Nadel, L. (2013). Long-axis specialization of the human hippocampus. *Trends in Cognitive Sciences*, *17*(5), 230–240. https://doi.org/10.1016/j.tics.2013.03.005

Quyen, M. L. V., Staba, R., Bragin, A., Dickson, C., Valderrama, M., Fried, I., & Engel, J. (2010). Large-Scale Microelectrode Recordings of High-Frequency Gamma Oscillations in Human Cortex during Sleep. *Journal of Neuroscience*, *30*(23), 7770–7782. https://doi.org/10.1523/JNEUROSCI.5049-09.2010

Radulovic, J., Kammermeier, J., & Spiess, J. (1998). Relationship between Fos Production and Classical Fear Conditioning: Effects of Novelty, Latent Inhibition, and Unconditioned Stimulus Preexposure. *The Journal of Neuroscience*, *18*(18), 7452–7461. https://doi.org/10.1523/JNEUROSCI.18-18-07452.1998

Rahsepar, B., Norman, J. F., Noueihed, J., Lahner, B., Quick, M. H., Ghaemi, K., Pandya, A., Fernandez, F. R., Ramirez, S., & White, J. A. (2023). Theta-phase-specific modulation of dentate gyrus memory neurons. *eLife*, *12*, e82697. https://doi.org/10.7554/eLife.82697

Ramirez, S., Liu, X., Lin, P.-A., Suh, J., Pignatelli, M., Redondo, R. L., Ryan, T. J., & Tonegawa, S. (2013). Creating a False Memory in the Hippocampus. *Science*, *341*(6144), 387–391. https://doi.org/10.1126/science.1239073

Ramirez, S., Liu, X., MacDonald, C. J., Moffa, A., Zhou, J., Redondo, R. L., & Tonegawa, S. (2015). Activating positive memory engrams suppresses depression-like behaviour. *Nature*, *522*(7556), 335–339. https://doi.org/10.1038/nature14514

Rapp, P. R., Deroche, P. S., Mao, Y., & Burwell, R. D. (2002). Neuron Number in the Parahippocampal Region is Preserved in Aged Rats with Spatial Learning Deficits. *Cerebral Cortex*, *12*(11), 1171–1179. https://doi.org/10.1093/cercor/12.11.1171

Ratzliff, A. H., Santhakumar, V., Howard, A., & Soltesz, I. (2002). Mossy cells in epilepsy: Rigor mortis or vigor mortis? *Trends in Neurosciences*, *25*(3), 140–144. https://doi.org/10.1016/S0166-2236(00)02122-6

Raymond, C. R. (2007). LTP forms 1, 2 and 3: Different mechanisms for the 'long' in long-term potentiation. *Trends in Neurosciences*, *30*(4), 167–175. https://doi.org/10.1016/j.tins.2007.01.007

Redondo, R. L., Kim, J., Arons, A. L., Ramirez, S., Liu, X., & Tonegawa, S. (2014). Bidirectional switch of the valence associated with a hippocampal contextual memory engram. *Nature*, *513*(7518), 426–430. https://doi.org/10.1038/nature13725

Reijmers, L. G., Perkins, B. L., Matsuo, N., & Mayford, M. (2007). Localization of a Stable Neural Correlate of Associative Memory. *Science*, *317*(5842), 1230–1233. https://doi.org/10.1126/science.1143839

Ribak, C. E., Harris, A. B., Vaughn, J. E., & Roberts, E. (1979). Inhibitory, GABAergic nerve terminals decrease at sites of focal epilepsy. *Science (New York, N.Y.)*, *205*(4402), 211–214. https://doi.org/10.1126/science.109922

Ribak, C. E., Seress, L., & Amaral, D. G. (1985). The development, ultrastructure and synaptic connections of the mossy cells of the dentate gyrus. *Journal of Neurocytology*, *14*(5), 835–857. https://doi.org/10.1007/BF01170832

Robinson, N. T. M., Descamps, L. A. L., Russell, L. E., Buchholz, M. O., Bicknell, B. A., Antonov, G. K., Lau, J. Y. N., Nutbrown, R., Schmidt-Hieber, C., & Häusser, M. (2020). Targeted Activation of Hippocampal Place Cells Drives Memory-Guided Spatial Behavior. *Cell*, *183*(6), 1586-1599.e10. https://doi.org/10.1016/j.cell.2020.09.061

Roux, L., Hu, B., Eichler, R., Stark, E., & Buzsáki, G. (2017). Sharp wave ripples during learning stabilize the hippocampal spatial map. *Nature Neuroscience*, *20*(6), 845–853. https://doi.org/10.1038/nn.4543

Roy, D. S., Arons, A., Mitchell, T. I., Pignatelli, M., Ryan, T. J., & Tonegawa, S. (2016). Memory retrieval by activating engram cells in mouse models of early Alzheimer's disease. *Nature*, *531*(7595), 508–512. https://doi.org/10.1038/nature17172

Roy, D. S., Park, Y.-G., Kim, M. E., Zhang, Y., Ogawa, S. K., DiNapoli, N., Gu, X., Cho, J. H., Choi, H., Kamentsky, L., Martin, J., Mosto, O., Aida, T., Chung, K., & Tonegawa, S. (2022). Brain-wide mapping reveals that engrams for a single memory are distributed across multiple brain regions. *Nature Communications*, *13*, 1799. https://doi.org/10.1038/s41467-022-29384-4

Ryan, T. J., Roy, D. S., Pignatelli, M., Arons, A., & Tonegawa, S. (2015). Engram Cells Retain Memory Under Retrograde Amnesia. *Science (New York, N.Y.)*, *348*(6238), 1007–1013. https://doi.org/10.1126/science.aaa5542

Sagar, S. M., Sharp, F. R., & Curran, T. (1988). Expression of c-fos Protein in Brain: Metabolic Mapping at the Cellular Level. *Science*, *240*(4857), 1328–1331. https://doi.org/10.1126/science.3131879

Samborska, V., Butler, J. L., Walton, M. E., Behrens, T. E. J., & Akam, T. (2022). Complementary task representations in hippocampus and prefrontal cortex for generalizing the structure of problems. *Nature Neuroscience*, *25*(10), Article 10. https://doi.org/10.1038/s41593-022-01149-8

Santhakumar, V., Bender, R., Frotscher, M., Ross, S. T., Hollrigel, G. S., Toth, Z., & Soltesz, I. (2000). Granule cell hyperexcitability in the early post-traumatic rat dentate gyrus: The 'irritable mossy cell' hypothesis. *The Journal of Physiology*, *524*(1), 117–134. https://doi.org/10.1111/j.1469-7793.2000.00117.x

Santoro, A. (2013). Reassessing pattern separation in the dentate gyrus. *Frontiers in Behavioral Neuroscience*, *7*. https://doi.org/10.3389/fnbeh.2013.00096

Sara, S. J. (2009). The locus coeruleus and noradrenergic modulation of cognition. *Nature Reviews Neuroscience*, *10*(3), Article 3. https://doi.org/10.1038/nrn2573

Sasaki, T., Piatti, V. C., Hwaun, E., Ahmadi, S., Lisman, J. E., Leutgeb, S., & Leutgeb, J. K. (2018). Dentate network activity is necessary for spatial working memory by supporting CA3 sharp-wave ripple generation and prospective firing of CA3 neurons. *Nature Neuroscience*, *21*(2), 258–269. https://doi.org/10.1038/s41593-017-0061-5

Satvat, E., Schmidt, B., Argraves, M., Marrone, D. F., & Markus, E. J. (2011). Changes in Task Demands Alter the Pattern of zif268 Expression in the Dentate Gyrus. *The Journal of Neuroscience*, *31*(19), 7163–7167. https://doi.org/10.1523/JNEUROSCI.0094-11.2011

Scharfman, H. E. (1995). Electrophysiological evidence that dentate hilar mossy cells are excitatory and innervate both granule cells and interneurons. *Journal of Neurophysiology*, *74*(1), 179–194. https://doi.org/10.1152/jn.1995.74.1.179

Scharfman, H. E. (2007). The CA3 “backprojection” to the dentate gyrus. In *Progress in Brain Research* (Vol. 163, pp. 627–637). Elsevier. https://doi.org/10.1016/S0079-6123(07)63034-9

Scharfman, H. E. (2016). The enigmatic mossy cell of the dentate gyrus. *Nature Reviews Neuroscience*, *17*(9), 562–575. https://doi.org/10.1038/nrn.2016.87

Scharfman, H. E. (2019). The Dentate Gyrus and Temporal Lobe Epilepsy: An “Exciting” Era. *Epilepsy Currents*, *19*(4), 249–255. https://doi.org/10.1177/1535759719855952

Schmidt, U., Weigert, M., Broaddus, C., & Myers, G. (2018). Cell Detection with Star-Convex Polygons. In A. F. Frangi, J. A. Schnabel, C. Davatzikos, C. Alberola-López, & G. Fichtinger (Eds.), *Medical Image Computing and Computer Assisted Intervention – MICCAI 2018* (pp. 265–273). Springer International Publishing. https://doi.org/10.1007/978-3-030-00934-2_30

Schönheit, B., Zarski, R., & Ohm, T. G. (2004). Spatial and temporal relationships between plaques and tangles in Alzheimer-pathology. *Neurobiology of Aging*, *25*(6), 697–711. https://doi.org/10.1016/j.neurobiolaging.2003.09.009

Schuette, P. J., Reis, F. M. C. V., Maesta-Pereira, S., Chakerian, M., Torossian, A., Blair, G. J., Wang, W., Blair, H. T., Fanselow, M. S., Kao, J. C., & Adhikari, A. (2020). Long-Term Characterization of Hippocampal Remapping during Contextual Fear Acquisition and Extinction. *Journal of Neuroscience*, *40*(43), 8329–8342. https://doi.org/10.1523/JNEUROSCI.1022-20.2020

Scoville, W. B., & Milner, B. (1957). Loss of Recent Memory After Bilateral Hippocampal Lesions. *Journal of Neurology, Neurosurgery & Psychiatry*, *20*(1), 11–21. https://doi.org/10.1136/jnnp.20.1.11

Semon, R. (1921). The mneme. *London: Allen*.

Senzai, Y. (2019). Function of local circuits in the hippocampal dentate gyrus-CA3 system. *Neuroscience Research*, *140*, 43–52. https://doi.org/10.1016/j.neures.2018.11.003

Senzai, Y., & Buzsáki, G. (2017). Physiological properties and behavioral correlates of hippocampal granule cells and mossy cells. *Neuron*, *93*(3), 691-704.e5. https://doi.org/10.1016/j.neuron.2016.12.011

Seress, L. (1988). Interspecies comparison of the hippocampal formation shows increased emphasis on the regio superior in the Ammon's horn of the human brain. *Journal Fur Hirnforschung*, *29*(3), 335–340.

Sheintuch, L., Geva, N., Baumer, H., Rechavi, Y., Rubin, A., & Ziv, Y. (2020). Multiple Maps of the Same Spatial Context Can Stably Coexist in the Mouse Hippocampus. *Current Biology*, *0*(0). https://doi.org/10.1016/j.cub.2020.02.018

Shen, J., Yao, P.-T., Ge, S., & Xiong, Q. (2021). Dentate granule cells encode auditory decisions after reinforcement learning in rats. *Scientific Reports*, *11*(1), Article 1. https://doi.org/10.1038/s41598-021-93721-8

Shimomura, O. (1979). Structure of the chromophore of Aequorea green fluorescent protein. *FEBS Letters*, *104*(2), 220–222. https://doi.org/10.1016/0014-5793(79)80818-2

Shin, J. D., Tang, W., & Jadhav, S. P. (2019). Dynamics of Awake Hippocampal-Prefrontal Replay for Spatial Learning and Memory-Guided Decision Making. *Neuron*. https://doi.org/10.1016/j.neuron.2019.09.012

Shpokayte, M., McKissick, O., Guan, X., Yuan, B., Rahsepar, B., Fernandez, F. R., Ruesch, E., Grella, S. L., White, J. A., Liu, X. S., & Ramirez, S. (2022). Hippocampal cells segregate positive and negative engrams. *Communications Biology*, *5*(1), 1009. https://doi.org/10.1038/s42003-022-03906-8

Siegle, J. H., & Wilson, M. A. (2014). Enhancement of encoding and retrieval functions through theta phase-specific manipulation of hippocampus. *eLife*, *3*. https://doi.org/10.7554/eLife.03061

Skaggs, W. E., & McNaughton, B. L. (1996). Replay of Neuronal Firing Sequences in Rat Hippocampus During Sleep Following Spatial Experience. *Science*, *271*(5257), 1870–1873. https://doi.org/10.1126/science.271.5257.1870

Sloviter, R. S. (1987). Decreased hippocampal inhibition and a selective loss of interneurons in experimental epilepsy. *Science (New York, N.Y.)*, *235*(4784), 73–76. https://doi.org/10.1126/science.2879352

Sloviter, R. S. (1994). The functional organization of the hippocampal dentate gyrus and its relevance to the pathogenesis of temporal lobe epilepsy. *Annals of Neurology*, *35*(6), 640–654. https://doi.org/10.1002/ana.410350604

Solstad, T., Boccara, C. N., Kropff, E., Moser, M.-B., & Moser, E. I. (2008). Representation of Geometric Borders in the Entorhinal Cortex. *Science*, *322*(5909), 1865–1868. https://doi.org/10.1126/science.1166466

Soriano, E., & Frotscher, M. (1994). Mossy cells of the rat fascia dentata are glutamate-immunoreactive. *Hippocampus*, *4*(1), 65–69. https://doi.org/10.1002/hipo.450040108

Spellman, T., Rigotti, M., Ahmari, S. E., Fusi, S., Gogos, J. A., & Gordon, J. A. (2015). Hippocampal–prefrontal input supports spatial encoding in working memory. *Nature*, *522*(7556), Article 7556. https://doi.org/10.1038/nature14445

Squire, L. R., Shimamura, A. P., & Amaral, D. G. (1989). 12—Memory and the Hippocampus. In J. H. Byrne & W. O. Berry (Eds.), *Neural Models of Plasticity* (pp. 208–239). Academic Press. https://doi.org/10.1016/B978-0-12-148955-7.50016-3

Stark, E., Roux, L., Eichler, R., & Buzsáki, G. (2015). Local generation of multineuronal spike sequences in the hippocampal CA1 region. *Proceedings of the National Academy of Sciences*, *112*(33), 10521–10526. https://doi.org/10.1073/pnas.1508785112

Stefanelli, T., Bertollini, C., Lüscher, C., Muller, D., & Mendez, P. (2016). Hippocampal Somatostatin Interneurons Control the Size of Neuronal Memory Ensembles. *Neuron*, *89*(5), 1074–1085. https://doi.org/10.1016/j.neuron.2016.01.024

Strange, B. A., Witter, M. P., Lein, E. S., & Moser, E. I. (2014). Functional organization of the hippocampal longitudinal axis. *Nature Reviews Neuroscience*, *15*(10), Article 10. https://doi.org/10.1038/nrn3785

Straube, T., Korz, V., Balschun, D., & Uta Frey, J. (2003). Requirement of β-adrenergic receptor activation and protein synthesis for LTP-reinforcement by novelty in rat

dentate gyrus. *The Journal of Physiology*, *552*(Pt 3), 953–960. https://doi.org/10.1113/jphysiol.2003.049452

Straube, T., Korz, V., & Frey, J. U. (2003). Bidirectional modulation of long-term potentiation by novelty-exploration in rat dentate gyrus. *Neuroscience Letters*, *344*(1), 5–8. https://doi.org/10.1016/S0304-3940(03)00349-5

Sullivan, D., Csicsvari, J., Mizuseki, K., Montgomery, S., Diba, K., & Buzsáki, G. (2011). Relationships between hippocampal sharp waves, ripples, and fast gamma oscillation: Influence of dentate and entorhinal cortical activity. *The Journal of Neuroscience: The Official Journal of the Society for Neuroscience*, *31*(23), 8605–8616. https://doi.org/10.1523/JNEUROSCI.0294-11.2011

Sun, X., Bernstein, M. J., Meng, M., Rao, S., Sørensen, A. T., Yao, L., Zhang, X., Anikeeva, P. O., & Lin, Y. (2020). Functionally Distinct Neuronal Ensembles within the Memory Engram. *Cell*, *181*(2), 410-423.e17. https://doi.org/10.1016/j.cell.2020.02.055

Suzuki, W. L., & Amaral, D. G. (1994). Perirhinal and parahippocampal cortices of the macaque monkey: Cortical afferents. *Journal of Comparative Neurology*, *350*(4), 497–533. https://doi.org/10.1002/cne.903500402

Takeuchi, T., Duszkiewicz, A. J., Sonneborn, A., Spooner, P. A., Yamasaki, M., Watanabe, M., Smith, C. C., Fernández, G., Deisseroth, K., Greene, R. W., & Morris, R. G. M. (2016). Locus coeruleus and dopaminergic consolidation of everyday memory. *Nature*, *537*(7620), 357–362. https://doi.org/10.1038/nature19325

Tamamaki, N., Abe, K., & Nojyo, Y. (1987). Columnar organization in the subiculum formed by axon branches originating from single CA1 pyramidal neurons in the rat hippocampus. *Brain Research*, *412*(1), 156–160. https://doi.org/10.1016/0006-8993(87)91452-1

Tanaka, K. Z., He, H., Tomar, A., Niisato, K., Huang, A. J. Y., & McHugh, T. J. (2018). The hippocampal engram maps experience but not place. *Science*, *361*(6400), 392–397. https://doi.org/10.1126/science.aat5397

Tanaka, K. Z., Pevzner, A., Hamidi, A. B., Nakazawa, Y., Graham, J., & Wiltgen, B. J. (2014). Cortical Representations Are Reinstated by the Hippocampus during Memory Retrieval. *Neuron*, *84*(2), 347–354. https://doi.org/10.1016/j.neuron.2014.09.037

Tang, W., Shin, J. D., & Jadhav, S. P. (2023). Geometric transformation of cognitive maps for generalization across hippocampal-prefrontal circuits. *Cell Reports*, *42*(3). https://doi.org/10.1016/j.celrep.2023.112246

Taube, J., Muller, R., & Ranck, J. (1990). Head-direction cells recorded from the postsubiculum in freely moving rats. I. Description and quantitative analysis. *The Journal of Neuroscience*, *10*(2), 420–435. https://doi.org/10.1523/JNEUROSCI.10-02-00420.1990

Tayler, K. K., Tanaka, K. Z., Reijmers, L. G., & Wiltgen, B. J. (2013). Reactivation of Neural Ensembles during the Retrieval of Recent and Remote Memory. *Current Biology*, *23*(2), 99–106. https://doi.org/10.1016/j.cub.2012.11.019

Teyler, T. J., & DiScenna, P. (1986). The hippocampal memory indexing theory. *Behavioral Neuroscience*, *100*(2), 147–154. https://doi.org/10.1037//0735-7044.100.2.147

Teyler, T. J., & Rudy, J. W. (2007). The hippocampal indexing theory and episodic memory: Updating the index. *Hippocampus*, *17*(12), 1158–1169. https://doi.org/10.1002/hipo.20350

Thompson, C. L., Pathak, S. D., Jeromin, A., Ng, L. L., MacPherson, C. R., Mortrud, M. T., Cusick, A., Riley, Z. L., Sunkin, S. M., Bernard, A., Puchalski, R. B., Gage, F. H., Jones, A. R., Bajic, V. B., Hawrylycz, M. J., & Lein, E. S. (2008). Genomic Anatomy of the Hippocampus. *Neuron*, *60*(6), 1010–1021. https://doi.org/10.1016/j.neuron.2008.12.008

Tolman, E. C. (1948). Cognitive maps in rats and men. *Psychological Review*, *55*(4), 189–208. https://doi.org/10.1037/h0061626

Tonegawa, S., Liu, X., Ramirez, S., & Redondo, R. (2015). Memory Engram Cells Have Come of Age. *Neuron*, *87*(5), 918–931. https://doi.org/10.1016/j.neuron.2015.08.002

Tosches, M. A., Yamawaki, T. M., Naumann, R. K., Jacobi, A. A., Tushev, G., & Laurent, G. (2018). Evolution of pallium, hippocampus, and cortical cell types revealed by single-cell transcriptomics in reptiles. *Science*, *360*(6391), 881–888. https://doi.org/10.1126/science.aar4237

Treves, A., & Rolls, E. T. (1994). Computational analysis of the role of the hippocampus in memory. *Hippocampus*, *4*(3), 374–391. https://doi.org/10.1002/hipo.450040319

van de Ven, G. M., Trouche, S., McNamara, C. G., Allen, K., & Dupret, D. (2016). Hippocampal Offline Reactivation Consolidates Recently Formed Cell Assembly Patterns during Sharp Wave-Ripples. *Neuron*, *92*(5), 968–974. https://doi.org/10.1016/j.neuron.2016.10.020

van Dyck, C. H., Swanson, C. J., Aisen, P., Bateman, R. J., Chen, C., Gee, M., Kanekiyo, M., Li, D., Reyderman, L., Cohen, S., Froelich, L., Katayama, S., Sabbagh, M., Vellas, B., Watson, D., Dhadda, S., Irizarry, M., Kramer, L. D., & Iwatsubo, T. (2023). Lecanemab in Early Alzheimer's Disease. *New England Journal of Medicine*, *388*(1), 9–21. https://doi.org/10.1056/NEJMoa2212948

Van Groen, T., & Wyss, J. M. (1990). Extrinsic projections from area CA1 of the rat hippocampus: Olfactory, cortical, subcortical, and bilateral hippocampal formation projections. *Journal of Comparative Neurology*, *302*(3), 515–528. https://doi.org/10.1002/cne.903020308

VanElzakker, M., Fevurly, R. D., Breindel, T., & Spencer, R. L. (2008). Environmental novelty is associated with a selective increase in Fos expression in the output elements of the hippocampal formation and the perirhinal cortex. *Learning & Memory*, *15*(12), 899–908. https://doi.org/10.1101/lm.1196508

Vaz, A. P., Wittig, J. H., Inati, S. K., & Zaghloul, K. A. (2020). Replay of cortical spiking sequences during human memory retrieval. *Science*, *367*(6482), 1131–1134. https://doi.org/10.1126/science.aba0672

Vaz, A. P., Wittig, J. H., Inati, S. K., & Zaghloul, K. A. (2023). Backbone spiking sequence as a basis for preplay, replay, and default states in human cortex. *Nature Communications*, *14*(1), Article 1. https://doi.org/10.1038/s41467-023-40440-5

Vertes, R. P., Hoover, W. B., Szigeti-Buck, K., & Leranth, C. (2007). Nucleus reuniens of the midline thalamus: Link between the medial prefrontal cortex and the hippocampus. *Brain Research Bulletin*, *71*(6), 601–609. https://doi.org/10.1016/j.brainresbull.2006.12.002

Vetere, G., Kenney, J. W., Tran, L. M., Xia, F., Steadman, P. E., Parkinson, J., Josselyn, S. A., & Frankland, P. W. (2017). Chemogenetic Interrogation of a Brain-wide Fear Memory Network in Mice. *Neuron*, *94*(2), 363-374.e4. https://doi.org/10.1016/j.neuron.2017.03.037

Villeda, S. A., Plambeck, K. E., Middeldorp, J., Castellano, J. M., Mosher, K. I., Luo, J., Smith, L. K., Bieri, G., Lin, K., Berdnik, D., Wabl, R., Udeochu, J., Wheatley, E. G., Zou, B., Simmons, D. A., Xie, X. S., Longo, F. M., & Wyss-Coray, T. (2014). Young blood reverses age-related impairments in cognitive function and synaptic plasticity in mice. *Nature Medicine*, *20*(6), Article 6. https://doi.org/10.1038/nm.3569

Villette, V., Malvache, A., Tressard, T., Dupuy, N., & Cossart, R. (2015). Internally Recurring Hippocampal Sequences as a Population Template of Spatiotemporal

Information. *Neuron*, *88*(2), 357–366. https://doi.org/10.1016/j.neuron.2015.09.052

Wang, G.-W., & Cai, J.-X. (2006). Disconnection of the hippocampal–prefrontal cortical circuits impairs spatial working memory performance in rats. *Behavioural Brain Research*, *175*(2), 329–336. https://doi.org/10.1016/j.bbr.2006.09.002

Weigert, M., Schmidt, U., Haase, R., Sugawara, K., & Myers, G. (2020). Star-convex Polyhedra for 3D Object Detection and Segmentation in Microscopy. *2020 IEEE Winter Conference on Applications of Computer Vision (WACV)*, 3655–3662. https://doi.org/10.1109/WACV45572.2020.9093435

Werk, C. M., & Chapman, C. A. (2003). Long-term Potentiation of Polysynaptic Responses in Layer V of the Sensorimotor Cortex Induced by Theta-patterned Tetanization in the Awake Rat. *Cerebral Cortex*, *13*(5), 500–507. https://doi.org/10.1093/cercor/13.5.500

West, M. J., & Gundersen, H. J. G. (1990). Unbiased stereological estimation of the number of neurons in the human hippocampus. *Journal of Comparative Neurology*, *296*(1), 1–22. https://doi.org/10.1002/cne.902960102

Wilmerding, L. K., Kondratyev, I., Ramirez, S., & Hasselmo, M. E. (2023). Route-dependent spatial engram tagging in mouse dentate gyrus. *Neurobiology of Learning and Memory*, *200*, 107738. https://doi.org/10.1016/j.nlm.2023.107738

Wilmerding, L. K., Yazdanbakhsh, A., & Hasselmo, M. E. (2022). Impact of optogenetic pulse design on CA3 learning and replay: A neural model. *Cell Reports Methods*, *2*(5), 100208. https://doi.org/10.1016/j.crmeth.2022.100208

Wilson, M. A., & McNaughton, B. L. (1993). Dynamics of the hippocampal ensemble code for space. *Science*, *261*(5124), 1055–1058. https://doi.org/10.1126/science.8351520

Wilson, M., & McNaughton, B. (1994). Reactivation of hippocampal ensemble memories during sleep. *Science*, *265*(5172), 676–679. https://doi.org/10.1126/science.8036517

Wood, E. R., Dudchenko, P. A., Robitsek, R. J., & Eichenbaum, H. (2000). Hippocampal Neurons Encode Information about Different Types of Memory Episodes Occurring in the Same Location. *Neuron*, *27*(3), 623–633. https://doi.org/10.1016/S0896-6273(00)00071-4

Xavier, G. F., & Costa, V. C. I. (2009). Dentate gyrus and spatial behaviour. *Progress in Neuro-Psychopharmacology and Biological Psychiatry*, *33*(5), 762–773. https://doi.org/10.1016/j.pnpbp.2009.03.036

Xavier, G. F., Oliveira-Filho, F. J. B., & Santos, A. M. G. (1999). Dentate gyrus-selective colchicine lesion and disruption of performance in spatial tasks: Difficulties in "place strategy" because of a lack of flexibility in the use of environmental cues? *Hippocampus*, *9*(6), 668–681. https://doi.org/10.1002/(SICI)1098-1063(1999)9:6<668::AID-HIPO8>3.0.CO;2-9

Yang, Y., & Wang, J.-Z. (2017). From Structure to Behavior in Basolateral Amygdala-Hippocampus Circuits. *Frontiers in Neural Circuits*, *11*. https://www.frontiersin.org/articles/10.3389/fncir.2017.00086

Yang, Y., Wang, Z.-H., Jin, S., Gao, D., Liu, N., Chen, S.-P., Zhang, S., Liu, Q., Liu, E., Wang, X., Liang, X., Wei, P., Li, X., Li, Y., Yue, C., Li, H., Wang, Y.-L., Wang, Q., Ke, D., … Wang, J.-Z. (2016). Opposite monosynaptic scaling of BLP–vCA1 inputs governs hopefulness- and helplessness-modulated spatial learning and memory. *Nature Communications*, *7*, 11935. https://doi.org/10.1038/ncomms11935

Yap, E.-L., Pettit, N. L., Davis, C. P., Nagy, M. A., Harmin, D. A., Golden, E., Dagliyan, O., Lin, C., Rudolph, S., Sharma, N., Griffith, E. C., Harvey, C. D., & Greenberg, M. E. (2021). Bidirectional perisomatic inhibitory plasticity of a Fos neuronal network. *Nature*, *590*(7844), 115–121. https://doi.org/10.1038/s41586-020-3031-0

Yu, A. J., & Dayan, P. (2005). Uncertainty, Neuromodulation, and Attention. *Neuron*, *46*(4), 681–692. https://doi.org/10.1016/j.neuron.2005.04.026

Zaki, Y., Mau, W., Cincotta, C., Monasterio, A., Odom, E., Doucette, E., Grella, S. L., Merfeld, E., Shpokayte, M., & Ramirez, S. (2022). Hippocampus and amygdala fear memory engrams re-emerge after contextual fear relapse. *Neuropsychopharmacology*, *47*(11), 1992–2001. https://doi.org/10.1038/s41386-022-01407-0

**CURRICULUM VITAE**